Development of Small Molecule Inhibitors Targeting HSP90 C-terminal Dimerization in BCR-ABL1 positive Leukemia

Inaugural-Dissertation

Zur Erlangung des Doktorgrades
der Mathematisch-Naturwissenschaftlichen Fakultät
der Heinrich-Heine-Universität Düsseldorf

vorgelegt von

Niklas Dienstbier
aus Neuss

Düsseldorf, Januar 2024

Aus dem Institut für Kinder-Onkologie, -Hämatologie und Klinische Immunologie der Heinrich-Heine-Universität Düsseldorf

Gedruckt mit der Genehmigung der Mathematisch-Naturwissenschaftlichen Fakultät der Heinrich-Heine-Universität Düsseldorf

Berichterstatter:

1. Prof. Dr. Thomas Kurz

2. Prof. Dr. Julia Hauer

Tag der mündlichen Prüfung:

27.10.2023

Table of Contents

List of Abbreviations

Abbreviation	Full Name
CML	Chronic Myeloid Leukemia
ADP	Adenosine-Di-Phosphate
AHA1	Activator of HSP90 ATPase homologue 1
ALDH1A1	Aldehyde Dehydrogenase 1 Family Member A1
APS	Ammonium Persulfate
ATP	Adenosine-Tri-Phosphate
AX	Aminoxyrone
BCR	Breakpoint Cluster Region
BSA	Bovine Serum Albumin
CA1	Coumermycin A1
CC domain	coiled-coil domain
CD26 etc.	Cluster of Differentiation
CETSA	Cellular Thermal Shift Assay
ChIP-SEQ	Chromatin Immunoprecipitation Sequencing
CTD	Carboxy(C)-terminal Domain
CXCR-4	C-X-C chemokine receptor type 4
DMSO	Dimethylsulfoxid
DPBS	Dulbecco's phosphate buffered saline
DTT	Dithiothreitol
ER	Endoplasmatic Reticulum
FACS	Fluorescence-Activated Cell Sorting
FCS	Fetal Calf Serum
FDA	Food and Drug Administration
FISH	Fluorescence In-Situ Hybridization
FITC	Fluorescein-5-isothiocyanat
FP	Fluorescence Polarization
GAPDH	Glyceraldehyde 3-phosphate dehydrogenase
GFP	Green Fluorescent Protein
GHKL	Gyrase, HSP90, Histidine Kinase, MutL
GM	Geldanamycin
Grp94	Glucose-regulated protein 94
GST	Glutathione S-transferase
HCL	Hydrochloric Acid
HER2	human epidermal growth factor receptor 2
HIVEP1	Human Immunodeficiency Virus Type I Enhancer-Binding Protein 1
HOP	HSC70/HSP90-organizing protein
HSCT	hematopoietic stem cell transplantation
HSE	Heat Shock Element
HSF1	Heat Shock Factor 1
HSP	Heat-Shock-Protein
HSR	Heat Shock Response
IDTA	Isothermal Dose Gradient Thermal Shift Assay

ITDRF	isothermal dose-response fingerprint
JAK2	Janus Kinase 2
LRP5	Low-Density Lipoprotein Receptor-Related Protein 5
LSC	Leukemic Stem Cells
MAPK	Mitogen-activated protein kinase
MCR	major cytogenetic response
MD	Middle Domain
MDR1	Multidrug Efflux Pump1
MMR	major molecular response
MST	Microscale Thermophoresis
NDNF	Neuron Derived Neurotrophic Factor
NIR	Near Infrared
NSG	Next Generation Sequencing
NTD	Amino(N)-terminal Domain
PCR	Polymerase Chain Reaction
PDX	Patient Derived Xenograph
PEG	Polyethylenglycol
PEI	Polyethylenimine
PI3K	Phosphoinositide kinase
PP2A	Protein phosphatase 2
PPID	Peptidylprolyl Isomerase D
PU	Purin
RAF-1	rapidly accelerated fibrosarcoma
RFP	Red Fluorescent Protein
RIPA	Radio-Immunoprecipitation Assay
RT	Room Temperature
SAR	Structure Activity Relation
SDS	Sodiumdodecylsulfate
SEC-SAXS	Size Exclusion Chromatopgraphy Small-Angle X-ray scattering
SH	Src-homolgy
STAT5	Signal transducer and activator of transcription 5
TAE	Tris-acetate-EDTA
TBS	Tris-buffered saline
TEMED	Tetramethylethylethylenediamine
TKI	Tyrosine Kinase Inhibitor
TLR4	Toll-like Receptor 4
TM	Tanespimycin
TPR	Tetratricopeptide Repeat
TRAP1	Tumor Necrosis Factor Associated Protein 1
TR-FRET	Time Resolved Förster Resonace Energy Transfer
WES	Whole Exome Sequencing

List of Figures

List of Tables

Abstract

Despite significant advances in treating BCR-ABL1-positive leukemias in the last decade, treating relapsed and refractory cases remains difficult. In addition, Chemotherapy and tyrosine kinase inhibitors cause serious side effects and affect patients' quality of life. Therefore, it is necessary to develop new targeted therapy. Heat shock protein 90 (HSP90) is involved in the folding and maturation of the oncoprotein BCR-ABL1 and is frequently overexpressed in leukemic cells. The increased levels of HSP90 are associated with poor prognosis in patients. Consequently, HSP90 is an attractive target for novel targeted therapies.

The cellular role of HSP90 was explored using genetic knockdowns of the two cytosolic isoforms of HSP90α and β in BCR-ABL1 positive cells. Interestingly, a robust balancing mechanism between the two isoforms was found, keeping the absolute levels of HSP90 constant. Furthermore, the resistance mechanisms against the orphan-drug designated N-terminal specific HSP90 inhibitor Zelavespib (PU-H71) and the C-terminal specific inhibitor Coumermycin A1 were deciphered. PU-H71-resistant cells are characterized by significantly increased expression of HSP90α and ALDH1A1. Elevated HSP90α levels stabilize the kinases SRC and AKT, recapitulating the activation of the classical RPS6 signaling pathway and thus protecting cells from PU-H71 treatment. In addition, these cells have acquired an HSP90α S164F mutation that restricts the flexibility of HSP90. In contrast, Coumermycin A1 resistant cells are characterized by increased expression of the efflux pump MDR1 but also show alterations in the RPS6 signaling pathway.

Finally, a first-in-class C-terminal specific inhibitor of HSP90 dimerization was investigated and validated. The inhibitors **5b** and **VWK147** decrease cell viability in a broad spectrum of leukemic cells, including cells from relapsed patients. Various biochemical, biophysical, and cellular experiments have validated that **5b** and **VWK147** bind at the C-terminus of HSP90 and disrupt dimerization. Furthermore, initial *in vivo* experiments in mice xenograft and zebrafish models demonstrated promising effects of **5b** with low associated toxicity. However, **5b** lacks solubility in formulations suitable for *in vivo* applications. Consequently, **5b** and **VWK147** provide an ideal basis for developing improved drugs of this new promising drug class.

Zusammenfassung

Trotz großer Fortschritte in der Behandlung von Patienten mit BCR-ABL1 positiven Leukämien, bleibt es weiterhin herausfordernd Patienten mit einem Rezidiv oder einer therapierefraktären Erkrankung zu behandeln. Chemotherapie und Tyrosin-Kinase-Inhibitoren verursachen schwerwiegende Nebenwirkungen und beinträchtigen die Lebensqualität der Patienten. Daher ist es notwendig neue zielgerichtete Therapie zu entwickeln, um Toxizität einzusparen. Das Hitzeschock Protein 90 (HSP90) ist maßgeblich an der Faltung des Onkoproteins BCR-ABL1 beteiligt und ist in Leukämiezellen häufig überexprimiert. Dies geht mit einer schlechten Prognose für die Patienten einher. HSP90 ist somit eine attraktive Zielstruktur neue zielgerichtete Therapien zu entwickeln.

In BCR-ABL1 positiven Zellen konnte durch den genetischen *knockdown* der beiden zytosolischen Isoformen HSP90α und β ein robuster Mechanismus identifiziert werden, der die Balance in der Expression beider Isoformen sichert und die absolute Menge des HSP90 Proteins innerhalb der Zelle auf einem konstanten Niveau hält. Außerdem konnte ich Mechanismen entschlüsseln, die zur Resistenz gegen den N-terminalen HSP90 Inhibitor Zelavespib (PU-H71) und den C-terminal spezifischen Inhibitor Coumermycin A1 führen. PU-H71 resistente Zellen sind durch eine signifikant erhöhte Expression von HSP90α und ALDH1A1 charakterisiert. HSP90α Überexpression stabilisiert die Kinasen SRC und AKT, welche den klassischen RPS6 Signalweg aktivieren. Außerdem zeigen diese Zellen eine HSP90α S164F Mutation. Coumermycin A1 resistente Zellen hingegen sind vor allem durch eine erhöhte Expression der Effluxpumpe MDR1 ausgezeichnet.

Darüber hinaus wurde ein *first-in-class* C-terminus spezifischer Inhibitor, der die Dimerisierung von HSP90 verhindert, untersucht und validiert. Die Inhibitoren **5b** und **VWK147** reduzieren die Viabilität von unterschiedlichen Leukämiezellen einschließlich primärer Zellen von Patienten mit rezidivierten Erkrankungen. Durch biochemische, biophysikalische und zelluläre Experimente konnte ich zeigen, dass **5b** und **VWK147** an den C-terminus von HSP90 binden und so seine Dimerisierung blockieren können. In initialen *in vivo* Experimenten zeigte **5b** ein vielversprechendes Potential trotz Einschränkungen in seiner Löslichkeit. Daher bieten die Komponenten **5b** und **VWK147** eine ideale Grundlage, optimale Medikamente dieser neuen Wirkstoffklasse zu entwickeln.

1 Introduction

1.1 Leukemia

1.1.1 Hematopoiesis

The generation of new blood cells (hematopoiesis) is based on hematopoietic stem cells (HSCs) that predominantly reside in the bone marrow and are characterized by low cell cycle rate and pluripotency.[2] Depending on stimulation with stem cell factors (SCFs), those cells can develop into oligopotent lymphoid (common lymphoid precursor = CLP) or myeloid (common myeloid precursor = CML) precursor cells. Further specialization is mediated by colony-stimulating factors (CSF) that determine the fate of the progenitor cells, whereby a higher specialization grade is accompanied by decreased pluripotent potential. In general, lymphoid stem cells can develop into natural killer (NK) cells, T-cells, or B-cells, whereas myeloid stem cells can develop into monocytes, megakaryocytes, neutrophils, and red blood cells (**Figure 1**).[3] The explicit cell fate mechanism by which each hematopoietic effector cell develops is highly complex and still, to date, not fully understood and part of extensive research.
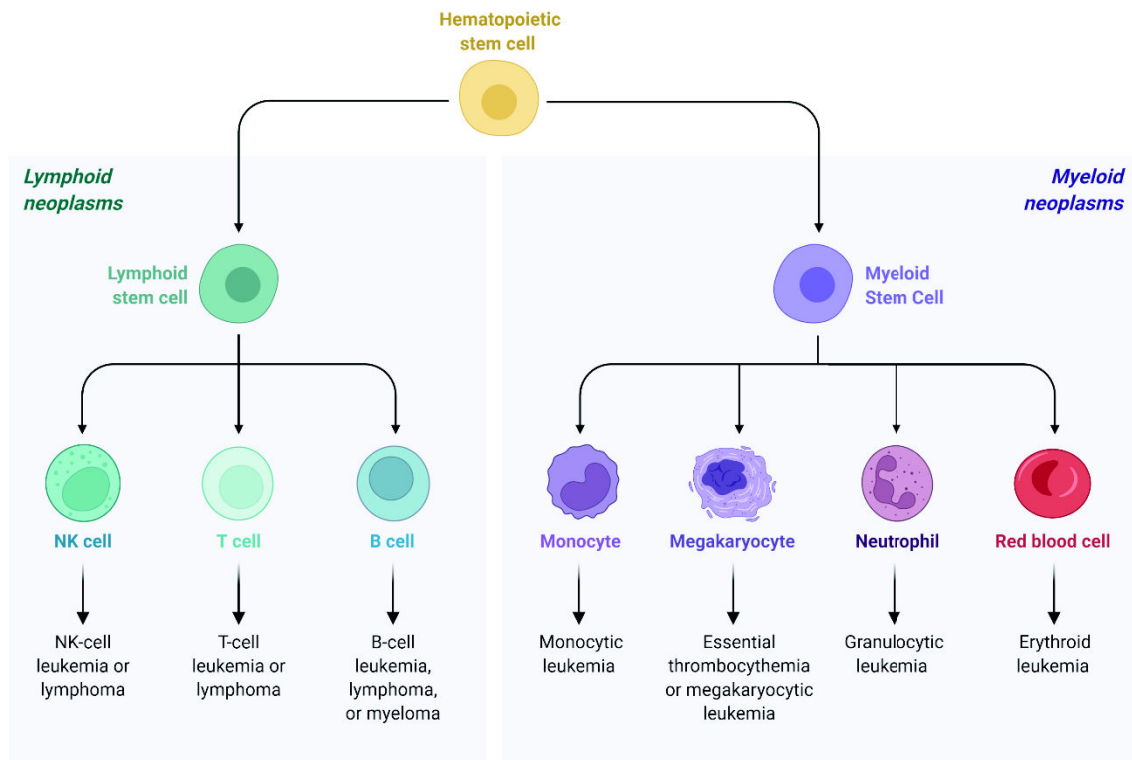
Figure 1: Schematic depiction of different hematological malignancies. Hematopoietic stem cells can take two routes of origin, including the lymphoid and myeloid route. Depending on distinct aberration some cells acquire malignant potential and develop leukemia. Created with BioRender utilizing the BioRender template "Blood Cancers" [1]

1.1.2 Leukemia

Despite strict immune modulatory regulation of the hematopoiesis and clearance of non-functional or damaged cells, some hematopoietic cells possess inherited and somatic genetic alterations leading to dysregulated and proliferation independent of growth factors.[4–6] This fundamental principle was postulated by *Greaves & Janossy* almost 45 years ago and is still valid for most leukemias.[6] Over the last years, several risk factors have been implicated and can be separated into environmental hazards (e.g. smoking, ionizing radiation, infections) and genetic predispositions like down syndrome.[7,8] Leukemic cells in the bloodstream are often characterized by an underdeveloped phenotype and are non- or semi-functional.[4,9] The displacement of functional hematopoietic cells in their corresponding niche by non-functional leukemic cells in patients results in leukocytosis, thrombocytosis, anemia, and splenomegaly. These disruptions of the hematopoietic equilibrium manifest in the form of diverse and nonspecific symptoms like fever, fatigue, and weight loss. Therefore, the majority of leukemias are detected in routine blood tests.[10]

The traditional classification of major leukemia subgroups is based on the progression speed (acute or chronic) and the lineage (lymphoid or myeloid) (**Figure 1**). First, acute leukemia develops rapidly and is characterized by non-functional, highly proliferative leukemic cells that generally induce more severe symptoms but are more susceptible to chemotherapy. Secondly, chronic leukemia develops more slowly with semi-functional leukemic cells resulting in a lower symptomatic burden and increasing the difficulty of detecting it. Combining the progression speed with the lineage origin of the malignant cells yields a classification into the four most prevalent types of leukemia: Acute lymphoblastic leukemia (ALL), acute myeloid leukemia (AML), chronic lymphocytic leukemia (CLL) and chronic myeloid leukemia (CML). However, the World Health Organization (WHO) guidelines consensus suggests using a more dynamic classification system based on differential protein expression and genetic alterations to account for oncogenic drivers and mosaic variants of those subtypes.[11]

1.1.3 Childhood leukemia

The prevalence of cancer entities between adults and children differs vastly, with children much more affected by hematological tumors. Besides central nervous system tumors, hematological malignancies account for 40% of all cancers in children.[12] Within the group of hematological malignancies, children are affected by leukemia much more frequently than adults, who are more often afflicted by lymphoma. A recent

comparative study from *Bolouri et al.* in AML demonstrated that children acquire 10-fold increased genetic structural alterations than adults, who have significantly more somatic mutations.[13] These genetic differences may be one of the reasons for the observed differences in incidence. Interestingly, the leukemic incidence in children is mainly attributed to ALL, accounting for up to 80% of all pediatric leukemias with predominant B-cell origin (85% B-cell lineage, 15% T-cell lineage) with a peak incidence between 2-6 years.

Pediatric leukemia is often characterized by chromosomal translocations or aberrations that happen early in development.[14] However, these oncogenic translocations often require additional mutations in crucial signaling pathways to manifest the disease. For example, ETV6-RUNX1 or RUNX1-RUNXT1 translocations are detected in newborns much more frequently (~100-fold)[15] than the incidence of ALL or AML would suggest.[16] A recent study utilizing DNA-based GIPFEL (genomic inverse PCR for exploration of ligated breakpoints) screening has demonstrated that 5% of healthy newborns already carry an ETV6-RUNX1 fusion.[17]

The origin of these additional acquired mutations is controversial, and several hypotheses emerged, focusing on environmental factors such as radiation, chemical exposure, and infections.[18] The "delayed infection" hypothesis suggests that contact with pathogens early in life fuel ALL pathogenesis by disrupting B-cell genome integrity, thus predisposing cells to other aberrations.[19–21] This principle was recapitulated in PAX5^{+/-} mice that developed leukemia following pathogen exposure after transfer from a pathogen-free environment providing experimental evidence of this mechanism.[22,23] However, the complex picture of childhood leukemia remains elusive.

1.1.4 BCR-ABL1 positive Leukemia

In CML, it was proven for the first time that a chromosomal translocation (*t(9;22)*) is the underlying cause of cancer.[24] More detailed investigations revealed that the gene encoding for the kinase ABL1 (Abelson murine leukemia) is located on the translocated chromosome 9. In contrast, all translocations in chromosome 22 happened in a distinct region labeled "breakpoint cluster region" (BCR).[25,26] This translocation will result in the expression of a chimeric mRNA[27,28] and, subsequently, the BCR-ABL1 oncoprotein (**Figure 2**).[27]
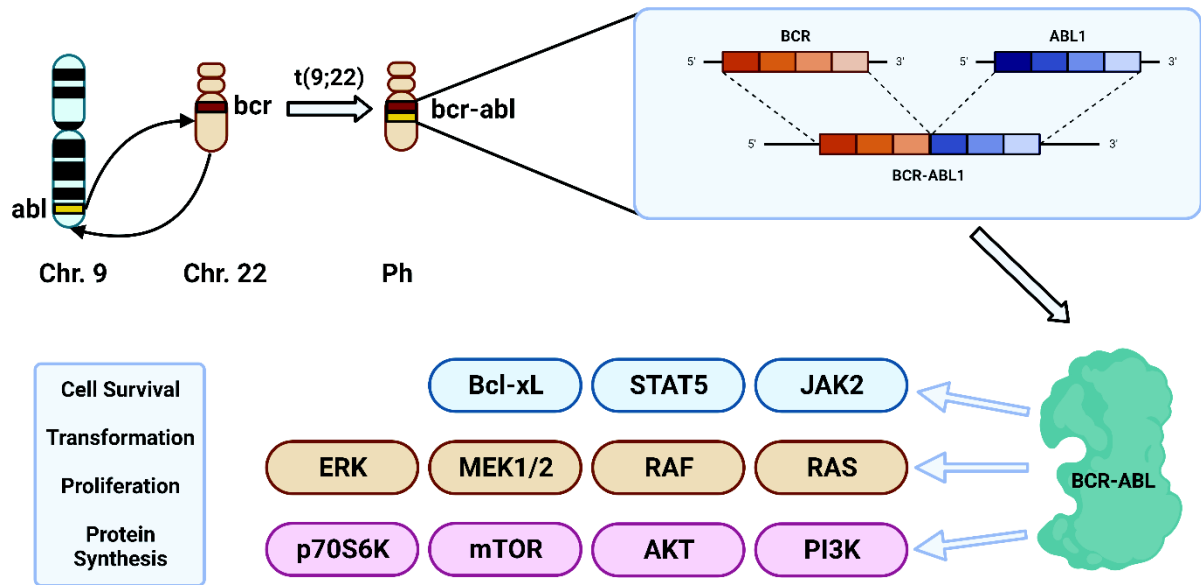
Figure 2: The molecular basis for BCR-ABL1. Translocation of Chr. 9 and Chr. 22 results in the Philadelphia Chromosome that encodes for a hybrid mRNA of BCR-ABL1. This hybrid mRNA is translated into the constitutively active oncoprotein BCR-ABL1, that activates several cellular pathways mediating oncogenic potential. Image created utilizing Biorender Software.

The tyrosine kinase ABL1 regulates a multitude of cellular processes. It is tightly regulated by an SH2/SH3 (Src-homology) negative regulator domain and an 80 AA N-terminal cap sequence stabilizing the inactive conformation.[29] Caused by the translocation, those two crucial regulatory domains are lost, mediating the oncogenic potential of BCR-ABL1 by enabling constitutively active tyrosine kinase signaling.[30] Mice transduced with BCR-ABL1 develop CML-like myeloproliferative disorders, confirming that isolated BCR-ABL1 signaling has sufficient oncogenic potential in an *in vivo* model.[31]

Three central downstream pathway axes are involved in driving BCR-ABL1-orchestrated transformation[32] (**Figure 2**): First, Signal transducer and activator of transcription 5 (STAT5) that mediates a plethora of survival and proliferation factors and prevents apoptosis via BCL-xL.[33,34] Secondly, the phosphoinositide kinase (PI3K) / AKT signaling axis that confers cell survival and prevents apoptosis,[35,36] and lastly the Ras/mitogen-activated protein kinase (MAPK) pathway that can induce BCR-ABL1-dependent transformation.[37] Importantly, loss of STAT5a with co-occurring P210$^{BCR/ABL}$ induction in primary murine bone marrow cells reconstituted in mice resulted in 21% of mice developing CML compared to 80-100% with active STAT5a.[38] This further confirms the importance of STAT5 signaling in BCR-ABL1-mediated axes.

In addition, BCR-ABL1 ensures cell cycle progression by inhibition and altered localization of the cell cycle inhibitor p27.[39,40] Interestingly, BCR-ABL1 translocation is not the only way of ABL-induced transformation. For example, a modified form of the c-ABL protein has been found in K562 cells with enhanced, constitutive tyrosine kinase activity independent of BCR, resulting in the oncogenic transformation of hematopoietic cells.[41–43].

1.1.5 Treatment of BCR-ABL1⁺ leukemia

For many years, the only curative option for BCR-ABL1⁺ leukemia was allogeneic hematopoietic stem cell transplantation (HSCT) accompanied by chemotherapy to bridge the time until a suitable donor was found. However, considering the availability of eligible donors and transplantation-mediated co-morbidities, the overall survival rate was only 30-40%.[44] Finally, a breakthrough was achieved with the development of Imatinib (Gleevec), a tyrosine kinase inhibitor (TKI), which was approved in 2001 (2003 for pediatric CML) for Ph-positive CML first-line treatment by the Food and Drug Administration (FDA), targeting BCR-ABL1 activity.[45] Due to the availability of crystal structures and extensive research, it is well understood that Imatinib engages close to the ATP-binding site of BCR-ABL1 and thus prevents enzyme activity. Especially important is the phenylamino-pyrimidine of Imatinib interacting with the hydroxyl group of T315 of BCR-ABL1 since cancer cells frequently exploit this interaction to acquire resistance.[46]

Generally, treatment response in BCR-ABL1⁺ leukemia is measured based on the surveillance method. Patients can achieve a hematologic response, cytogenetic response, or molecular response. The molecular response measures the amount of BCR-ABL1 transcript detected, with a major molecular response (MMR) being defined as BCR-ABL1 transcript < 0-1% international scales (IS). The cytogenetic response accounts for the portion of cells in the bone marrow with Ph-chromosome, whereas the hematologic response is based on the white blood cell and platelet count.[47,48] However, significant downsides of TKI treatment are acquired resistance after the TKI treatment is stopped and severe side effects such as pleural effusion and vascular events originating from chronic TKI treatment.[49–51]

1.1.6 Tyrosine-Kinase-Inhibitor resistance

Since TKIs and many other anti-proliferative drugs mainly disrupt the cell cycle and cell survival signaling and thus target the proliferating population of leukemic cells, they fail to eradicate persisting dormant or non-proliferative leukemia stem cells (LSCs).[52–54]

Additionally, recent studies linked characteristic surface expression markers of CML-LSC to TKI-resistance, such as CD26[55], CD36[56], and CD93.[57] These mechanisms are diverse, including interfering with the CXCR-4-axis, fatty acid uptake, and enhanced stemness, respectively. One pathway that has been found frequently to affect response to TKIs is the β-catenin signaling pathway.[58] β-catenin-induced resistance to TKI is mediated through JAK2 and PP2A, which maintain survival signaling and substitute BCR-ABL1 downstream to ensure proliferation and survival.[59] In addition, master regulators like c-MYC, HSP90, and the loss of tumor suppressor p53 are involved in maintaining the stemness phenotype, avoiding TKI response, and increasing the risk of relapse.[10]

Furthermore, the strict binding conditions of Imatinib near the ATP pocket (e.g. interaction with the hydroxyl group of T315) confers its specificity, rendering it susceptible to resistance mechanisms evolving around point mutations in BCR-ABL1 like T315I, E255K, and M351T. 38% of patients without major cytogenetic response (MCR) harbor mutations in BCR-ABL1 upon imatinib treatment.[60] These mutations enhance constitutive BCR-ABL1 signaling and confer severe resistance toward TKIs. Especially, mutations targeting the ATP phosphate-binding loop (P-loop) of BCR-ABL1 confer treatment resistance.[60] The development of second-generation TKIs like Nilotinib and Dasatinib, which showed significant improvement in affinity towards BCR-ABL1 compared to Imatinib, still failed to overcome T315I mutation-mediated resistance.[61,62]

Considering T315I mutation can be found in up to 20% of CML cases,[63] recent efforts led to the development of the newest generation of BCR-ABL1 TKI Ponatinib, specifically designed to be effective against imatinib-resistant clones. So far, the third-generation TKI Ponatinib is only approved in adults but shows decent efficacy against the T315I mutation.[64] However, several studies confirmed promising effects in children with a phase 1/2 clinical trial recruiting (NCT03934372).

Based on these findings and the severe treatment-induced side effects of TKIs, there is an urgent need for novel treatment options. Modern drug development consequently focuses on the combinatory usage of highly specific drugs targeting overarching cell-fate mechanisms like autophagy, protein homeostasis, and epigenetic modulations. One of those master regulators is the heat shock protein 90 (HSP90).

1.2 Heat shock protein 90 (HSP90)

Heat shock protein 90 (HSP90) stabilizes, folds, transports, and regulates the activity of over 400 client proteins.[65] Considering its immense importance, it is unsurprising that HSP90 comprises 1-2% of the total protein amount in a cell, increasing to 4-6% upon stress.[66]

1.2.1 HSP90 Structure

Without ATP bound, HSP90 occupies a homodimer, V-shaped conformation.[67,68] The two monomers consist of several distinct domains that fulfil complementary functions. (**Figure 3**) The amino-terminal domain (NTD) is essential for ATP binding and contains a conserved loop, the so-called lid region. The middle domain (MD) is necessary for ATP hydrolysis and client protein binding. Both domains are interconnected via a flexible charged linker. Lastly, the carboxy-terminal domain (CTD) contributes to HSP90 dimerization and contains the important recognition motif MEEVD.[69,70]
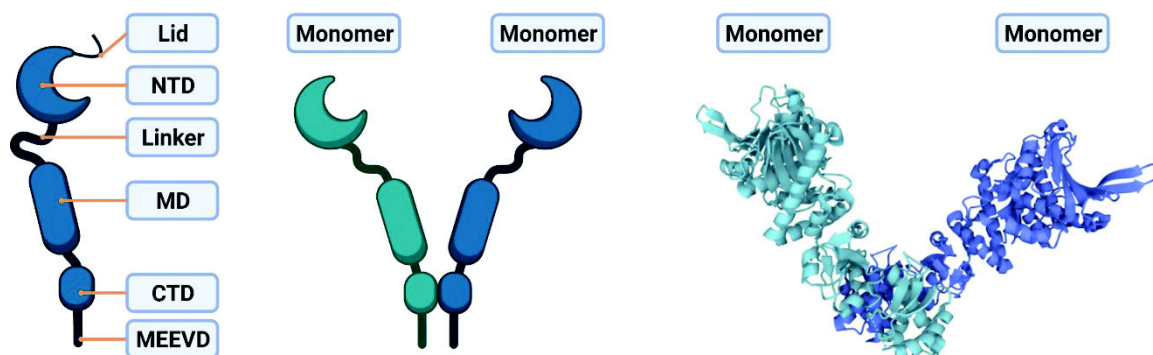
Figure 3: Schematic depiction of HSP90. (a) Important structural properties of HSP90 monomer. (b) HSP90 occupies a V shaped conformation. (c) Cartoon depiction of HSP90 crystal structure. Image created using Mol Viewer (PDB ID = 2IOQ) and BioRender.

Structurally, the ATP binding pocket is well conserved but is embedded in a deep pocket between a highly twisted β-sheet and an α-helix formed by the N-terminal domain.[70–72] The charged linker region contains KEKE (lysine-glutamate-lysine-glutamate) motifs and is exclusive for eukaryotic cells. This region has been shown to participate in steroid receptor binding, includes the nuclear localization signal, and has several regulatory implications upon phosphorylation or methylation that regulate the association between HSP90 and the proteasome.[73–76] Surprisingly, genetic studies have shown that the linker region is not essential for life-sustaining functions.[77]

1.2.2 HSP90 chaperone cycle

HSP90 undergoes a unique conformational cycle that starts with the engagement of ATP to the NTD, inducing a conformational change into the *intermediate state* by closing off the lid region (**Figure 4**). In this state, the NTDs of both monomers come in proximity and dimerize, called the *closed 1-state*. The *closed 2-state* is characterized by an interaction of the NTDs with the middle domains, enabling ATP hydrolysis. Subsequently, HSP90 returns to the open conformation by releasing ADP + P and dissociating the NTDs. Interestingly, ATP hydrolysis by HSP90 is, compared to other ATPases, very slow due to the complex conformational cycle involved.[78]
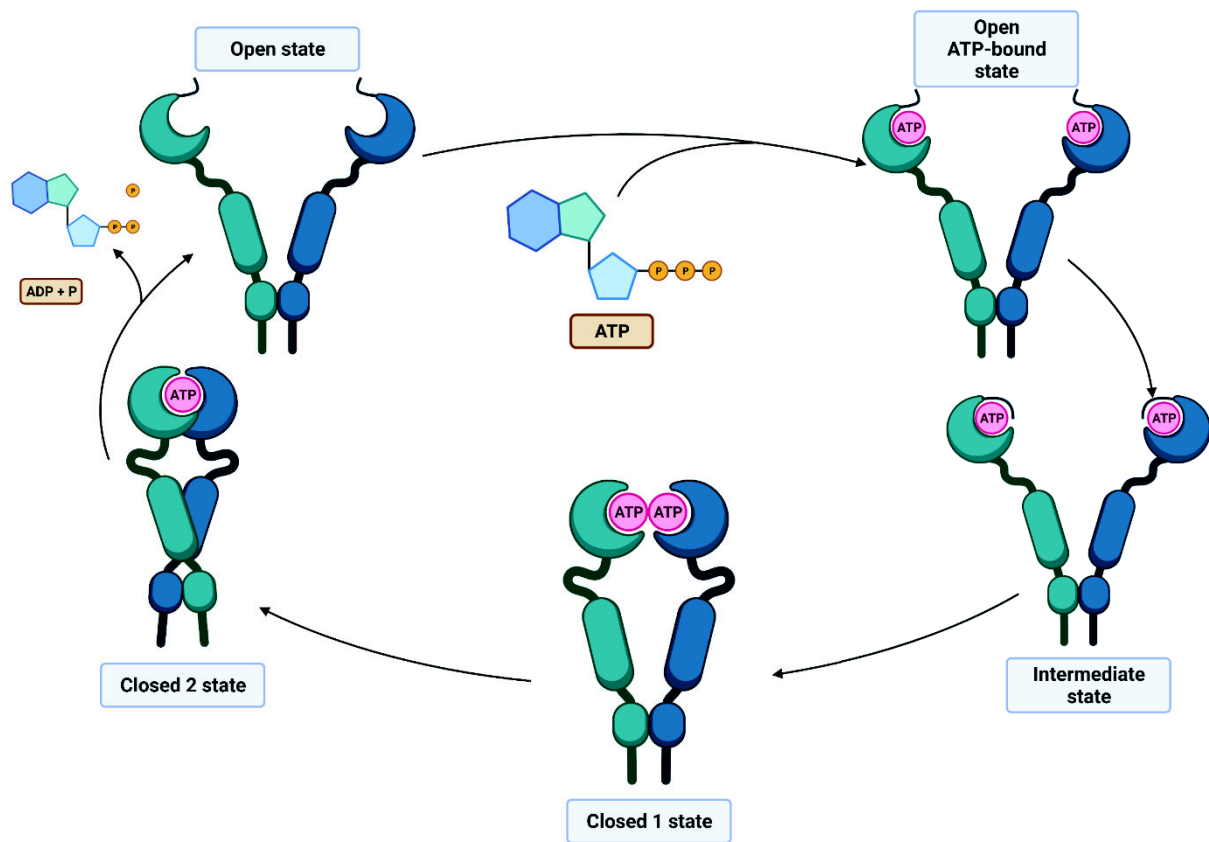
Figure 4: The HSP90 conformational cycle. After HSP90 has bound ATP, the lid regions close marking the intermediate state. After a dimerization of the NTDs HSP90 achieves the closed 1 state, whereas the closed 2 state is characterized by the interaction of both NTD and middle domains. This enables ATP hydrolysis. Adapted from *Schopf et. al*.[79] Image created using BioRender.

Co-chaperones orchestrate this conformational cycle with distinct roles depending on the cycle phase. AHA1 (Activator of HSP90 ATPase homolog 1) regulates the propagation into the *closed 1-state*, whereas p23 monitors the ATPase activity of HSP90 based on the *closed 2-state*. The co-chaperones CDC37 and HSC70/HSP90-organizing protein (HOP) have a shared responsibility in the phases before *closed 1-*

and after *closed 2-state*.[79] HSP90 has different motifs to mediate those interactions. One important motif located in the C-terminal domain is the MEEVD recognition motif which enables interaction with the tetratricopeptide repeat (TPR) domains of other chaperones.[80]

1.2.3 HSP90 paralogs and isoforms

Four isoforms of HSP90 exist in eucaryotic cells and differ significantly in cellular localization (**Figure 5**). Glucose-regulated protein 94 (GRP94) is localized in the endoplasmic reticulum, whereas tumor necrosis factor-associated protein 1 (TRAP1) is localized in the mitochondria.[81] Besides Grp94 and Trap1, there are also two cytosolic isoforms, HSP90α and HSP90β, originating from gene duplication, thus showing remarkably high amino acid similarity.[82]
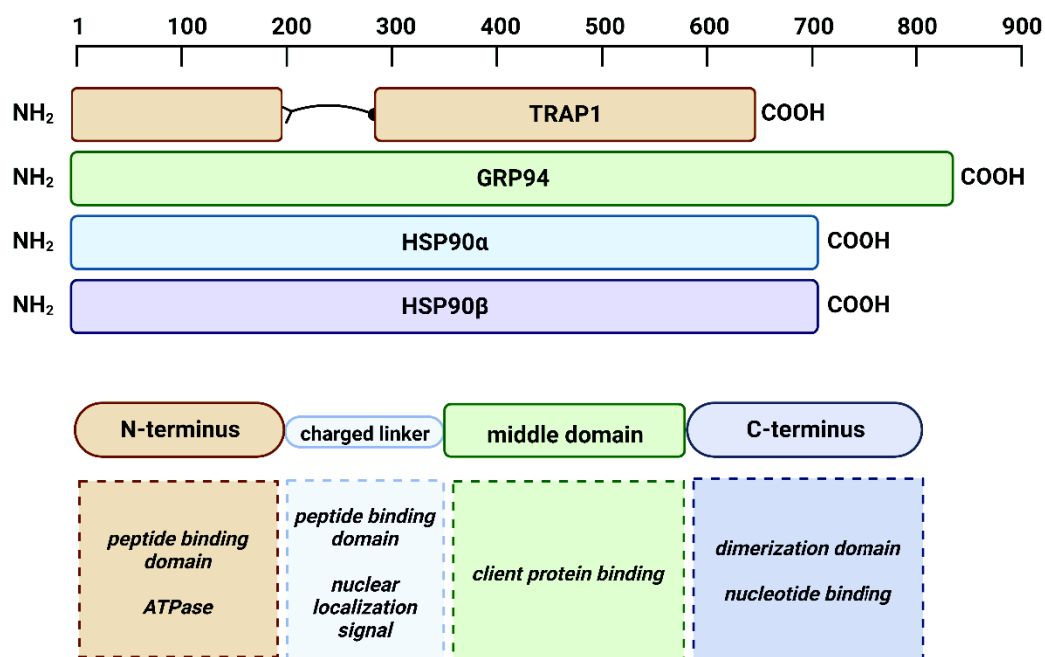
Figure 5: Structural similarity of different HSP90 isoforms: The four HSP90 isoforms (TRAP1, GRP94, HSP90α and HSP90β) have similar conserved structural properties, but differ in cellular localization and roles within the cell. Notably, HSP90α and HSP90β, have a very high amino acid similarity. Adapted from *Sreedhar et al.*[81], created using Biorender.

The general structure of the four isoforms is highly conserved and consists of an N-terminal region responsible for peptide binding and the ATPase function, a charged linker containing a nuclear localization signal, a middle domain important for client protein interaction, and a C-terminal domain that facilitates dimerization and nucleotide binding (**Figure 5**).[81] GRP94 can achieve its role as ER specific chaperone due to its

KDEL motif in its C-terminal domain that serves as an endoplasmic retention signal to ensure proper endoplasmic localization.[76]

HSP90α and HSP90β have an 86% identical amino acid sequence but fulfill specialized roles in the cell.[83] To orchestrate these roles, both isoforms are differentially expressed based on subtle changes in non-coding regions that are exploited by transcription factors such as heat shock factor 1 (HSF1).[84] Physiologically, HSP90β is constitutively expressed, whereas the baseline expression of HSP90α is moderate. However, upon stress induction, HSP90α levels increase strongly due to specialized enhancer regions called heat shock elements (HSEs) located upstream of HSP90α, which are engaged by HSF1 to induce the expression. This mechanism consists of a proximal and distal HSE at the transcription start site of HSP90α. Under physiological conditions, HSF1 only occupies the proximal HSE, whereas, under stress, both HSEs can be bound by activated HSF1, as demonstrated by ChIP-SEQ analysis. Occupation of both HSEs results in a DNA loop formation that enables the synergistic expression of HSP90α due to structural enhancement.[81,85,86]

Another isoform-specific regulation is a sequence of post-translational modification sites specific for HSP90α, altering the interaction with downstream targets such as CHIP and HOP[87] or DNA repair proteins.[88]

1.2.4 Heat Shock Response

The heat shock response (HSR) is a biological safeguard mechanism and one of the primary pro-survival responses which protect cells from proteotoxic stress. Initially, it was found as a reaction to elevated temperature, but as research continues, it has been found to have a variety of roles and implications in different diseases. The HSR is characterized by a strong upregulation of heat shock proteins (HSPs) which manage and reverse the proteotoxic stress. A vital role in this mechanism is attributed to the transcription factor heat shock factor 1 (HSF1), which detects and reacts to altered proteostasis (**Figure 6**).[89,90] Interestingly, HSP90 and HSP70 regulate HSF1 by binding it in a transcriptionally incompetent monomeric form. This mechanism has been confirmed by adding HSP90 to a temperature-induced heat shock system resulting in significantly reduced trimerization of HSF1 and less binding to the corresponding HSEs (**Figure 6**).[91]

During stress and accompanying accumulation of misfolded proteins, HSF1, and nonnative proteins, compete for HSP90-binding, thus releasing HSF1 monomers into the cytoplasm (**Figure 6**). This accumulation of unbound HSF1 monomers in the cytoplasm enables homotrimerization and strongly depends on the HSF1 concentration.[91] Subsequently, the HSF1 trimer relocates into the nucleus and associates with distinct transcriptional binding sites called Heat Shock Elements (HSE).
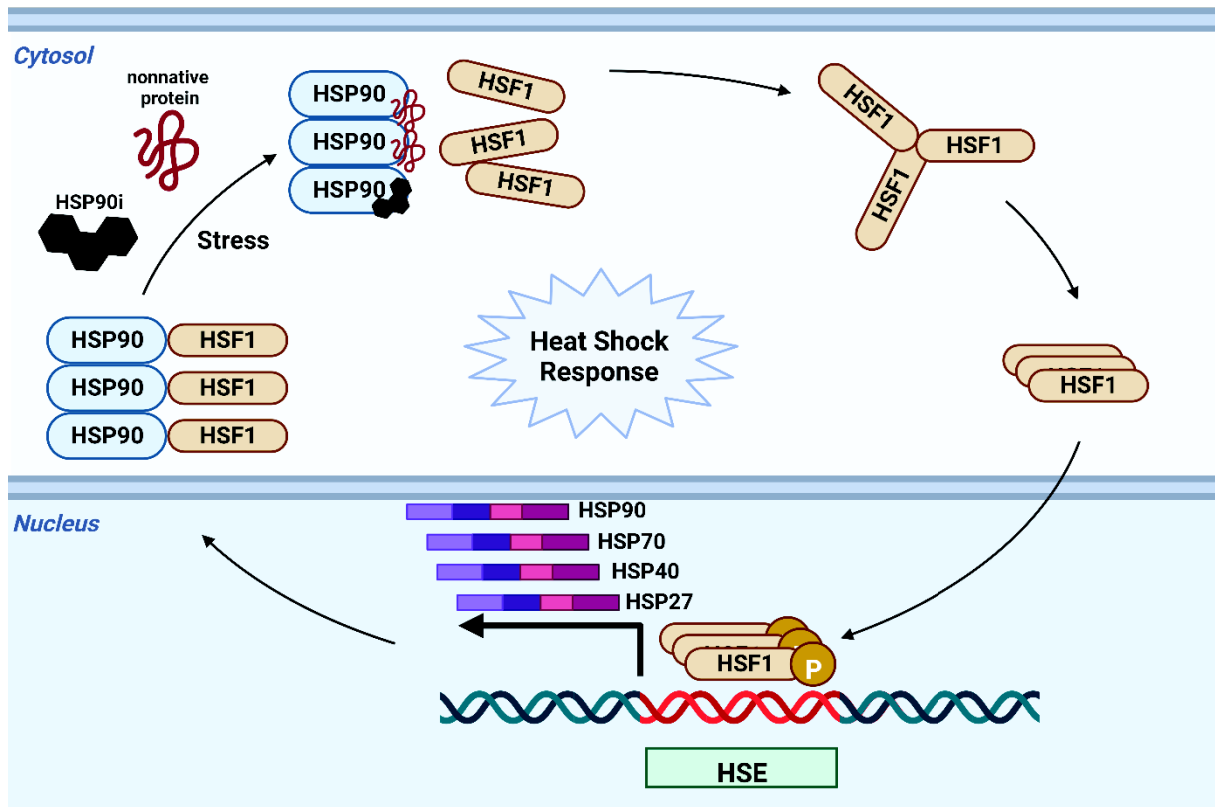
Figure 6: The Heat Shock Response. Upon stress, there is an accumulation of non-native proteins occupying the binding pockets of HSP90 proteins, releasing increasing amounts of HSF1 monomers into the cytoplasm. HSF1 trimerizes, is phosphorylated and thus translocates into the nucleus, where it can bind HSE, inducing the expression of a multitude of heat-shock family proteins.

To enhance transcription activity and enable transactivation competence, HSF1 is hyperphosphorylated resulting in the expression of the HSF1-dependent gene panel, including most notably, HSP90, HSP70, HSP40, and HSP27, which mediate the heat shock response due to various downstream interaction (**Figure 6**).[92,93]

1.2.5 HSP90β and BCR-ABL1 localization

More recent studies revealed that the function of BCR-ABL1 is strongly associated with its subcellular localization. The cytoplasmatic localization of BCR-ABL1 is mediated by the N-terminal coiled-coil domain (CC domain) and manifests predominately pro-survival downstream signaling.[94] However, it has been shown that BCR-ABL1 loses transforming capabilities and induces apoptosis of CML cells through activation of p73 when directed into the nucleus by drug transduction or a nuclear transport system. [95,96]
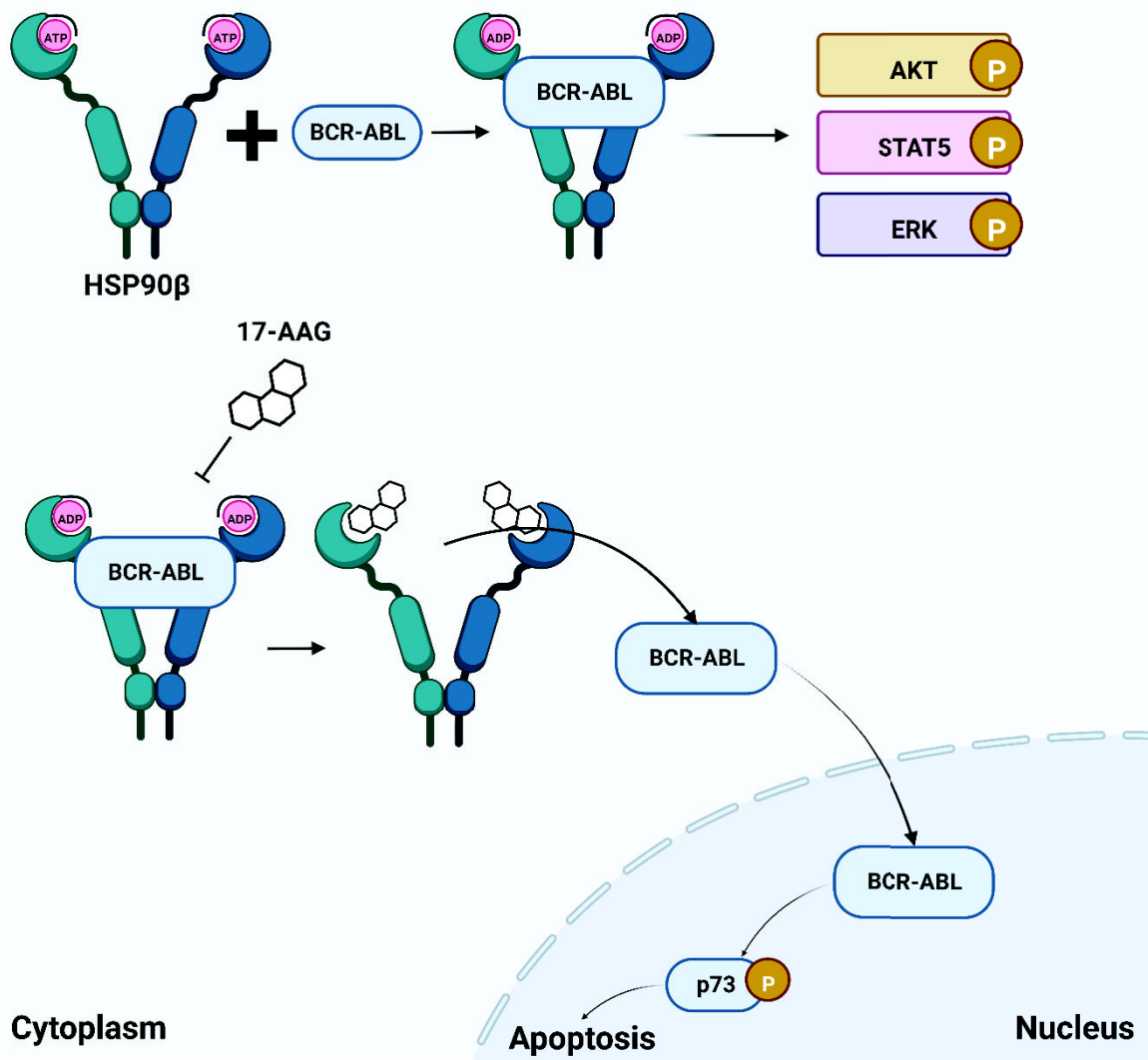
Figure 7: Schematic depiction of the HSP90β specific regulation of BCR-ABL1 localization. (a) BCR-ABL1 signaling with intact HSP90β results in the activation of downstream kinases mediating cell growth and survival. (b) Upon 17AAG inhibition of HSP90β BCR-ABL is released from the HSP90β-BCR-ABL complex and translocates into the nucleus, where it activates p73 and thus inducing apoptosis. Adapted from *Peng et al.*[100]

Since BCR-ABL1 is one of the most critical downstream clients of HSP90 in leukemia, it is unsurprising that many studies have confirmed that HSP90 inhibition decreases levels of BCR-ABL1 and induces apoptosis in various leukemic entities.[97–99]

However, recently *Peng et al.* implicated that the aforementioned cytoplasmatic retainment of BCR-ABL1 is regulated by forming a BCR-ABL1-HSP90β complex, enabling the oncogenic transformation of cells (**Figure 7**).[100] Interestingly, this regulation seems to be paralog specific. HSP90β directly binds the CC domain of BCR-ABL1 and thus stabilizes cytoplasmatic BCR-ABL1 and prevents its degradation. This protection activates several downstream kinases, including AKT, STAT5, and MAPK axes (**Figure 7**).

Treatment of cells with the N-terminal inhibitor 17-AAG disrupts the BCR-ABL1-HSP90β complex due to a competitive binding event on the N-terminal part of HSP90β. Consequently, BCR-ABL1 dissociates from HSP90β, translocates into the nucleus, inhibits cytoplasmatic BCR-ABL1 signaling, and induces p73 signaling, namely p21 and PUMA expression via its c-ABL kinase domain activity (**Figure 7**).[100]

1.2.6   Cancer Hallmarks and HSP90

Since HSP90 is involved in stabilizing, maturing, and properly folding over 400 client-proteins,[101] it is consequently involved in regulating most crucial cellular processes like cell proliferation, DNA damage response, and cell survival. While this contributes to regulated protein homeostasis in healthy cells, cancer cells hijack these fundamental mechanisms to promote uncontrolled proliferation.[102] In recent years, it became evident that several oncogenic kinases, including BCR-ABL1,[100] RAS/RAF,[103] AKT/PI3K,[104] and many others, depend on functional HSP90. This HSP90 addiction compensates for high protein turnover and failing safeguard mechanisms of neglected protein quality checkpoints.[105] Mechanisms and cellular processes essential for transformation, cancer survival, and treatment resistance were defined by *Hanahan and Weinberg* as six hallmarks of cancer,[106] which were updated more recently to ten hallmarks of cancer.[107] Interestingly, HSP90 can influence all ten hallmarks of cancer, making it a desirable drug target for researchers and clinicians.[102]

In patients, HSP90 is upregulated in leukemia[108], breast[109], and pancreatic[110,111] cancers, compared to their benign counterparts, accelerating malignant transformation and tumor progression by advancing cell cycle progression via tyrosine kinases stabilization.[81,108,112–114]

1.2.7 HSP90 in leukemia

Many oncoproteins described as major leukemic drivers, such as c-KIT, FLT3-ITD, and BCR-ABL1, depend on HSP90 signaling. For example, treating malignant mast cells with HSP90i diminishes c-KIT activity and downstream survival signaling.[115,116] Furthermore, 17-AAG disrupts cell proliferation of FLT3-expressing leukemia[117] and BCR-ABL1 signaling.[100,115,118] It has been shown that patient-derived leukemic cells express significantly more HSP90 protein than peripheral mononuclear cells.[108,119] This increase in total HSP90 is mediated by elevated HSP90α mRNA.[108,120] Interestingly, this seems specific for HSP90 since other chaperones like HSP27 and HSP70 were not affected to such an extent.

In recent years, the role of HSP90 in leukemia was also investigated in a clinical context. A comparative study by *Sedlackova et al.* showed that HSP90α levels are elevated in untreated leukemic patients compared to healthy donors.[121] Furthermore, *Tian et al.* demonstrated direct clinical implications correlating with HSP90α expression.[122] First, refractory and relapsed acute leukemia patients show elevated levels of HSP90α. Secondly, untreated patients with high HSP90α expression had diminished remission rates implicating a correlation between HSP90α levels and poor leukemia prognosis.[122] Similar findings have been reported that expression levels of heat-shock proteins have prognostic significance in acute myeloid leukemia[118] and myelodysplastic syndromes.[123] Additionally, HSF1, the central regulator of the heat shock protein expression, is often dysregulated in leukemia and affected by treatment therapy.[124] In contrast, HSF2 is upregulated lineage-specific and dictates hematopoietic lineage commitment, as demonstrated in K562 cells.[125]

In summary, HSP90 plays a significant role in leukemia, affects leukemia-specific signaling axes, and has direct clinical implications. Consequently, HSP90 is a promising drug target for advanced targeted therapy in leukemia.

1.3 HSP90 Inhibitors

1.3.1 Natural Compound N-terminal HSP90 Inhibitors

Geldanamycin, a benzoquinone ansamycin antibiotic originally intended to inhibit gram-negative bacteria's gyrase activity, was the first discovered HSP90 inhibitor in 1994. However, due to the structural similarities between the HSP90 ATP-binding domain and bacterial gyrase, it has been shown that geldanamycin binds to the ATP-binding domain located in the N-terminus of HSP90 destabilizing HSP90 client proteins in cancer cell lines.[72]

Figure 8: Co-crystal structure of HSP90 and Geldanamycin. Geldanamycin binds to the ATP-binding domain located in the N-terminus of HSP90. Geldanamycin is colored in orange whereas HSP90 is colored in green. Figure was generated based on the PDB ID: 1YET based on crystal structures by *Stebbins et al.* [72]

After the availability of the co-crystal structure of HSP90 with ADP and geldanamycin, the development of N-terminal inhibitors was significantly accelerated.[70,72,126] Based on structure-activity relationship (SAR) studies, the ansamycin class was developed further by optimizing the 17-methoxy group resulting in compounds like 17-AAG (tanespimycin) or 17-DMAG (alvespimycin) overall yielding four ansamycin-type drugs investigated in clinical trials.[127–129] Another natural compound found to disrupt HSP90 with even greater specificity/potency than geldanamycin is the fungal polyketide radicicol, a resorcyclic acid lactone.[130] Next, advanced synthetic resorcinol-based inhibitors such as NVP-AUY922 (Luminespib) and STA-9090 (Ganetespib) have been developed based on radicicol co-crystal structures in complex with HSP90 and high throughput drug screening against yeast HSP90. Five resorcinol-based inhibitors are evaluated in clinical trials, including phase II and III studies. [116,129,131–134]

1.3.2 Purine-based N-terminal HSP90 Inhibitors

The first fully synthetic HSP90 inhibitor was a purine-based scaffold that also targets the ATP-binding pocket of HSP90. It was developed by rational design mimicking the conformation of ATP in GHKL-ATP binding sites.[135] It contains a purine connected to a phenyl moiety via a linker and an alkyl or aminoalkyl moiety. In principle, these three structural characteristics mimic the physiological ATP binding. The purine mimics the adenine, the phenyl moiety accounts for the phosphates, and the alkyl moiety is based on the ribose location. However, achieved co-crystal structures suggest a conformational change of the phosphate binding pocket, resulting in a slightly different binding mode of the phenyl-moiety than anticipated.[136] Based on the optimization of the phenyl-moiety, which enhances HSP90 specificity, and improved pharmacokinetics, achieved with changes of the alkyl moiety, several potent purine-based HSP90 inhibitors were developed.[137] The improved oral bioavailability and lower overall toxicity of purine-based HSP90 inhibitors hold promising advantages over classical N-terminal HSP90 inhibitors. The most successful purine-based HSP90 inhibitor is Zelavespib (PU-H71). Zelavespib has been validated in numerous publications in preclinical studies demonstrating potent HSP90 inhibition and apoptosis induction in heavily resistant tumor entities such as diffuse large B-cell lymphoma (DLBCL) or triple-negative breast cancer. [138,139] As of recently, Zelavespib was granted orphan drug designation for myelofibrosis.

1.3.3 Aminocoumarin-based C-terminal HSP90 Inhibitors

Initially, it has been reported that a second class of bacterial antibiotics, namely amino coumarin-based antibiotics (coumermycin A1, novobiocin, and clorobiocin), degrade HSP90 client proteins such as HER2 and RAF-1.[140] However, further investigation revealed that this class binds a so far unrecognized binding pocket at the HSP90 C-terminus.[141] Considering that most amino coumarin-based HSP90 inhibitors do not induce an HSR[142–144], significant effort was put into developing new C-terminal HSP90 inhibitors to improve HSR-related toxicity.[145–154] Nevertheless, missing co-crystal structures, complex C-terminal dynamics, and poor pharmacological properties have made this investigation challenging. Several binding mode theories have been proposed, including an allosteric regulation of the N-terminal nucleotide binding site and disruption of the C-terminal dependent dimerization.[155] Investigation of HSP90 co-

chaperones suggests that amino coumarin compounds modulate the association of HSP90 with HSP70, p23, and CDC37.[141,156]

1.3.4 Peptidomimetics-based C-terminal HSP90 inhibitors

New classes of C-terminal HSP90 inhibitors emerge, such as the aminoxyrone (AX) helix mimetic, which successfully disrupts C-terminal HSP90 dimerization in CML.[97] This new class of peptidomimetic foldamer C-terminal HSP90 inhibitors was developed to target the C-terminal mediated dimerization of HSP90 based on hot spot residue predictions.[97,157] In detail, AX has a 2_8-helical conformation mimicking conserved residues in the HSP90 C-terminal domain responsible for dimerization (I688, Y689, I692, L696) accounting for the spatial arrangement of the peptide side chains in the HSP90 α-helix H5 resulting in a computational modeled binding event of AX between H4 and H5 (**Figure 9**).[158,159]
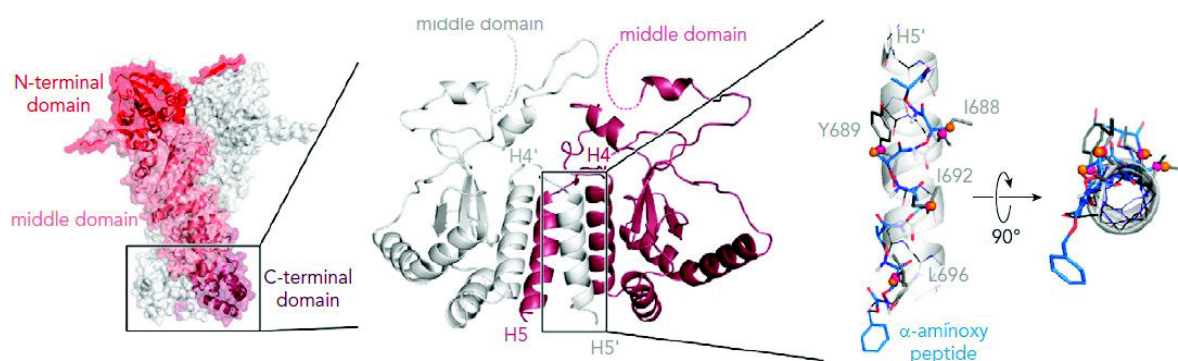
Figure 9: Aminoxyrone mimics the C-terminal interaction surface of HSP90. The conserved hot spots I688, Y689, I692, L696 in the peptide chain of helix H5 located in the C-terminal domain of HSP90 is exploited by aminoxyrone. Figure adapted from *Bhatia et al*.[97]

Bhatia et al. demonstrated that AX binds HSP90 at the C-terminus and disrupts dimer formation, confirmed by an auto-display assay and sedimentation velocity analysis. In addition, AX inhibited the chaperone activity of HSP90 in a cell-based luciferase refolding assay, and several *in-vitro* and biochemical assays confirmed binding to HSP90 oligomers. Notably, AX destabilizes BCR-ABL1, blocking essential pro-survival signaling axes such as AKT, STAT5a, and MYC. On top of that, AX did not induce a classical HSR, which usually contributes to dose-limiting toxicity, and had less pronounced toxicity effects on healthy blood fractions reducing potential side effects.[97] Furthermore, AX showed potency in the leukemic stem cell fraction, which significantly contributes to relapse and therapy resistance, and against resistant cells that harbor

clinically relevant point mutations conferring TKI resistance, such as T315I, E255K, and M351T.[97] However, peptide-based compounds are non-optimal for clinical uses because of poor membrane permeability, susceptibility to proteolysis, and fast metabolization.[160] On top of that, due to the high molecular weight (994 g/mol) and lipophilic nature, AX is characterized by poor water-solubility and coherent low bioavailability rendering it unsuitable for further clinical studies.

1.3.5 HSP90 inhibitors in clinical trials

Considering HSP90 is a promising potential target for multi-resistance cancer types, significant effort was put into developing highly potent HSP90 inhibitors.

Over a dozen HSP90 inhibitors have been tested in numerous clinical trials, beginning with the clinical trial of 17-AAG several years ago.[161–164] However, dose-limiting toxicity and adverse side effects, particularly ocular toxicity and hepatotoxicity, terminated most clinical trials. Consequently, the FDA was hesitant to approve HSP90 inhibitors for clinical usage. Hepatoxicity of the ansamycin-based drugs is often attributed to high oxidative stress induced by superoxide formation by NQO1 and NADPH cytochrome P450 or NADH cytochrome b5 reductase.[165] In addition, most inhibitors have issues with low water solubility resulting in non-optimal bioavailability.[166,167] HSP90 N-terminal inhibitors require a 100-fold higher concentration in biochemical/biophysical HSP90 binding affinity assays than cell viability assays *in vitro*.[168] This discrepancy implies potential off-target mechanisms involved in inducing cellular toxicity. In contrast, the efficacy of C-terminal HSP90 inhibitors *in vitro* correlates better with their binding to HSP90 in biochemical assays.[168,169] However, the FDA recently designated PU-H71 (Zelavespib) as an orphan drug for myelofibrosis in combination with the JAK2 inhibitor Ruxolitinib. In addition, the HSP90 inhibitor Jeselhy (TAS-116, Pimitespib) has been approved by Japan's Ministry of Health for gastrointestinal stromal tumors (GIST) after a promising clinical trial [JapicCTI-184094].[170]

1.3.6 Mechanism of Resistance to HSP90 Inhibition

The failure of HSP90 inhibitors in clinical trials is based on several issues. One of the most important is acquired resistance to HSP90 inhibition. One central mechanism is caused by the HSR mentioned above. It has been shown that Geldanamycin treatment drastically increases the binding affinity of HSF1 to the HSEs by inhibition of HSP90 and thus inducing the HSR similarly to proteotoxic stress.[91] Upon HSP90 inhibition,

HSF-1 is phosphorylated and forms signalosomes which localize into the nucleus where it regulates downstream chaperones.[171] The subsequent overexpression of HSP70 and HSP27 triggers several adverse effects, including resistance and ocular toxicity.[172] For example, HSP70 over-expression prevents apoptosis by interfering with caspases,[173], whereas HSP27 blocks mitochondrial-induced cell death by disrupting cytochrome C.[174]

Besides these biological consequences of HSP90 inhibition, tumor cells possess an eclectic repertoire of mechanisms to deal with unwanted drugs. The four classical resistance mechanisms to acquire drug resistance are 1) overexpression of efflux pumps or transporters, 2) modification of the drug target to destabilize drug binding, 3) metabolizing or modifying the drug, and 4) constitutive activation of downstream effector proteins mediating survival signaling.[165] Cancer cells can acquire resistance to HSP90 inhibitors utilizing most of these mechanisms.

First, overexpression of the multidrug efflux pumps P-glycoprotein or MDR1 is reported as a response to treatment with benzoquinone ansamycins, whereas purine-based or advanced synthetic HSP90 inhibitors like BIIB021 remain unaffected.[175,176] Secondly, *Rouhi et al.* have reported that KRAS mutant lung cancer cells harbor a mutation in HSP90α Y142N, which abolishes a stabilizing hydrogen bond with its interaction partner S164.[177] Next, the quinone oxidoreductase 1 (NQO1), which is responsible for metabolizing benzoquinone ansamycin drugs, is reduced in several cancer entities.[164,165,178] One significant advantage of HSP90-targeting is that resistance requirement due to constitutive activation of downstream kinases is not very successful. This resistance mechanism fails due to the multitude of client proteins of HSP90. A more fruitful, HSP90-specific resistance mechanism is the misregulation of HSP90 co-chaperones mediating resistance to HSP90 inhibition. However, this mechanism of resistance is poorly described and needs additional investigation.[165]

1.4 Aim of the thesis:

This multi-disciplinary study addresses three major research topics concerning the role of HSP90 in BCR-ABL1-positive leukemia:

- First, this study investigates the role of the cytosolic isoforms HSP90α and β utilizing genetic knockdowns and implications on the heat shock response. Emphasis is put on the interplay between both paralogs.

- Secondly, the resistance mechanisms acquired by BCR-ABL1 positive cells against the orphan-drug designated N-terminal HSP90 inhibitor Zelavespib (PU-H71) and the C-terminal HSP90 Inhibitor Coumermycin A1 will be unraveled. In particular, the underlying adaptations of resistant cells on DNA-, RNA-, and protein-level will be elucidated based on acquired DNA copy number variations, point mutations, and changes in kinase signaling.

- Lastly, this study aims to investigate, validate, and characterize a first-in-class C-terminal inhibitor of HSP90 dimerization. For this, state-of-the-art biochemical, biophysical, and cellular validation methods will be conducted to study the mechanism of action, focusing on the interaction with HSP90, C- or N-terminal binding, and disruption of dimerization. Additionally, the compounds will be tested in initial *in vivo* experiments to further optimize this new class of drugs for *in vivo* applications addressing toxicity and solubility.

In summary, these findings will help with the current understanding of the role of HSP90 in BCR-ABL1 positive leukemia regarding its contribution to survival, the portfolio available for leukemic cells to escape HSP90 inhibition, and application possibilities for this new class of HSP90 inhibitors to overcome resistance and advance further in the direction of prospective clinical trials.

2 Material and Methods:

2.1 Material

2.1.1 Instruments:

Table 1: List of utilized instruments with distributing company.

Device	Company
Digital Scale	KERN & SOHN, Balingen, Germany
CytoFLEX Flow Cytometer	Beckman Coulter, Krefeld, Germany
JESS	Protein Simple, BioTechne, Wiesbaden, Germany
ThermoMixerC	Eppendorf, Hamburg, Germany
Microscope	Carl Zeiss, Oberkochen, Germany
NanoDrop Spectrophotometer ND-1000	Peqlab, Erlangen, Germany
Mice Injection Cage	NeoLab, Heidelberg, Germany
Caliper IVIS Lumina II Multispectral Imaging System	PerkinElmer, Rodgau, Germany
PowerPac™ Basic Power Supply	Bio-Rad, #1645050EDU
Laminar Flow Hood	Thermo Fisher Scientific, Schwerte, Germany
Ultrasonication Waterbath	Bio-Rad, Düsseldorf, Germany
37°C Incubator	Thermo Fisher Scientific, Schwerte, Germany
CO^2 Incubator	Binder, Tuttlingen, Germany
Microcentrifuge	Thermo Fisher Scientific, #75002555
Flow Cytometer Sorter MoFlo XDP	Beckman-Coulter, Krefeld, Germany
Tecan Spark10M	Tecan, Crailsheim, Germany
Tecan Infinite M1000pro (AG Stark, HHU)	Tecan, Crailsheim, Germany
D300e Digital Dispenser	Tecan, Crailsheim, Germany
MultidropTM Combi	Thermo Fisher Scientific, Schwerte, Germany
Maxwell RSC48	Promega, Walldorf, Germany
ABI 3130XL Genetic Analyzers	Applied Biosystems, Massachusetts, USA
NextSeq550	Illumina, San Diego, USA
TGradient Cycler (PCR Gradient Cycler)	Biometra, Göttingen, Germany
Western BLot Equipment	BioRad, Düsseldorf, Germany
GeneAMP PCR System2700	Applied Biosystems, Schwerte, Germany
Fluorescence 384 well plate	Thermo Fisher Scientific, #NUN384fb
Multifuge 3SR+	Heraeus, Hanau, Germany
Multifuge 4KR	Thermo Fisher Scientific, Schwerte, Germany
Vortex Genie 2	Neolab, Heidelberg, Germany
Mikro centrifuge	Neolab, Heidelberg, Germany #C1301B-230V
-20°C Freezer	Liebherr, Kirchdorf an der Iller, Germany
-80°C Freezer	Thermo Fisher Scientific, Schwerte, Germany
CFX384 Teal-Time PCR Detection System	Bio-Rad, Düsseldorf, Germany
Vi-Cell-XR	Beckman Coulter, Krefeld, Germany
Water Bath	GFL, Burgwedel, Germany
Axiovert 40C Microscope	Carl Zeiss, Oberkochen, Germany
MoFlo XDP High-Speed Cell Sorter	Beckman Coulter, Krefeld, Germany, #ML99030
Mr. Frosty^{TM} Freezing Container	Thermo Fisher Scientific, Schwerte, Germany

2.1.2 Chemicals:

Table 2: List of utilized chemicals with distributing company and catalog number.

Name	Company	Catalog number
2-Propanol	Carl Roth	#CN09.1
Laemmli Sample Buffer	Bio-Rad	#1610747
Bovine Serum Albumin (BSA)	Sigma-Aldrich	#9048-46-8
cOmplete EDTA-free Protease Inhibitor Cocktail	Roche	#11697498001
DMSO	Sigma-Aldrich	#D2438
Doxycycline	Sigma-Aldrich	#D5207
Methanol	Carl Roth	#8388.1
NaCl	Sigma-Aldrich	#7647-14-8
Natriumazid (NaN3)	Sigma-Aldrich	#S2002
N,N,N',N' - tetramethylethylene diamine (TEMED)	Amresco	#243C112
2-Mercaptoethanol	Gibco	#21985023
DMEM GlutaMax	Gibco	#31966-021
Fetal Bovine Serum (500 ml)	Sigma-Aldrich	#121031
RPMI Medium 1640 GlutaMax	Gibco	#61870-070
L-Glutamin	Sigma-Aldrich	#G3126
Penicillin Streptomycin	Gibco	#15140-122
RIPA Lysis Buffer	Thermo Fisher Scientific	#89901
Pierce BCA Protein Assay	Thermo Fisher Scientific	#23225
Ponceau S	Thermo Fisher Scientific	#A40000279
Puromycin	Sigma-Aldrich	#P8833
RetroNectin	TaKaRaBio	#T100
Tetracycline free FCS	TaKaRaBio	#T202
Ammonium Persulfate (APS)	Sigma-Aldrich	#A3678
Trypanblue	Thermo Fisher Scientific	#15250061
Tween20	Sigma-Aldrich	#P9416
DNA Ladder	New England BioLabs	#N3232S
Protein Ladder	Thermo Fisher Scientific	#AM992
Luciferase	Promega	#E1701
MethoCult™ H4230	STEMCELL Technologies	#04230
PhosStop^{Tm}	Roche	#4906837001
Luminol Peroxid	Cytiva Amersham	#RPN2236
Polyethylenimine (PEI)	Sigma-Aldrich	#764647
polybrene	Sigma-Aldrich	#TR-1003-G
Kolliphor RH40	Sigma-Aldrich	#07076
D-Glucose (Dextrose)	Sigma-Aldrich	#G7021
DTT	Thermo Fisher	#15508013
Acrylamide 30% 19:1	Sigma-Aldrich	#A3699
Bromphenol blue	Active Motif	#100602
CytoFLEX Sheath FLuid	Beckman Coulter	#B51503
Dulbecco's phosphate buffered saline (DPBS)	Gibco/Thermo	#14040117
Ethanol	Carl Roth	#5054.1
Glycerol	Sigma-Aldrich	#G5516
Hydrochloric Acid (HCl)	Carl Roth	#4625.1
Lenti-X Concentrator	TaKaRaBio	#631232
Pageruler^{TM} Prestained Protein Ladder	Thermo Scientific	#26616

PVDF blotting membrane (AmerhamTM HybondTM P 0.45)	GE Healthcare	#10600023
Sodium Dodecyl Sulfate (SDS)	Carl Roth	#0183.1
Trizma® Base	Sigma-Aldrich	#T1503
TrypLE™ Express Enzyme	Gibco	#12605010
XenoLight D-Luciferin - K+ Salt	PerkinElmer	#122799

2.1.3 Compounds:

Table 3: List of utilized compounds and experimental drugs.

Name	(putative) Class	Subclass	Origin (Company)	Catalog
Geldanamycin (GM)	N-terminal HSP90i	Natural	Sigma-Aldrich	# G3381
Tanespimycin (17-AAG)	N-terminal HSP90i	Geldanamycin based	Selleck Chemicals	#S1141
Zelavespib (PU-H71)	N-terminal HSP90i	Purin-based	Selleck Chemicals	# S8039
Ganetespib (STA-9090)	N-terminal HSP90i	Radiciol-based	Selleck Chemicals	#S1159
Luminespib (NVP-Auy922)	N-terminal HSP90i	Radiciol-based	Selleck Chemicals	#S1069
Novobiocin	C-terminal HSP90i	Aminocoumerin	Sigma-Aldrich	#N1628-1
Coumermycin A1 (CA1)	C-terminal HSP90i	Aminocoumerin	Sigma-Aldrich	#27715
5a	C-terminal HSP90i	experimental	AG Kurz	
5b	C-terminal HSP90i	experimental	AG Kurz	LSK82
5c	C-terminal HSP90i	experimental	AG Kurz	
5d	C-terminal HSP90i	experimental	AG Kurz	
6	C-terminal HSP90i	experimental	AG Kurz	
7a	C-terminal HSP90i	experimental	AG Kurz	
7b	C-terminal HSP90i	experimental	AG Kurz	
VWK147	C-terminal HSP90i	experimental	AG Kurz	

2.1.4 Buffers:

Table 4: List of utilized buffer and buffer compositions.

Buffer Name	Recipe
Lysis Buffer	RIPA Buffer + Complete + PhosStop
Washing Buffer	DPBS + Complete
10/18 DRD	10% DMSO 18% Cremaphor RH40 3.6% Dextrose 68.4% H20
1x SDS-PAGE Buffer	25 mM Tris 192 mM glycine 0.1% SDS
1x Transferbuffer	25 mM Tris 192 mM glycine 20% (v/v) methanol
TAE-Buffer	242 g Tris base 57.1 acetic acid 100 ml of 500 mM EDTA (pH 8.0)

	Ad 1 L dH2O
Blocking Buffer	5% (w/v) BSA in TBST
10% APS	5% (w/v) Ammonium Persulfate in dH2O
5x laemmli Loading Buffer	6 ml 20% SDS 7.5 ml 1.5 M Tris ph 6.8 18 mg bromphenol blue 4.8 ml 2-Mercaptoethanol 9 ml Gylcerol Adjust to 30 ml
10% SDS	20% (w/v) SDS in dH2O
TBS + Twenn (TBST)	14 mM NaCl 2 mM Tris 0.1% (w/v) Tween 20 pH 7.6

2.1.5 Commercial Kits and Consumables:

Table 5: List of utilized commercial kits and consumables.

Assay	Company	Catalog Number
HSP90 CTD TR-FRET Assay kit	BPS Bioscience	#50289
HSP90 NTD assay kit	BPS Bioscience	#50293
PierceTm BCA Protein Assay Kit	Thermo Fisher Scientific	#23225
Dual-Luciferase Reporter Assay	Promega	#E1910
QIAprep Spin Miniprep Kit	Qiagen	#27106
QIAquick PCR Purification Kit	Qiagen	#28104
Maxwell® RSC simplyRNA Cells Kit	Promega	#AS1390
Maxwell RSC Blood DNA kit	Promega	#AS1400
CytoSNP-12 v2.1 array	Illumina	# WG-320-2101
QuantiTect Reverse Transcription Kit	Qiagen	#205311
CellTiter-Glo® Luminescent Cell Viability Assay	Promega	#G7573
CellTiter-Glo® 2.0 Cell Viability Assay	Promega	#G9243
JESS 12-230 kDa seperation module 25x cartridges	BioTechne	SM-W004
JESS Protein Normalization Module	BioTechne	DM-PN02
JESS Anti-Rabbit detection Module	BioTechne	DM-001
Sure Select Human All Exon v7 kit	Agilent	#5191-4028
ECLTM Western Blotting Detection Reagents	GE Healthcare	#RPN2106
0.5 ml Insulin syringe U-100 0.30 x 12 mm	B. Braun Omnican 50	#9151168

384 well low Flange White Flat Bottom Polystyren TC-treated Microplate	Corning	#3570
Nunc MicroWell 96-Well, Nunclon Delta-Treated, Flat-Bottom Microplate	Thermo Scientific	#136101
D300e dispensehead cassettes T8 plus	Life Sciences Tecan HP	#30097370
D300e Dispensehead cassettes D4 Plus	Life Sciences Tecan HP	#30097371
Aspiration pipette (2 ml)	Sarsted Inc	#NC1425570
BD Microtainer Blood Collection Tubes	BD	#365965
Cell Culture flasks and plates	Greiner Bio-One	#690175
Centrifugation Tubes 15 ml	Greiner	#188271
Centrifugation Tubes 50 ml	Greiner	#210261
CLINITUBES capillary tubes 100 µL	Radiometer	#942-878-D957G-70
Safe-Lock Tubes 0.5 ml	Eppendorf	#0030121023
Safe-Lock Tubes 1.5 ml	Eppendorf	#0030120086
Safe-Lock Tubes 2 ml	Eppendorf	#0030120094
pluriStrainer Mini 20 µM	pluriSelect	#43-10020-40
serological pipette 5 ml	Greiner CELLSTAR	#P7865
serological pipette 10 ml	Greiner CELLSTAR	#CLS4488
serological pipette 25 ml	Greiner CELLSTAR	#CLS4487
TipOne Pipette tips	starlab	#S1111

2.1.6 Software:

Table 6: List of utilized software and distributing company.

Software	Company
Living Image Software	Perkin Elmer, Rodgau, Germany
GraphPadPrism 7.0	GraphPad by Dotmatics
Compass 2.0	Bio-Techne GmbH, Wiesbaden, Germany
D300e Control Titration Wizard	Tecan, Crailsheim, Germany
TecanSparkControl	Tecan, Crailsheim, Germany
Partek FLow	Partek, Chesterfield, USA
CytExper 2.4	Beckman Coulter, Krefeld, Germany
Living Image	PerkinElmer, Rodgau, Germany

2.1.7 Cell line and Patient Information:

Table 7: List of utilized cell lines and patient samples.

Name	Cancer type	Company Catalog	Cell line or Patient
K-562	CML, BCR ABL+	DSMZ (ACC10)	Cell line
SUP-B15	B cell precursor ALL	DSMZ (ACC389)	Cell line
HL-60	Acute myeloid leukemia	DSMZ(ACC3)	Cell line
MV-4-11	Acute monocytic leukemia	DSMZ(ACC102)	Cell line
KASUMI-1	Acute myeloid leukemia	DSMZ(ACC220)	Cell line

THP-1	Acute monocytic leukemia	DSMZ(ACC16)	Cell line
MOLT-4	T cell leukemia	DSMZ(ACC362)	Cell line
MOLM-13	Acute myeloid leukemia	DSMZ(ACC554)	Cell line
TALL-1	T cell leukemia	DSMZ(ACC521)	Cell line
HSB-2	T cell leukemia	DSMZ(ACC435)	Cell line
PEER	T cell leukemia	DSMZ(ACC6)	Cell line
SUP-T1	T cell lymphoma	DSMZ(ACC140)	Cell line
JURKAT	T cell leukemia	DSMZ(ACC282)	Cell line
KOPT-K1	T cell leukemia	CVCL_4965	Cell line
DND-41	T cell leukemia	DSMZ(ACC525)	Cell line
HPB-ALL	T-cell leukemia	DSMZ(ACC483)	Cell line
HEK293T	Kidney Cell	DSMZ	Cell line
Pat1	AML		PDX
Pat2	ALL		PDX
Pat3	B-ALL		PDX
Pat4	B-ALL		PDX
Pat5	B-ALL		PDX
Pat6	B-ALL		PDX
Pat7	B-ALL		PDX
Pat8	B-ALL		PDX
Pat9	AML		PDX
Pat10	B-ALL		PDX
Pat11	AML		PDX
Pat12	B-ALL		PDX
Pat13	B-ALL		PDX

2.1.8 Primer for Sanger Sequencing:

Primer	Sequence
HSP90AA1_HATPase_F	CCCCAATCACCTACAGACAGA
HSP90AA1_HATPase_R	CCAGACCCAAGACCAACCGATG
w-ABCB1-mut-F	AGTCCAAGAACTGGCTTTGCT
w-ABCB1-mut-R	GCAGGCTATAGGTTCCAGGC
w-TNFSF11-mut-F	GGTTGGGCCAAGATCTCCAA
w-TNFSF11-mut-R	TCCGGATCCAGTAAGGAGGG
w-TNFRSF9-mut-F	GTCCCCACTCTGTTAAGCCC
w-TNFRSF9-mut-R	TCAAACTTTGGCAAACCGGC
w-LRP5-mut-F	AGCTCTGATTCCCAGTTGGC
w-LRP5-mut-R	AGAGCCCCTACTCCTGTGAG
w-KNTC1-mut-F	GCGAGAGTTGATCACGTTGC
w-KNTC1-mut-R	CCCCCTTTGCTCAAGATGGT
w-PCDH15-Pr-F	ATACTCACCCCATCTGGCCT
w-PCDH15-Pr-R	AAGTAATTCACTATACTAAG
w-HIVEP1-PCr-F	TCACCACATCCTGACCCTCA
w-HIVEP1-PCr-R	GCAAGCCTGGGGTACTTAGG
w-NDNF-PCr-F	AGCAGTTCATGCAGTGGTCA
w-NDNF-PCr-R	TGCAGAAAGCAGTGACCACA

2.1.9 Antibodies:

Table 8: List of utilized antibodies, species, dilution, and catalog number.

Target	Species	Dilution (Western Blot)	Dilution (JESS)	Catalog Number
β-actin	Mouse	1:2000	1:50	#MAB8929
HSP90 total	Rabbit	1:2000	1:100	CST#4877
HSP90α	Rabbit	1:2000	1:100	CST#8165
HSP90β	Rabbit	1:1000	1:100	CST#5087
HSP70	Rabbit	1:1000	-	CST#4872
HSP27	Mouse	1:1000	-	CST#2402
HSP40	Rabbit	1:2000	-	CST#4871
HSF-1	Rabbit	1:1000	-	CST#4356
p-AKT (S473)	Rabbit	1:750	1:30	CST#4060
AKT (pan)	Mouse	1:1000	1:50	CST#2920
ADLH1A1	Rabbit	1:1000	-	CST#54135
GAPDH	Mouse	1:2000	-	CST#97166
GAPDH	Rabbit	1:2000	-	CST#5174
SRC	Rabbit	1:1000	-	CST#2109
p-SRC	Rabbit	1:1000	-	CST#2101
p-p90RSK(S380)	Rabbit	1:1000	-	CST#9335
p90 RSK (RSK1)	Rabbit	1:1000		CST#8408
MDR1/ABCB1	Rabbit	1:1000	-	CST#13342
pS6 (S240/244)	Rabbit	1:1000	-	CST#5364
p38 MAPK	Rabbit	1:1000	-	CST#9212
P44/42 MAPK	Rabbit	1:1000	-	CST#9102
p-p44/42 (T202/Y204)	Rabbit	1:2000	-	CST#4370
S6 Ribosomal Protein	Rabbit	1:1000	-	CST#2217
p-S6 Ribosomal Protein (S235/S236)	Rabbit	1:2000	-	CST#4858
p-S6 Ribosomal Protein (S240/S244)	Rabbit	1:1000	-	CST#5364
p-p70 S6 Kinase (T389)	Rabbit	1:1000	-	CST#9234
p70 S6 Kinase	Rabbit	1:1000	-	CST#2708
MAPK4	Mouse	1:1000		#MA5-26208
TLR4	Rabbit	1:1000		#48-2300

2.2 Methods:

Cell Harvest:

Approximately $5*10^6$ cells were counted by the Vi-Cell-XR (Beckman Coulter) and harvested in their linear growth phase if viability exceeds 90% by centrifugation (400 x g, RT) to generate a pellet. After discarding the supernatant, cell pellets were subsequently stored on ice. Next, the pellet was resuspended vigorously in 100-1000 µL ice-cold PBS supplemented with cOmplete™ (1:50) and PhosSTOP™ (1:10) and centrifuged (400 x g, 4°C) with subsequent removal of the supernatant. This washing step was repeated thrice to remove any residual FCS. After the last wash step, the cell pellet was snap-frozen in liquid nitrogen.

Cell Lysis:

After thawing the cell pellet on ice, it was dissolved vigorously in 50 µL (per $1*10^6$ cells) ice-cold RIPA lysis buffer supplemented with cOmplete™ (1:50) and PhosSTOP™ (1:10). Lysis was incubated for at least 60 min on ice with regular vortexing. Afterward, lysates were centrifuged (10000 x g, 4°C), and the supernatant was transferred into a new Eppendorf two times.

BCA-Assay:

For protein concentration measurement Pierce™ BCA Protein Assay Kit (Thermo Fisher-Scientific # 23225) was utilized per the manufacturers' instructions. In short, the working solution was prepared by mixing 50 parts of BCA reagent A with 1 part of BCA reagent B. 200 µL working solution was pipetted into a 96-well plate per well in triplicates. For the standard curve, 0, 1, 2, 3, 4, 5 µL BSA standard (2 mg/ml) was pipetted into prepared wells, whereas 2 µL per well lysate was added for samples incubated at 37°C for 30 mins. Absorbance was measured at 562 nm in a Tecan Spark 10M.

Cellular Thermal Shift Assay (CETSA):

One 80% confluent T175 (50 ml) of K562 cells was prepared for every condition, which equals roughly $1*10^6$ cells/ml. After treatment with indicated compounds or DMSO for 6h or 24h, cells were harvested by centrifugation (400 x g, RT) and subsequent five times washing steps with ice-cold PBS supplemented with cOmplete™ (400 x g, 4°C). After the last washing step, the pellet was dissolved thoroughly in ice-cold 1.3 ml PBS (+cOmplete™), and an equal volume of 100 µL of this concentrated cell suspension was aliquoted in 12 200 µL PCR tubes.

Thermal shift assay
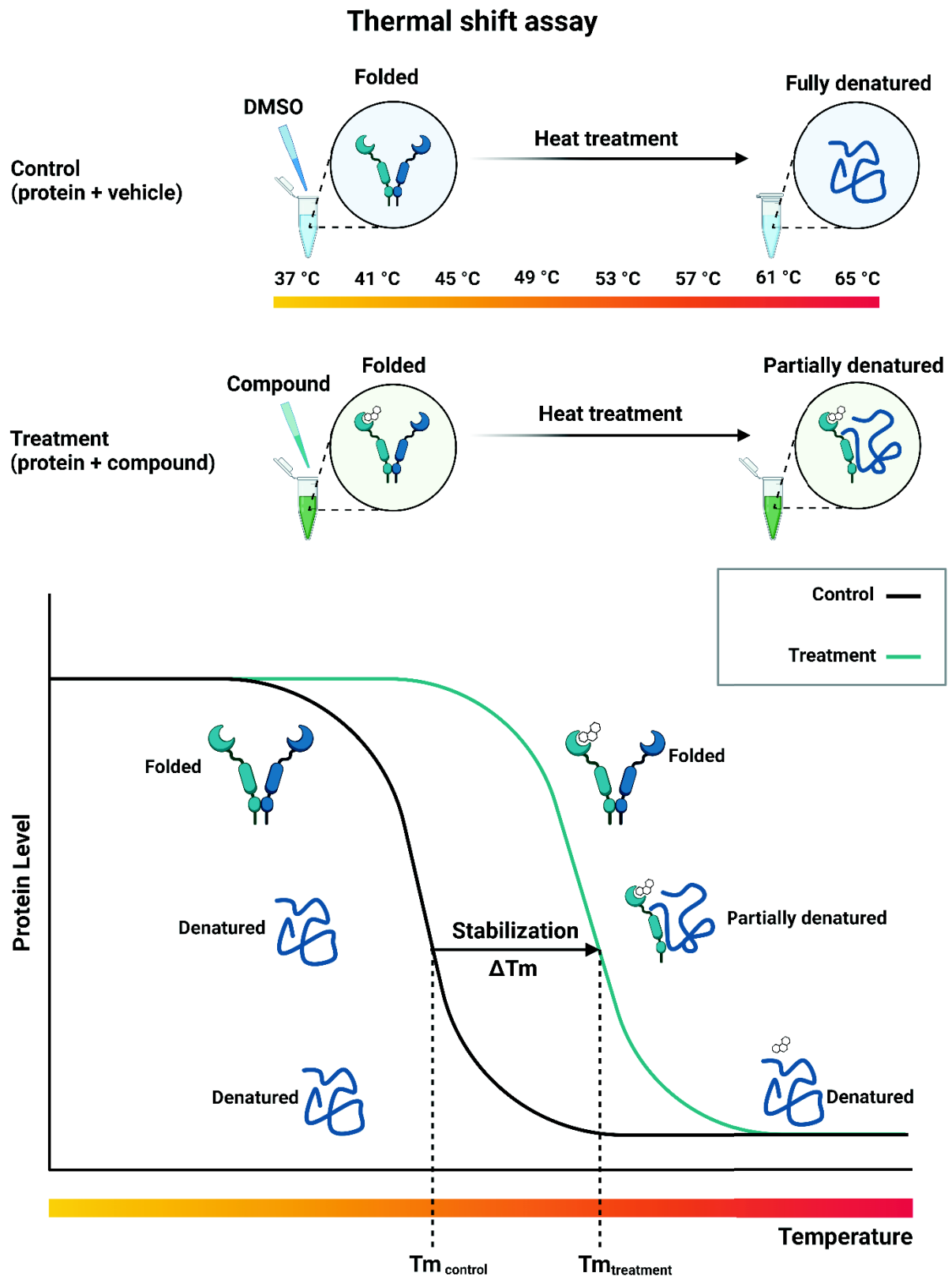
Figure 10: Principle of the Thermal Shift Assay. After cells were treated with indicated compounds, a temperature gradient was applied to the lysate. Successful binding of the compound to the target will stabilize it, reducing its susceptibility towards thermal stabilization. Afterwards (digital) Western Blot is performed to quantify amounts of denatured protein and a shift in the melting Temperature (ΔT_M) can be calculated. Figure created with BioRender and adapted from the Biorender thermal shift template.

Subsequently, the cell suspension was treated with a previously optimized temperature gradient (45-53°C) in the $T_{gradient}$ thermal cycler (BIOMETRA) for 3 min and 30 sec sharp. The treatment was stopped immediately by snap-freezing the sample in liquid nitrogen. Lysis was performed by three freeze-thawing cycles in liquid nitrogen and at 25°C in the GeneAMP PCR System2700 (BIOMETRA). Lysates were transferred into new precooled 1.5 ml reaction tubes, centrifuged two times at 10000 x g at 4°C for 20 mins, and the supernatant was transferred into a 0.5 ml reaction tube. As a quality control, a follow-up BCA assay was performed to confirm the temperature-dependent decrease of detectable protein concentration.

The mean value of the two lowest temperatures was used to estimate the appropriate protein range (20 μg/well) for subsequent western blot or quantitative simple western immunoassay (JESS, BioTechne).

Data analysis was performed utilizing GraphPadPrism 8.0.2 software. In short, the AUC (area under the curve) values of the electropherograms generated by quantitative simple western immunoassay were normalized to the lowest temperature (0% degradation). Then, non-linear regression (sigmoid dose-response curve) was applied to generate T_M values for controls and conditions. The T_M values describe the calculated temperature at which 50% of the protein is degraded. Finally, subtracting T_M values of the treatment conditions from the experimental controls quantifies differences in melting temperature (ΔT_M values).

Isothermal Dose Gradient Thermal Shift Assay (IDTA):

For performing the isothermal dose gradient thermal shift CETSA, one 80% confluent 10 cm dish (10 ml) of K562 cells was prepared with roughly $1*10^6$ cells/ml for every compound concentration and the DMSO control. The cells were treated with the indicated compound concentration gradient for 6h or 24h, then centrifuged (400 x g, RT) and washed five times (400 x g, 4°C) in ice-cold PBS (+cOmplete™). The pellet was dissolved in 100 μL ice-cold PBS (+cOmplete™), transferred into a precooled 200 μL PCR tube, incubated at the previously optimized temperature for 3 min 30 sec sharp in the $T_{gradient}$ thermal cycler (BIOMETRA), and the reaction was stopped immediately by snap-freezing the sample in liquid nitrogen. Optimizing the temperature was crucial and should be based on the degradation of the DMSO control in previous CETSA assays. Suppose a stabilizing effect of the compound was expected. In that case, the optimal temperature completely degrades the protein in the DMSO control and vice-versa. Lysis and subsequent analysis are identical to the CETSA protocol.

Western Blot:

Acrylamide gels were prepared as per available standard protocols. In short, 30% acrylamide, 1.5 M TRIS-HCL (pH = 8.8), 10% SDS, H_2O, and 10% APS were mixed. Finally, TEMED was added, and the resolving gel was mixed vigorously and pipetted into prepared gel chambers (BioRad). Next, 300 µL 2-Propanol was added to ensure a smooth edge between both gel parts. After 45 min of polymerization, 2-Propanol was removed with filter paper, the prepared stacking gel was poured on top, and a well-comb was inserted. Prepared gels were stored at 4°C for up to two weeks.

Lysates were supplemented with 5x Laemmli buffer and denatured for 5 min at 95°C in a thermal cycler (BioRad). Subsequently, SDS-PAGE was performed with 10-40 µg protein per lane in a Bio-Rad Chamber filled with 1x SDS-PAGE sample buffer starting with constant 50V during stacking phase and increased to 100V during separation volt for 1.5h-2.5h (depending on gel percentage and desired targets). The PageRuler™ Prestained Protein Ladder (#26616, Thermo Fisher Scientific) was used for size determination.

After SDS-PAGE, the gel and membrane were equilibrated for 15 min in cold 1x transfer buffer, and the blotting chamber was assembled. Depending on the desired targets, the transfer was performed for 16h overnight at 30 V without additional cooling or 100 V for 60 min with cooling. Membranes were washed shortly in TBS and stained with Ponceau S (#A40000279, Thermo Fisher Scientific) to confirm the successful transfer. After the Ponceau S staining membranes were washed 3 times in TBS-T to remove residual Ponceau S and blocked for 1h at RT with 5% BSA in TBS-T. Subsequently, membranes were washed three times in TBS-T, incubated with primary antibody for 2h at RT or overnight at 4°C, and then washed three times with TBS-T to be probed with secondary antibody diluted 1:1000 in TBS-T for 1h. After three wash steps in TBS-T, one additional wash in TBS was performed to remove residual tween. Membranes were then detected by luminol peroxide solution and visualized using the JESS system.

Capillary based automated Western Blotting (JESS):

Digital western blotting was performed per the manufacturer's instructions (JESS, Protein Simple, BioTechne). In short, after preparing DTT, 5x fluorescent master mix, and biotinylated ladder, samples were adjusted to their optimized final protein concentration with 0.1x sample buffer in 200 µL PCR tubes and supplemented with 1:5 fluorescent master mix. Afterward, samples were denatured at 95°C for 5 mins sharp

in a PCR Cycler (GeneAMP PCR System2700, Applied Biosystems), and 3 µL per well was applied to the JESS plate. Primary antibody dilutions and multiplex conditions can be found in the antibody appendix. The plate was filled per the manufacturer's instructions and centrifuged at 1000 x g at RT for 5 min. A 12-230 kDA separation module with 25 cartridges (SM-W0004, BioTechne) or protein normalization kit (AM-PN01) was utilized for the JESS run. Separation was performed for 25 min at 375 volts, blocking for 5 min with antibody diluent 2, primary antibody incubation for 30 min, and secondary antibody incubation for 30 min. Generally, the only condition adjusted was primary antibody incubation for up to 90 min with phospho-proteins. Signal detection was performed with an anti-rabbit detection module (DM-001, BioTechne), whereas an anti-mouse secondary NIR antibody (#043-821, BioTechne) was utilized for multiplexing.

HSP90 C-terminal domain Time-resolved fluorescence resonance energy transfer (TR-FRET) assay:

To evaluate the C-terminal binding affinity of compounds, a C-terminal specific time-resolved fluorescence energy transfer (TR-FRET) assay was conducted utilizing the HSP90 CTD TR-FRET assay kit (#50289, BPS Bioscience). In this, whether a compound binds, the C-terminus is measured by the compound's capability to disrupt the interaction of truncated HSP90 (C-terminal domain) with the C-terminal specific co-chaperone[179] cyclophilin D/PPID (**Figure 11**).

First, HSP90 Assay buffer was prepared by diluting 3x HSP90 Assay buffer 3-fold with molecular grade water (#AM992, Thermo Fisher Scientific). The donor-acceptor pair (Terbium-labeled donor, dye-labeled acceptor) was diluted 100x fold in 1x HSP90 assay buffer each and then pipetted 10 µL of each to every well. Next, HSP90α (C-terminus) and PPID were thawed slowly on ice and diluted in 1x HSP90 assay buffer to 2 ng/µL and 3 ng/µL, respectively. To bind their corresponding dyes, HSP90α was biotin-labeled, whereas PPID was GST-tagged. For the assay, each well contained 10 µL tb-labeled donor, 10 µL dye-labeled acceptor, 4 µL inhibitor, 10 µL PPID (3 ng/µL = 30 ng/reaction), 6 µL HSP90α (2 ng/µL = 12 ng/reaction). The positive control should measure minimal disruption and maximum FRET signal since the donor-acceptor pair connects in proximity without interference and thus contains 4 µL DMSO instead of inhibitor. The negative control includes no PPID and thus measures maximal disruption and minimum FRET signal since the donor-acceptor pair cannot connect in proximity. To ensure proper dye connectivity and inhibitor effect, the assay was incubated 2 hours

at RT protected from light and subsequently measured with a microplate reader (SPARK10M, Tecan). For the fluorescence measurement, two consecutive measurements were performed:

1) 340 nm / 620 nm (excitation/emission) wavelength, lag time = 60 µs, integration time = 500 µs.

2) 340 nm / 665 nm (excitation/emission) wavelength, lag time = 60 µs, integration time = 500 µs.

The TR-FRET ratio (665 nm emission / 620 nm emission) was utilized to calculate binding affinity after normalization to % activity by setting the negative control as zero percent activity and the positive control as one hundred percent activity [($FRET_{sample} - FRET_{neg}$)/($FRET_{pos} - FRET_{neg}$) * 100%].
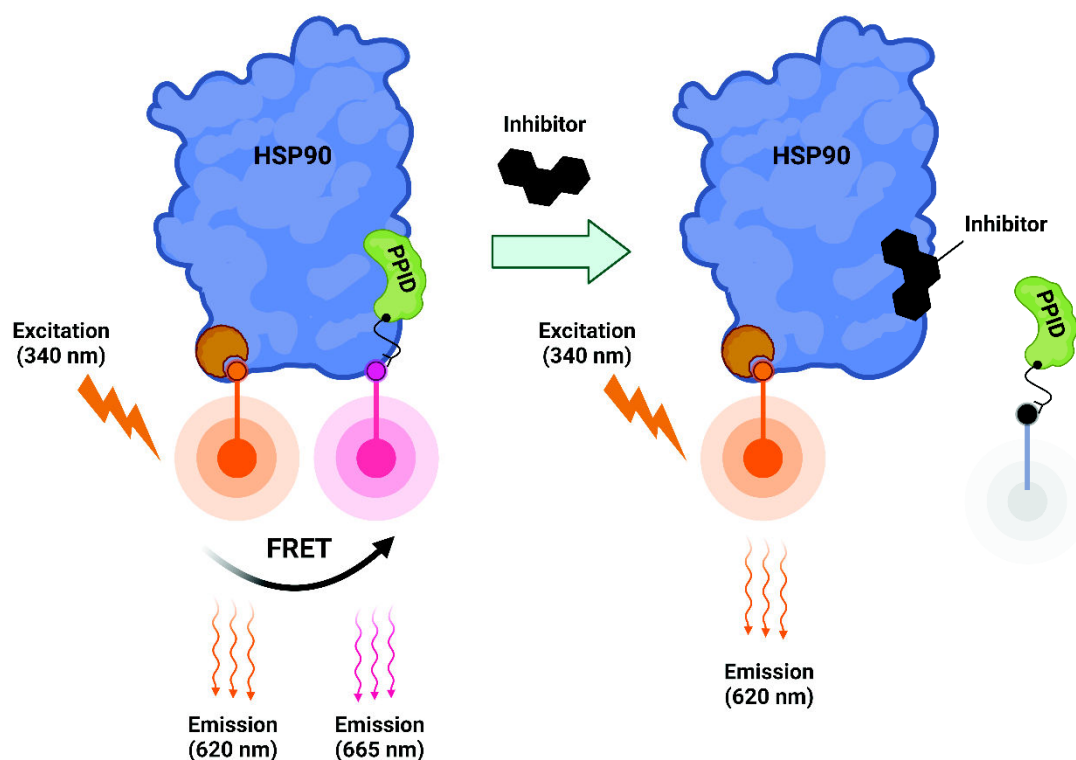
Figure 11: Principle of the HSP90 CTD-FRET assay. HSP90 and a C-terminal domain specific chaperone (PPID) are labeled with a FRET donor/acceptor pair. If donor and acceptor are in proximity, there will be energy transfer from donor to acceptor detectable by a shift in emitted fluorescence. Drugs that disrupt the interaction of HSP90 and PPID will prevent the energy transfer. Image created utilizing Biorender Software.

Fluorescence polarization (FP) measurements:

The binding affinity of compounds was evaluated utilizing the HSP90 NTD assay kit (#50293, BPS Bioscience). This competitive binding assay measures the ability of compounds to displace FITC-labeled geldanamycin (FITC-GM) from the ATP binding pocket (**Figure 12**).
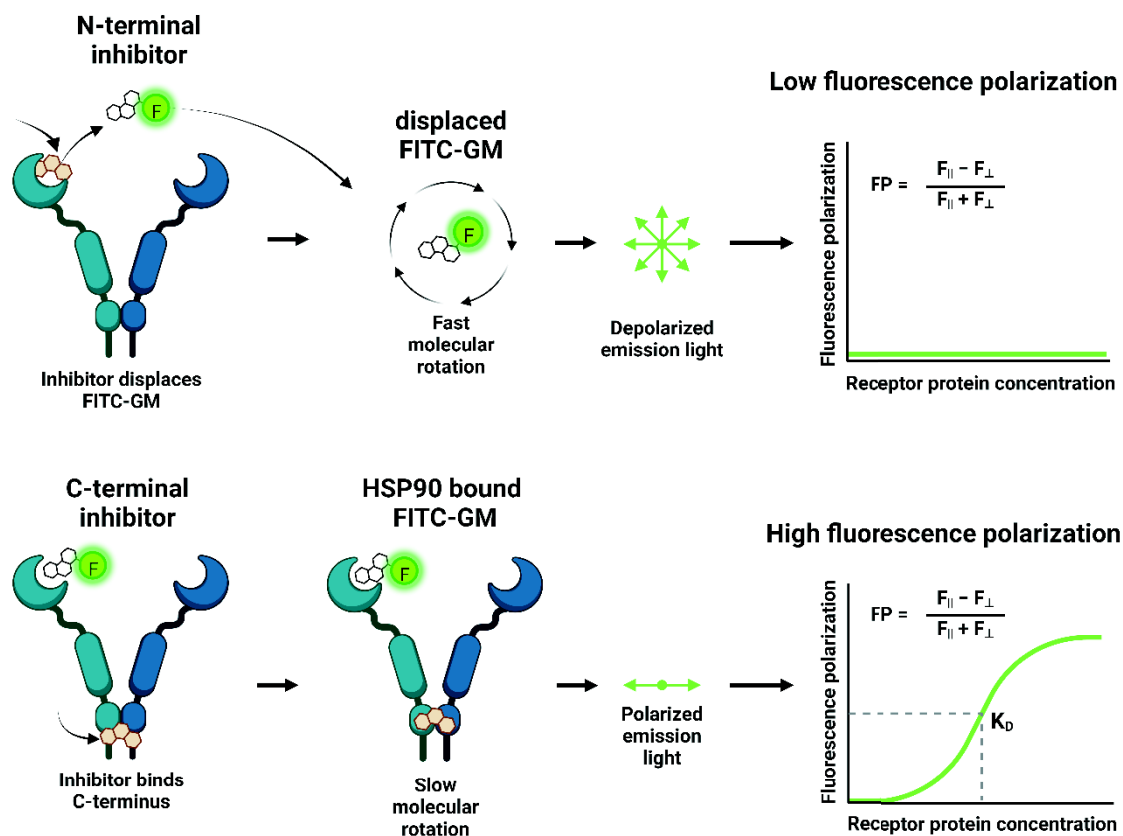
Figure 12: N-terminal Fluorescence polarization Assay. (a) principle of fluorescence polarization assay. (b) Schematic depiction of fluorescence polarization with a N-terminal and C-terminal HSP90 inhibitor. Created with BioRender and adapted from the BioRender fluorescence polarization template

After FITC-GM and HSP90α were thawed on ice, 100 nM FITC-GM was prepared by diluting the 2.5 µM stock solution 25-fold with 1x HSP90 assay buffer, and HSP90α was diluted to 17 ng/µL in 1x HSP90 assay buffer. For the assay, 65 µL of master mix containing 15 µl 5x HSP90 assay buffer 1 + 5 µL 40 mM DTT + 5 µL 2 mg/ml BSA + 40 µL H_2O was pipetted into every well of a black, low binding, microtiter plate (#79685, BPS Bioscience). To calibrate the background in the fluorescence polarization measurement, blank wells, which do not contain FITC-GM, were prepared by adding 10 µL of the inhibitor solvent (DMSO) and 25 µL 1x HSP90 assay buffer to the master mix to round up to 100 µL total volume per well.

The enzyme-positive control wells include 5 µL FITC-GM, 10 µL DMSO, and 340 ng HSP90α (20 µL) and account for 100% bound FITC-GM since there is no inhibitor to disturb the interaction between GM and HSP90α. This results in polarized light emission due to a slower molecular rotation than free-spinning FITC-GM, which affects the ratio of parallel and perpendicular light detected and subsequently leads to a high fluorescence polarization readout (**Figure 12**). Next, enzyme-negative control wells included 5 µL FITC-GM, 10 µL DMSO, and 20 µL 1x HSP90 assay buffer and account for 0% bound FITC-GM since there is no HSP90α in the solution to bind. Considering all FITC-GM molecules are freely spinning in solution and are not kept in place by the HSP90α protein, the emitted light is mainly depolarized due to fast molecular rotation resulting in a low fluorescence polarization readout (**Figure 12**). Finally, inhibitor test wells were prepared by adding 5 µL FITC-GM, 10 µL inhibitor dissolved in DMSO, and 340 ng HSP90α (20 µL). Note that HSP90α was pipetted into all well simultaneously to initiate the reaction. The prepared assay plate was incubated at room temperature and protected from light for 3h with gentle agitation.

Fluorescence polarization was measured in a microtiter-plate reader (Infinite M1000pro, Tecan) kindly provided by the working group of *Prof. Holger Stark* (*Pharmaceutical and Medicinal Chemistry, HHU*) at 470 nm excitation wavelength and 525 nm emission wavelength. The instrument-specific g-factor of 1.187 was used to calculate the polarization $(I_{\parallel} - G(I_{\perp})/ (I_{\parallel} + G(I_{\perp}))*1000$, whereas the percentage of HSP90-bound FITC-GM was calculated using $P_{norm} = (P_{Inhibitor}-P_{neg}) / (P_{pos} - P_{neg})*100$. If inhibitors have a higher binding affinity than FITC-GM to the HSP90α ATP binding pocket, they can displace FITC-GM in the binding pocket, resulting in a higher percentage of unbound FITC-GM. Unbound FITC-GM has a faster molecular rotation and emits depolarized light, thus reducing the fluorescence polarization.

Drug Screening:

Drug screening plates (384w, 96w) were prepared by micro-robotics (Tecan D300e). Compounds were diluted to 10 mM stock in DMSO and pipetted onto T8 cassette slots (#30097370, Tecan). After prior concentration range optimization, compounds were printed onto the plate in a logarithmic concentration range ranging from 5 nM up to 25 µM in triplicates in a randomized fashion. Afterward, all wells were normalized to the highest DMSO volume utilizing D4 cassettes (#30097371, Tecan). Plates were then sealed with parafilm, vacuumed, and stored at -20°C for further usage.

Approximately 60 mins before seeding, prepared plates were slowly thawed at RT protected from light. Cells were seeded at their previously optimized cell density (K562 = 40000 cells/ml, patient cells = 500000 cells/ml) in 30 µL/well in white 384-well plates, shaken for one minute, and incubated for 72h at 37°C, 5% CO2. The CellTiter-Glo® assay was utilized per the manufacturer's instructions with minor adjustments to detect viability. In short, CellTiter-Glo® reagent was dissolved in CellTiter-Glo® buffer and aliquoted into 10 ml aliquots. For the assay, a 10 ml aliquot was slowly thawed on 4°C and mixed with 40 ml PBS. This working solution was added 1:1 in volume to the cell suspension with a fluid dispenser (Multidrop). Plates were shaken for 2 min and incubated for 10 min protected from light. The colorimetric signal was measured using the Tecan Spark plate reader.

The evaluation was done in GraphPadPrism Software 7. After the de-randomization of data, they were normalized to the DMSO control set to 100%, and concentrations were logarithmically converted. Data were then plotted with non-linear regression utilizing the log (inhibitor) vs. normalized response (variable slope) function to determine IC_{50} values.

Resistance acquirement through clonal evolution:

To develop cell lines resistant to specific HSP90 inhibitors, K562 cells were seeded into a T125 flask. Cells were treated for 24h with a sublethal inhibitor concentration (3-day IC_{50}), centrifuged at 90 x g for 5 min at RT, and then recovered in a T25 flask until viability recovered beyond 50%. Then $1x10^6$ cells were seeded in every well of a six-well plate. One well was left untreated as backup, well two was treated with IC_{50}, well three IC_{50}+10%, well four IC_{50}+20%, well five IC_{50}+30%, and well six IC_{50}+40%. Recovery and treatment were repeated in cycles, with a periodic harvest of cell pellets to study the development and regular IC_{50} determination for the corresponding inhibitors.

Conditional knockdown (shRNA):

First, HEK293T cells were plated onto 10 cm dishes and incubated for 12-16h with a lentiviral backbone (125 = 18 µg/plate, 126 = 7 µg/plate, 127 = 4 µg/plate) and plasmid fragments of interest (V2, V3, N17, N18, N19 = 18 µg/plate, **Table 9**) in serum-free media with 1 µL Polyethylenimine(PEI)/plate. After incubation medium was changed, and cells were grown for 60h to generate the virus. The supernatant was isolated, filtered with a 0.45 µm filter, and centrifuged in an ultra-centrifuge (2h, 11000 rpm). The virus was then plated onto retronectin (#T202, TaKaRa) coated plates for 6h at 37°C.

After washing off the residual virus with PBS+5%BSA, $1x10^6$ K562 cells were added onto virus plates in a complete growth medium containing 8 µg/ml polybrene (#TR-1003-G, Sigma-Aldrich), centrifuged onto the plates (50 x g, 2 mins) and incubated overnight. Cells were harvested the next day, thoroughly washed to remove the residual virus, and plated with fresh medium on 12-well TC plates. After 24h recovery, puromycin selection (0.5 µg/ml) was started, and cells were monitored. After antibiotic selection, cells were recovered and incubated with 2 µg/ml doxycycline for 72h. GFP or RFP expression was quantified via FACS, and GFP (V2, V3) and RFP (N17, N18, N19, n.t.) positive cells were sorted by FACS (MoFlo XDP, Beckman-Coulter), recovered and frozen away. If not stated otherwise, for experiments, cells were induced with 2 µg/ml doxycycline for 72h and labeled as (+), whereas uninduced cells treated with the same volume of H_2O for 72h were labeled as (-).

Table 9: List of utilized shRNA constructs for the conditional knockdown.

Target	Cat.No. (Dharmacon)	Mature antisense sequence (5' – 3')
V2 (HSP90α)	RHS4696-200706063	TTAATATGCAGCTCTTTCC
V3 (HSP90α)	RHS4696-200765858	TAATATGCAGCTCTTTCCC
N17 (HSP90β)	V3SH11252-224926587	GAATGCTTCTTCACTACTT
N18 (HSP90β)	V3SH11252-227425710	CACTAATTTCCTTCTCTCG
N19 (HSP90β)	V3SH11252-230219424	CTAATCGACTTCTTCCATG

SNP-Array:

The copy number analysis was performed on the DNA of 12 cell lines, including the parental K562 cell line and the different drug-resistant K562 using the Illumina CytoSNP-12 v2.1 array encompassing 299,140 SNP markers according to the manufacturer´s suggestion. Beeline 2.0.3.3 software was used to convert idat to gct files. Data were processed and analyzed using the BlueFuse Multi 4.5 software from Illumina. Partek Flow was used to identify chromosomal imbalances in resistance-acquired K562 cells compared to the parental K562 cell line. The human reference genome was GRCh38/hg38. Dr. Layal Yasin and Dr. Rabea Wagener performed the analysis.

Whole exome sequencing (WES):

Whole-exome sequencing was performed on the parental K562 cell line and the PU-H71-resistant and Coumermycin A1-resistant K562 cells. Next-generation WES was performed using the Sure Select Human All Exon V7 kit (Agilent). The library was paired-end sequenced on an Illumina NextSeq550 (2x150bp) sequencer to yield an

average on-target coverage of 100x. Dr. Layal Yasin and Dr. Rabea Wagener performed a biostatistical analysis.

Quantitative Real-Time Polymerase Chain Reaction (qRT PCR):

RNA extraction was performed with the Maxwell RSC viral total nucleic acid purification kit (Promega, Madison, WI, USA) with the Maxwell RSC 48, following the manufacturer's instructions. 2 µg of total RNA was used for cDNA synthesis with random hexamers. Real-time PCR was carried out using primers targeting genes of interest (**Table 10**). Reactions were carried out in triplicates in three independent experiments. The geometric mean of the housekeeping gene B2M and GAPDH was used as an internal control to normalize the variability in expression levels.

Table 10: List of utilized primers for qRT PCR.

Target	Forward Primer Sequence	Reverse Primer Sequence
HSP90AA1	TCTGCCTCTGGTGATGAGATGG	CGTTCCACAAAGGCTGAGTTAGC
HSP90AA2	CAAGTCTGGGACCAAAGCGTTC	CTTTCTCAGCAACCAAATAAGCAG
HSP90AA1 X1	GTCTAGTTGACCGTTCCGCA	TAACAGGTGCCCTGCTTCTC
HSP90AB1	CTCTGTCAGAGTATGTTTCTCGC	GTTTCCGCACTCGCTCCACAAA
TRAP1	CTCTGTGGAGACGGACATAGTC	CTCCTTCTCTGATAGGCACTCG
HSP90B1 (94)	GGAGAGTCGTGAAGCAGTTGAG	CCACCAAAGCACACGGAGATTC
HSPA1B (70)	ACCTTCGACGTGTCCATCCTGA	TCCTCCACGAAGTGGTTCACCA
HSPB1 (27)	CTGACGGTCAAGACCAAGGATG	GTGTATTTCCGCGTGAAGCACC
DNAJB1 (40)	AGTTCAAGGAGATCGCTGAGGC	GCTGAAAGAGGTACCATTGGCAC

Sanger Sequencing:

Cells were harvested by centrifugation at 400 x g for 5 min and washed three times with PBS, then snap-frozen in liquid nitrogen. DNA was isolated utilizing the Maxwell® RSC Blood DNA Kit (Promega, #AS1400) and quantified via Nanodrop (Thermo Fisher Scientific) analysis. Primer pairs were generated, and PCR conditions were optimized on a DNA-Pool. After PCR was performed, samples were loaded onto agarose gel electrophoresis to validate the specificity of the product calculated by In-Silico PCR (UCSC Genome Browser). Subsequently, DNA was purified utilizing QIAquick PCR purification kit (Qiagen, #28104) as per the manufacturer's instructions, and samples were sent to the BMFZ (Biomedizinisches Forschungs Zentrum).

In vivo Formulation and solubility:

10/18 DRD (10% Dimethyl Sulfoxide, 18% Kolliphor RH40, 3.6% dextrose, 68.4% water) was adapted from *Shimamura* et al. [180] with several modifications in the

preparation process. The compound was dissolved in DMSO starting at 1 M at 60°C in a water bath. Additional DMSO was added slowly until the compound was fully dissolved at 60°C with ultra-sonification treatment. Stability in DMSO was monitored for up to three days on RT to ensure a stable solution and was documented as maximum stable DMSO solubility. The freshly prepared compound stock solution was then mixed in a ratio of 10% compound stock solution (DMSO), 18% Kolliphor RH40 and 72% H_2O supplemented with dextrose. To prepare Kolliphor RH40, it was melted down in a 50 ml Falcon in a 37°C water bath and aliquoted into 2 ml Eppendorf reaction tubes. Melted aliquots of Kolliphor RH40 were heated to 60°C to decrease viscosity and were pipetted dropwise with a cutoff tip into the prepared DMSO-based compound stock solution. The solution was thoroughly mixed to ensure a one-phase solution. Dextrose-water mix was also aliquoted and stored at 4°C to prevent potential contamination. To prepare the ready-to-use solution, preheated dextrose-water mix (60°C) was added and mixed vigorously without bubbles. It was ensured that the resulting solution was clear, one-phased, and had no apparent threads. The stability of this injection solution was monitored for at least seven days on RT before doing experiments with mice or zebrafish. Immediately before injection, the solution was heated to 37°C to not cause irritation in the mice and to ensure proper viscosity. Compounds utilized in this thesis were mainly limited by DMSO solubility.

Mouse Xenograft Experiments:

Luciferase-GFP[97] expressing MV-4-11 (1 X 10^6 cells) cells were transplanted via intravenous (i.v.) tail injection in NSG or NOD scid gamma (NOD.Cg-Prkdcscid Il2rgtm1Wjl/SzJ) mice (#005557; The Jackson Laboratory, Bar Harbor, ME). Tumor burden was monitored with the Caliper IVIS Lumina II Multispectral Imaging System after i.p. injection of D-Luciferin firefly sodium salt monohydrate as per manufacturer's instructions (Biosynth, Staad, Switzerland). Calculation were performed using the Living Image Software (Perkin Elmer, Rodgau, Germany). Kaplan-Meier curves were plotted to estimate the survival of the animals among different groups (n = 5 mice per group). Animal experiments were conducted in accordance with the German Animal Welfare Act under the authorization at the Animal Research Institute (ZETT), Heinrich-Heine-University Düsseldorf Aktenzeichen 81-02.04.2017.A441.

3 Results

List of publications that arise from the work of this thesis is seen below:

Co-targeting HSP90 alpha and CDK7 overcomes resistance against HSP90 inhibitors in BCR-ABL1+ leukemia cells.[181]

Vogt, Melina*; **Dienstbier, Niklas***; Schliehe-Diecks, Julian; Scharov, Katerina; Tu, Jia-Wey; Gebing, Philip; Hogenkamp, Julian; Bilen, Berna-Selin; Furlan, Silke; Picard, Daniel; Remke, Marc; Yasin, Layal; Bickel, David; Kalia, Munishikha; Iacoangeli, Alfredo; Lenz, Thomas; Stühler, Kai; Pandyra, Aleksandra; Hauer, Julia; Fischer, Ute; Wagener, Rabea; Borkhardt, Arndt; Bhatia, Sanil (2023):
In *Cell death & disease* 14 (12), p. 799. DOI: 10.1038/s41419-023-06337-3.

Development of a First-in-Class Small-Molecule Inhibitor of the C-Terminal HSP90 Dimerization.[182]

Bhatia, Sanil; Spanier, Lukas; Bickel, David; **Dienstbier, Niklas**; Woloschin, Vitalij; Vogt, Melina; Pols, Henrik; Lungerich, Beate; Reiners, Jens; Aghaallaei, Narges; Diedrich, Daniela; Frieg, Benedikt; Schliehe-Diecks, Julian; Bopp, Bertan; Lang, Franziska; Gopalswamy, Mohanraj; Loschwitz, Jennifer; Bajohgli, Baubak; Skokowa, Julia; Borkhardt, Arndt; Hauer, Julia; Hansen, Finn K.; Smits, Sander H. J.; Jose, Joachim; Gohlke, Holger; Kurz, Thomas (2022):
In *ACS central science* 8 (5), pp. 636–655. DOI: 10.1021/acscentsci.2c00013.

Solid-Phase Synthesis of Cereblon-Recruiting Selective Histone Deacetylase 6 Degraders (HDAC6 PROTACs) with Antileukemic Activity.[183]

Sinatra, Laura; Yang, Jing; Schliehe-Diecks, Julian; **Dienstbier, Niklas**; Vogt, Melina; Gebing, Philip; Bachmann, Luisa M.; Sönnichsen, Melf; Lenz, Thomas; Stühler, Kai; Schöler, Andrea; Borkhardt, Arndt; Bhatia, Sanil; Hansen, Finn K. (2022):
In *J. Med. Chem.* 65 (24), pp. 16860–16878. DOI: 10.1021/acs.jmedchem.2c01659.

Development of the first Geldanamycin-Based HSP90 Degraders[184]

Wurnig, Silas L.*; Vogt, Melina*; Hogenkamp, Julian; **Dienstbier, Niklas**; Borkhardt, Arndt; Bhatia, Sanil*; Hansen, Finn K.* (2023):
In *Frontiers in Chemistry*. DOI: 10.3389/fchem.2023.1219883

Small-molecule inhibitor of C-terminal HSP90 dimerization modulates autophagy and functions synergistically with mTOR inhibition to kill bladder cancer cells[185]

Sun, Yadong; Woloschin, Vitalij; Vogt, Melina; **Dienstbier, Niklas**; David, Céline; Schlütermann, David; Berning, Lena; Opitz, Heinz; Friedrich, Annabelle; Akgün, Seda; Mendiburo, María José; Borkhardt, Arndt; Wesselborg, Sebastian; Bhatia, Sanil*; Kurz, Thomas*; Stork, Björn* (2023):
Manuscript in preparation
* contributed equally to this work

3.1 Role of HSP90α and β isoforms in eliciting Heat Shock response

Considering the importance of HSP90 in BCR-ABL1 positive leukemia,[98,100] the role of HSP90α and β isoforms was investigated to decipher the underlying regulatory mechanisms to recapitulate HSP90 inhibition genetically.

First, BCR-ABL1 positive K562 cells were transduced with inducible shRNA targeting HSP90α and β transcripts to examine short-term feedback loops triggered by reduced HSP90 levels. Secondly, *Melina Vogt* (Ph.D. student in our working group) generated CRISPR-Cas9-based constitutive knockouts of HSP90α and β to study long-term adaptations to lost HSP90 signaling. Both models gave complementary insight into the regulation of the cytosolic HSP90 isoforms.

The successful knockdown of the shRNA model was validated on mRNA level utilizing quantitative PCR (**Figure 13**). Cells expressing shRNA against HSP90AA1 (V2+, V3+) demonstrated a significant loss of HSP90AA1 mRNA levels after doxycycline induction compared to K562 (K562+) and non-targeting control (n.t.+) treated with doxycycline or non-induced V2- and V3- (**Figure 13, upper panel, blue**).
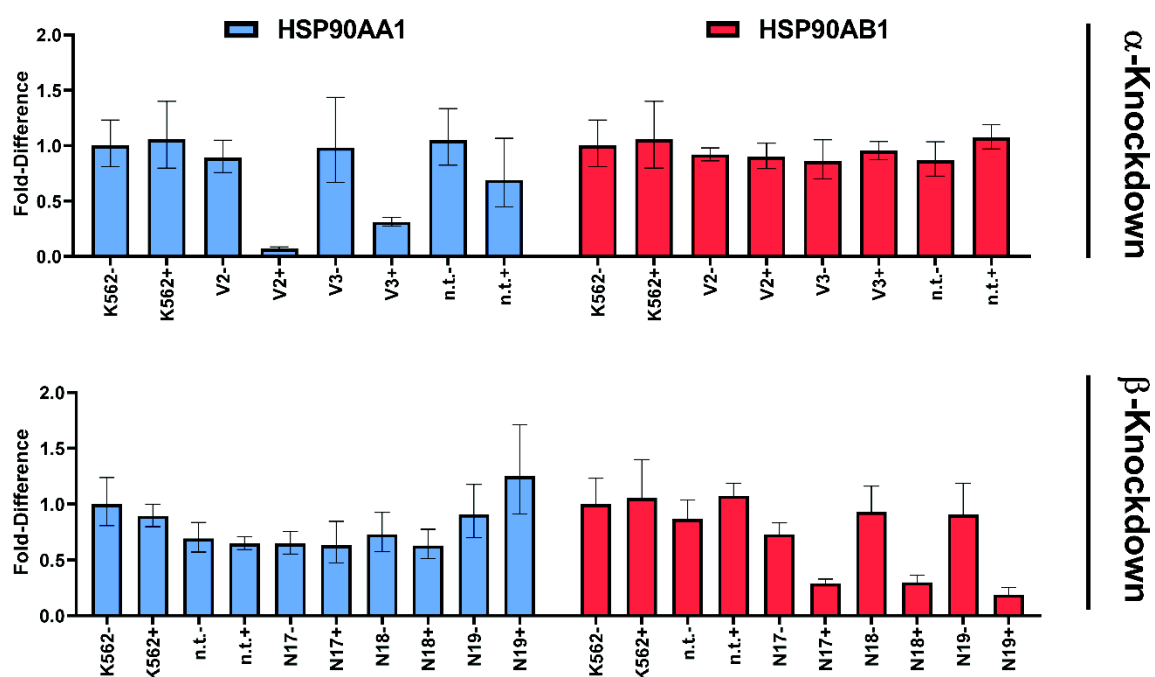
Figure 13: mRNA expression of HSP90AA1 (HSP90α) and HSP90AB1 (HSP90β) knockdown. Indicated cell lines are either treated with doxycycline 2 µg/ml (+) or same volume H2O (-) for 24h. Cells were harvested and RNA was isolated for qPCR analysis with primers against the HSP90AA1 and HSP90AB1 construct. Depicted are mean values and standard deviation of technical triplicates of one representative experiment. N.t. (non-targeting control). Figure adapted from *Vogt & Dienstbier* et al.[181]

However, the HSP90AA1 knockdown (V2+, V3+) did not affect the expression of the HSP90AB1 construct (**Figure 13, upper panel, red**). On the contrary, cells expressing shRNA against HSP90AB1 (N17+, N18+, N19+) demonstrated a significant loss of HSP90AB1 mRNA levels after doxycycline induction compared to K562 (K562+) and non-targeting control (n.t.+) treated with doxycycline or non-induced N17-, N18-, N19- (**Figure 13, lower panel, red**). Vice versa, HSP90AB1 knockdown (N17+, N18+, N19+) did not affect the expression of the HSP90AA1 mRNA (**Figure 13, lower panel, blue**).
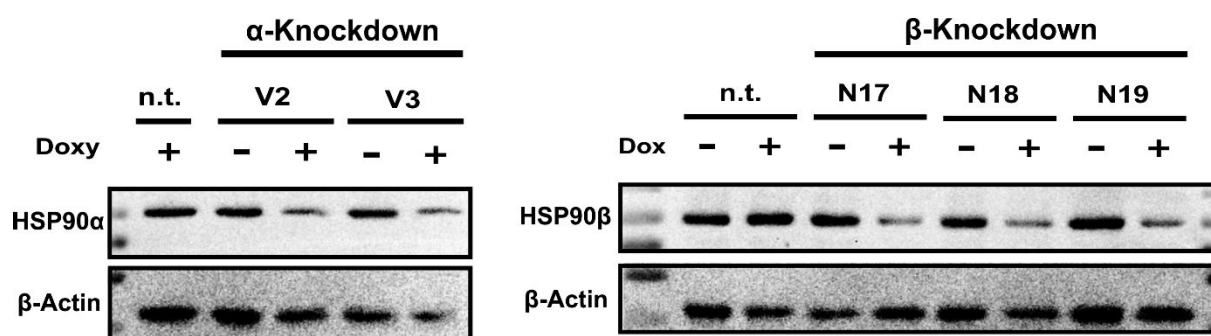
Figure 14: Protein expression of α and β knockdown. Indicated cell lines are either treated with doxycycline 2 µg/ml (+) or same volume H2O (-) for 24h. Cells were then harvested, protein was isolated and samples were subjected to western blot analysis. One representative blot out of four biological replicates is shown. Figure adapted from *Vogt & Dienstbier* et al.[181]

In addition, HSP90AA1 (V2+, V3+) knockdown resulted in decreased HSP90α protein levels, whereas HSP90AB1 knockdown (N17+, N18+, N19+) reduced HSP90β protein levels significantly compared to doxycycline-treated K562 (data not shown), non-targeting controls (n.t. +) and non-induced cell lines (**Figure 14**).
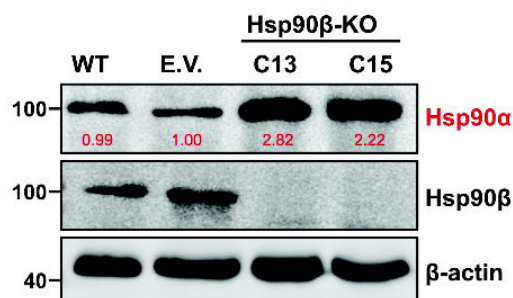
Figure 15: Western Blot Analysis of HSP90β-KO. WT = Wildtype, E.V. = empty vector, C13 and C15 = monoclonal HSP90β knockout. Western Blot and knockout cell lines were performed by *Melina Vogt.* One representative blot out of three biological replicates was performed. Figure adapted from *Vogt & Dienstbier* et al.[181]

Interestingly, constitutive loss of HSP90β in K562 cells resulted in a noticeable increase in HSP90α that has not been detected in short-term HSP90 knockdown (**Figure 15**). To better quantify this phenomenon, digital western blotting with the JESS system was performed to monitor changes in total HSP90 levels upon transient and constitutive HSP90α and HSP90β disruption (**Figure 16**).
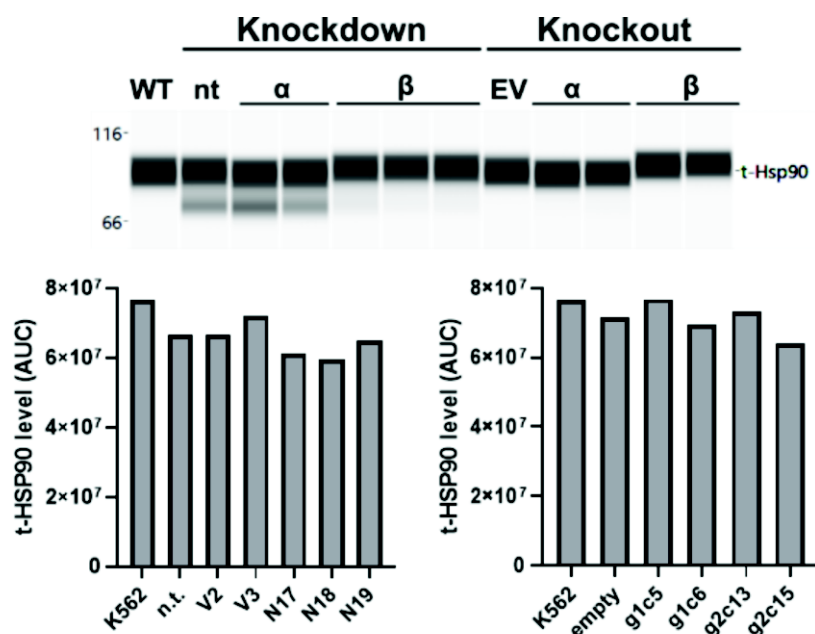
Figure 16: Digital Western Blot of HSP90 total levels. Depicted is the digital recalculation of measured electropherograms of total HSP90 protein. Electropherograms were quantified utilizing area under the curve (AUC) measurement. Note that differences in height depict changes in molecular weight. Knockout cell lines were provided by *Melina Vogt.* This experiment was performed once. Figure adapted from *Vogt & Dienstbier* et al.[181]

Despite successful HSP90α and β knockdown (**Figure 14**) and knockout (**Figure 15**) on protein level, no changes in total HSP90 levels were observed in quantitative digital Western Blotting (**Figure 16**). In addition to detecting total HSP90 levels, the assay allowed the estimation of HSP90α and β isoform ratios based on differences in molecular weight. HSP90β reduction resulted in an increased molecular weight of total HSP90 protein, indicating a shift to the slightly larger HSP90α. Contrarily, the loss of HSP90α decreased the molecular weight of total HSP90, indicating a shift to the slightly smaller HSP90β. In summary, this provides evidence of a mechanism between HSP90 α and β isoforms to balance out total HSP90 levels (**Figure 16**).

Next, the implications of HSP90α and β knockdown on the heat shock response were investigated by analyzing mRNA levels of the heat shock superfamily, including HSPA1A (HSP70), HSPB1 (HSP27), DNAJB1 (HSP40), and the paralogs TRAP1 and HSP90B1 (GRP94) (**Figure 17**).
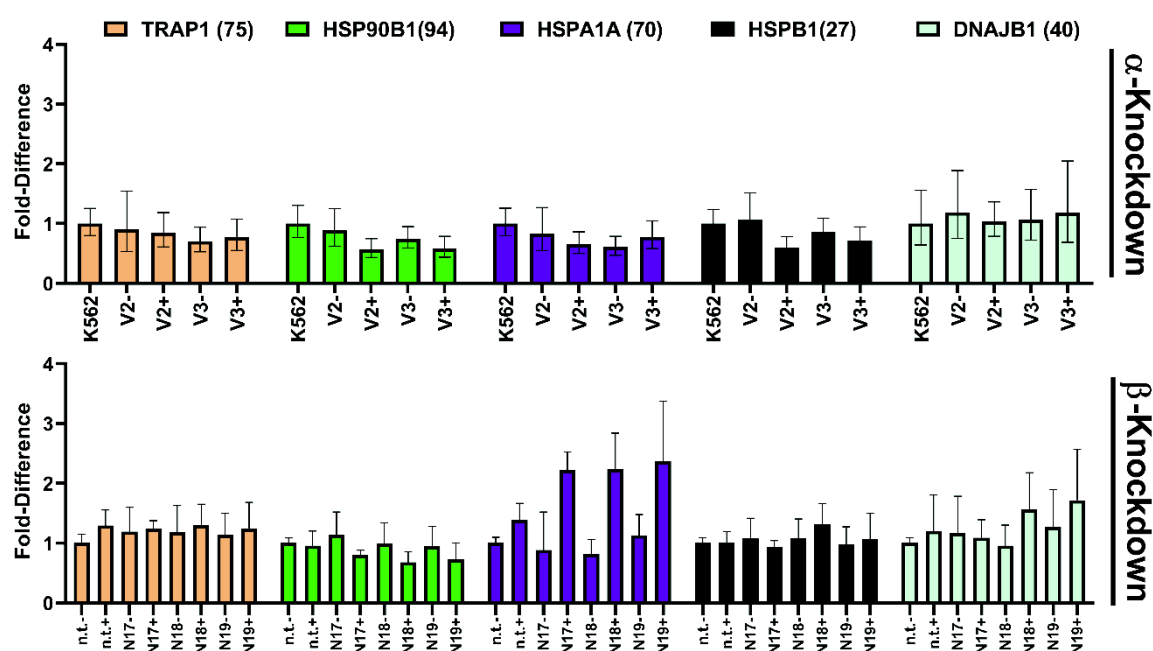
Figure 17: mRNA expression of HSP90AA1 and HSP90AB1 knockdown. Indicated cell lines are either treated with doxycycline 2 µg/ml (+) or same volume H2O (-) for 24h. Cells were harvested and RNA was isolated for qPCR performed with primers against the HSP90AA1 and HSP90AB1 construct. Depicted are mean values and standard deviation of technical replicates of one representative experiment.

HSP90AA1 and HSP90AB1 knockdown did not result in significant mRNA transcript changes in the heat shock family members TRAP1, HSP90B1, HSPB1, and DNAJB1. However, HSPA1A mRNA (translating to HSP70) was upregulated in HSP90AB1 knockdown cells (**Figure 17, lower panel, purple**). Subsequent Western Blot analysis revealed that neither 72h HSP90α nor HSP90β knockdown affected HSP70, HSP40, HSP27, or HSF-1 protein levels (**Figure 18**).
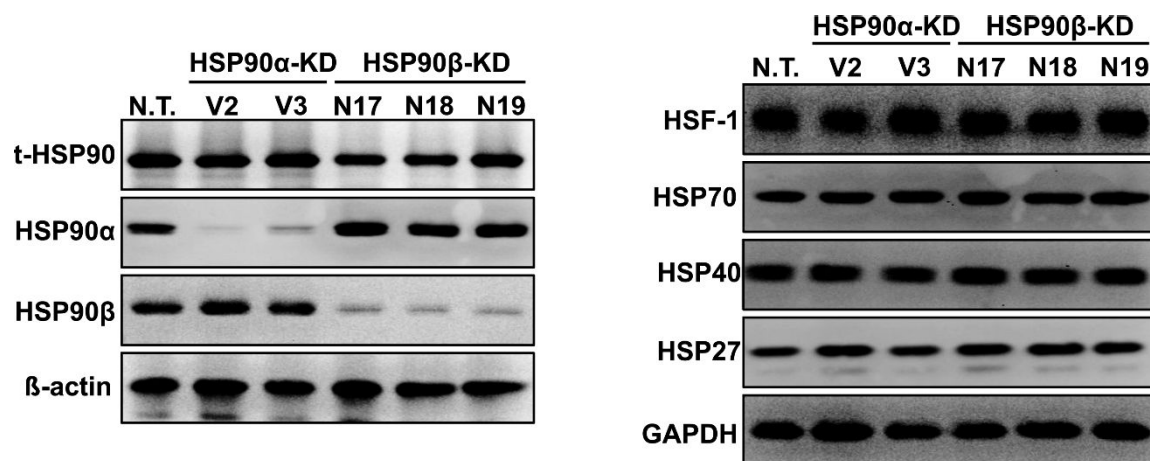
Figure 18: Western Blot analysis of heat-shock associated proteins. Indicated cell lines were induced with doxycycline 2 µg/ml for 27h. Cells were harvested and protein was isolated and samples were subjected to western blot analysis. Figure adapted from *Vogt & Dienstbier* et al.[181]

After consideration of the complex kinetics and doxycycline side effects accompanying transient shRNA knockdown, further analysis was performed with constitutive HSP90α and β knockout cell lines. Besides quantitative proteomics to decipher downstream signaling implications, consequences of HSP90α and β knockout on apoptosis and drug synergism were further validated *in vitro*. On top of that, the engraftment efficacy of HSP90α and β in xenograft mouse models was assessed to deduce clinical implications.[181]

3.2 Elucidating the resistance-acquisition mechanism towards HSP90 inhibitors

Resistance studies are crucial in evaluating HSP90 inhibitors further into clinical trials by anticipating adaptations of malignant cells to HSP90i treatment in patients. Therefore, it is necessary to decipher counteracting signaling mechanisms, feedback loops, and the acquisition of mutations that either disrupt drug binding or confer constitutive signaling. Thus, C-terminal and N-terminal specific HSP90 inhibitors were utilized to generate resistant cells for an advanced understanding of the underlying resistance mechanism. For this reason, the investigation included the advanced purine-based N-terminal HSP90 inhibitor PU-H71 (Zelavespib) and the C-terminal HSP90 inhibitor Coumermycin A1 (CA1).
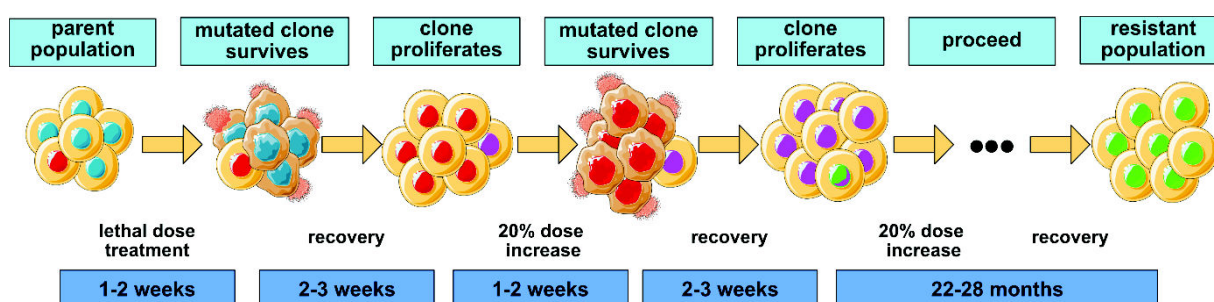
Figure 19: Development of HSP90i resistant cell lines utilizing clonal evolution. K562 cell lines were incubated with lethal doses of compounds for 1-2 weeks and recovered until viability overcomes 80% determined via trypan-blue staining. After recovery to high confluency another round of treatment was started with 20% increased dose. This procedure was repeated until a significant resistant clone was determined. Figure adapted from *Vogt & Dienstbier* et al.[181]

First, BCR-ABL1 positive K562 cells were subjected to a treatment-recovery scheme with escalating inhibitor doses to gradually increase resistance by clonal evolution (**Figure 19**). In between, cells were cryo-conserved for follow-up studies at fixed intervals defined by significant shifts in drug sensitivity (tolerated dose = 1.5x previous dose). Simultaneously, one set of K562 was subjected to chronic DMSO treatment to account for possible long-term DMSO effects. Drug sensitivity was evaluated regularly via CellTiter-Glo® cell viability assay to monitor changes in IC_{50} compared to parental K562 and DMSOr. Finally, distinct clones that mark significant progression of resistance were validated in a drug titration assay to quantify acquired resistance (**Figure 20**).
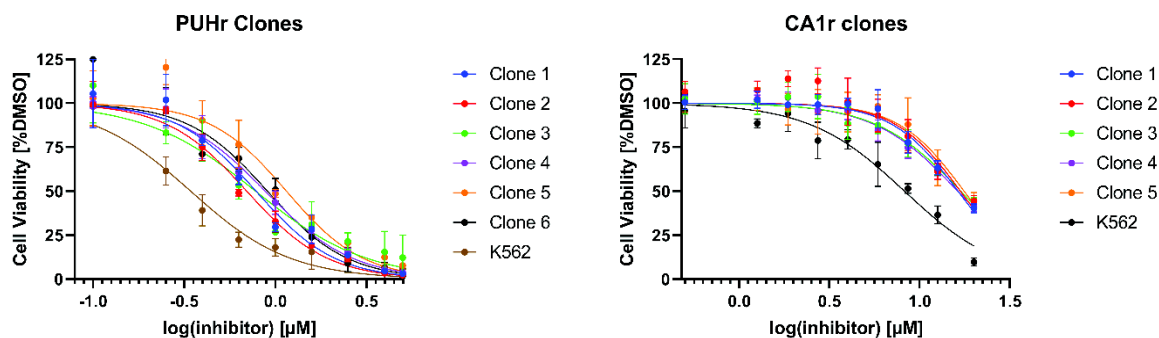
Figure 20: Drug titration assay between clones of different evolutionary stages. CellTiter-Glo® luminescence assay was conducted 72h after treatment with indicated inhibitor. Depicted are mean values and SD of technical triplicates (n = 3). One representative of two biological replicate is shown.

The half maximal inhibitory concentration (IC_{50}) upon PU-H71 treatment directly correlates with the corresponding number of treatment-recovery cycles PU-H71 resistant (PUHr) clones have undergone. Advanced clones are more resistant than clones subjected to fewer treatment cycles (**Figure 20, left panel**). Contrarily, Coumermycin A1-resistant (CA1r) clones acquired homogenous shifts in resistance to CA1 treatment that do not correlate with treatment cycles (**Figure 20, right panel).** Quantifying the most advanced clones confirmed a significant increase in IC_{50} values in PUHr (5.6-fold) and CA1r cells (3.6-fold) compared to the parental DMSOr control (**Figure 21**).
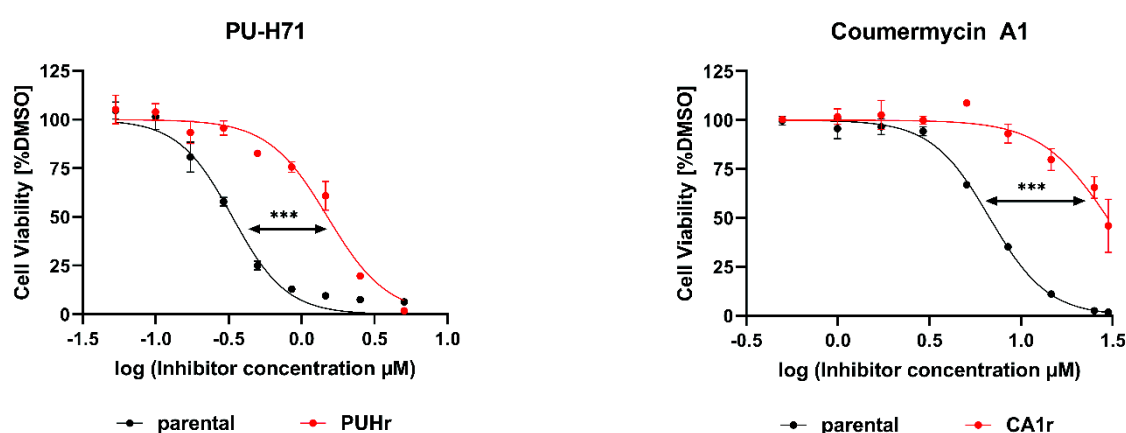
Figure 21: Validation of resistance acquirement. CellTiter-Glo® luminescence assay was conducted after treatment for 72h with indicated inhibitor. Depicted are mean values and SD of technical triplicates from one representative experiment. Unpaired t-test of both mean IC_{50} was performed evaluating to ***p < (0.0005). Figure adapted from *Vogt & Dienstbier* et al.[181]

Subsequently, cross-drug titration assays assessed the sensitivity of PUHr and CAr cells to different classes of HSP90 inhibitors to deduce whether a resistance mechanism is specific to a single inhibitor, a class of inhibitors or confers broad-spectrum resistance (**Figure 22**).
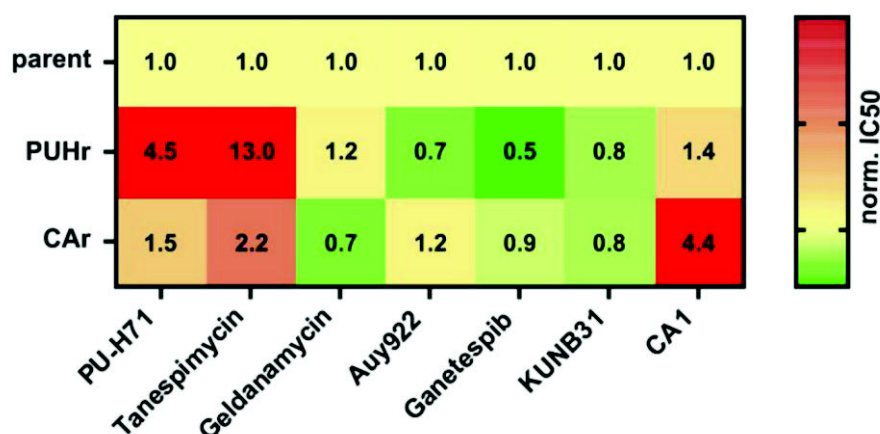
Figure 22: Cross resistance analysis against other HSP90 inhibitors. Cell viability of indicated cells was measured via CellTiter-Glo® assay after 72h treatment of indicated inhibitors. Inhibitors were used in dose concentrations titrated around the IC$_{50}$. IC$_{50}$ was calculated with graph pad prism utilizing non-linear regression (log(inhibitor) vs normalized response – variable slope). Normalized IC$_{50}$ were calculated by normalizing IC$_{50}$ values of PUHr and CA1r cells to the corresponding IC$_{50}$ of the same inhibitor concentration in DMSOr resulting in a fold-increase measurement. Figure adapted from *Vogt & Dienstbier* et al.[181]

Interestingly, PU-H71 resistance also confers resistance to the ansamycin-type inhibitor Tanespimycin (17-AAG), whereas the response to the C-terminal inhibitor Coumermycin A1 remained mainly unaffected. Furthermore, PUHr cells did not acquire resistance against the semi-synthetic radicicol-based N-terminal inhibitors Auy922 and Ganetespib or the beta-preferential HSP90 inhibitor KUNB31. Contrarily, Coumermycin A1 resistance also conferred cross-resistance to some N-terminal HSP90 inhibitors, including PU-H71 and Tanespimycin (**Figure 22**).

Considering the significant role of the heat shock response in resistance acquirement, protein levels of crucial heat shock protein (HSP) family members following HSP90 inhibition were assessed in the resistant cell lines (**Figure 23**).
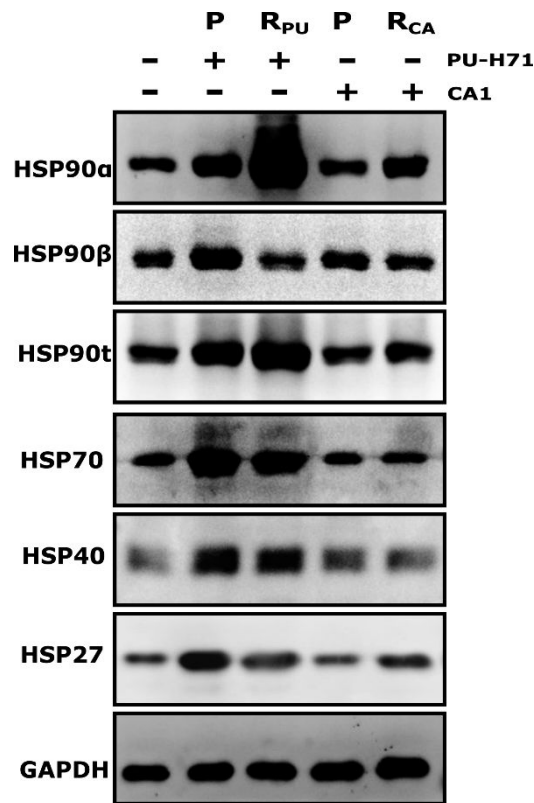
Figure 23: Western blot analysis of heat shock panel proteins. Cells were treated with either PU-H71 (350 nM), Coumermycin A1 (1 μM) or DMSO (-/-) for 24h before being harvested and prepared for protein analysis. P = Parental, R_{PU} = PU-H71 resistant cells, R_{CA} = Coumermycin A1 resistant cells. One representative blot out of 2-4 biological replicates is shown. Figure adapted from *Vogt & Dienstbier* et al.[181]

As expected, PU-H71 treatment of parental K562 cells resulted in the upregulation of proteins associated with the heat-shock response, namely HSP70, HSP40, and HSP27 (**Figure 23, lane 2**).[186] However, PUHr cells demonstrated an overall weaker classical heat shock response upon PU-H71 treatment than the parental lines indicated by less pronounced HSP70 and HSP27 induction (**Figure 23**, **lane 3**). In addition, PUHr cells showed remarkably increased HSP90α levels after PU-H71 treatment with slightly decreased levels of HSP90β. In accordance with previously published work,[129] Coumermycin A1 treatment did not induce a heat shock response in parental or CA1r cell lines (**Figure 23**, **lanes 4 and 5**).

Subsequently, RNA sequencing of PU-H71 resistant cells was performed to understand the underlying mechanism of resistance better and compared against DMSOr control cells (**Figure 24**). Analysis of the log2 fold change vs. -log10 FDR revealed several differentially up- and down-regulated mRNAs. Overlaying these hits with putative HSP90 client proteins yielded three especially interesting mRNAs:
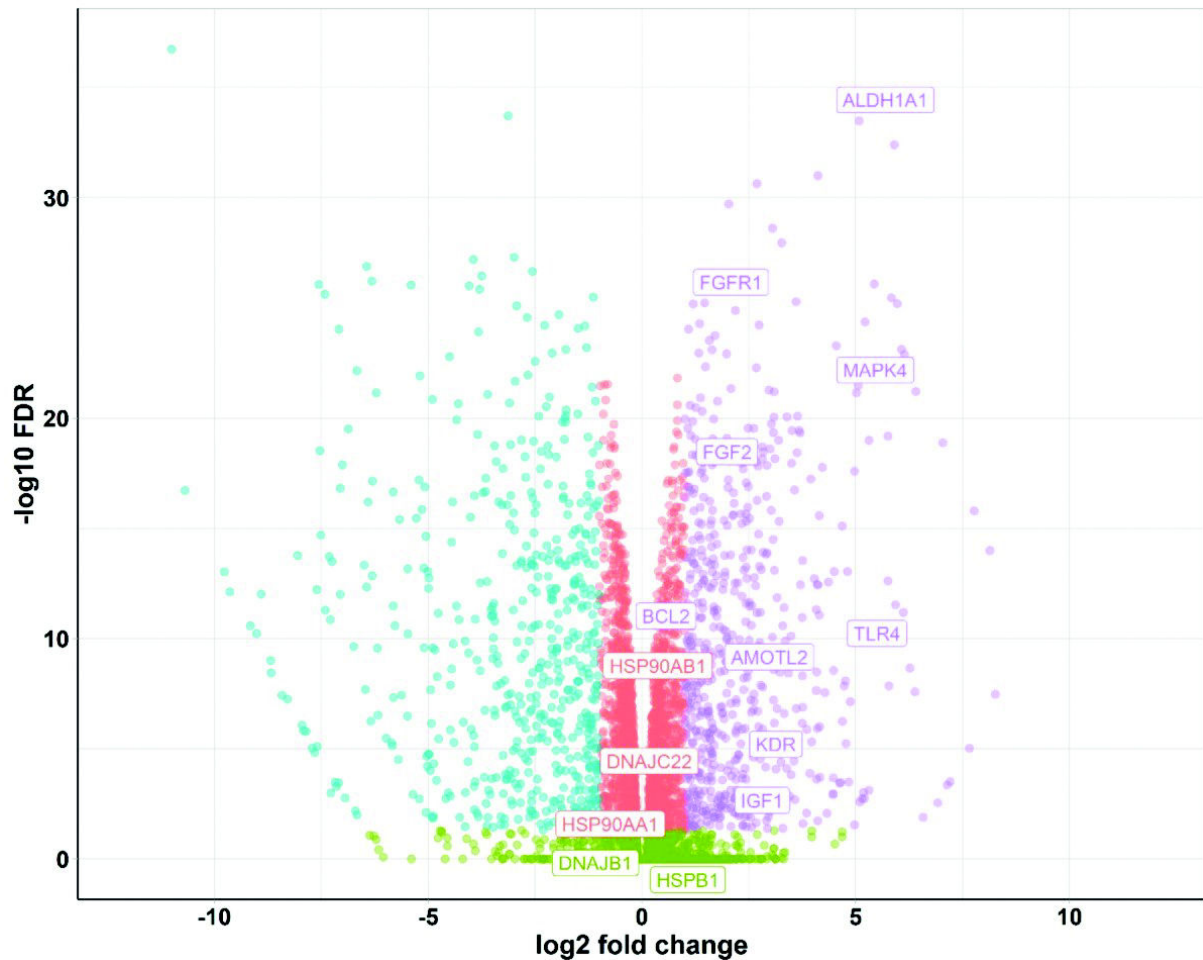
Figure 24: Differentially up or downregulated genes in PUHr cells compared to parental DMSOr. Annotated proteins are proteins of interested and marked into the clusters of significantly upregulated (violet), non-changed (red) or significantly downregulated (blue). n = 3. Figure adapted from *Vogt & Dienstbier* et al.[181]

Aldehyde Dehydrogenase 1 Family Member A1 (ALDH1A1), Mitogen-activated protein kinase 4 (MAPK4) and Toll-Like Receptor 4 (TLR4). Gene set enrichment analysis revealed that predominantly genes associated with stemness and fetal development are enriched in PUHr cells (data not shown).

For a complementary picture, the contribution of genetic alterations to the resistance mechanism was evaluated. First, whole exome sequencing (WES) was performed to identify single-nucleotide-polymorphism (**Table 11**) that results in point mutations. Secondly, SNP-Array analysis was utilized to investigate the amplification of specific gene loci (**Figure 27, Figure 28**).

Table 11: Whole Exome Sequencing Summary: Displayed are single-nucleotide polymorphisms in the genome of resistant cell lines compared to the parental control that have been successfully Sanger-Validated.

Gene	WES	Sanger Validation
HSP90AA1	Positive in both CMA1r and PUH71r	PUHr: positive (S164F)
		CA1r: positive (L29F)
CLMN	Positive in both CMA1r and PUH71r	PUHr: positive (E588Q)
		CA1r: positive (S217N)

In total, 100 (PUHr) and 59 (CA1r) genetic alterations have been found in whole exome sequencing analysis in resistant cells compared to the parental line, respectively. Notably, distinct single nucleotide variants in the *HSP90AA1* and *CLMN* (Calmin) gene loci were identified by WES (**Table 11**). PUHr cells acquired an 857C>T nucleotide exchange in the *HSP90AA1* locus (ENST00000216281.13, chr14:102085796G>A, hg38) which consequently leads to an amino acid exchange from serine to phenylalanine on position 164 (S164F). *HSP90AA1*[857C>T] was validated via sanger sequencing. Coumermycin A1 resistant cells harbored a mutation (ENST00000216281.13, chr14:102086292C>A, hg38) in the *HSP90AA1* locus as well, resulting in an L29F substitution on protein level. In addition, PUHr cells acquired an S217N mutation in the *CLMN* gene locus, whereas CA1r cells displayed an E588Q substitution. Additional validated polymorphism by sanger sequencing in both resistant cell lines include *LRP5* (Low-density lipoprotein receptor-related protein 5), *NDNF* (neuron-derived neurotrophic factor), and *HIVEP1* (Human Immunodeficiency Virus Type I Enhancer-Binding Protein 1). In contrast, a *TNFSF11* variant (Tumor Necrosis Factor Ligand Superfamily Member 11) is exclusive for CA1r.

Next, the consequences of the S164F HSP90α variant were investigated *in silico* utilizing crystal structure-based rational analysis of PU-H71 binding and molecular dynamics (MD) simulations (**Figure 25**). Initial unbiased MD simulations by *Dr. David Bickel* and *Dr. Munishikha Kalia*[181] suggest no direct interference with the PU-H71 binding mode, which aligns with a distance of 0.9 nm separating the mutation side from the PU-H71 binding site (**Figure 25**).
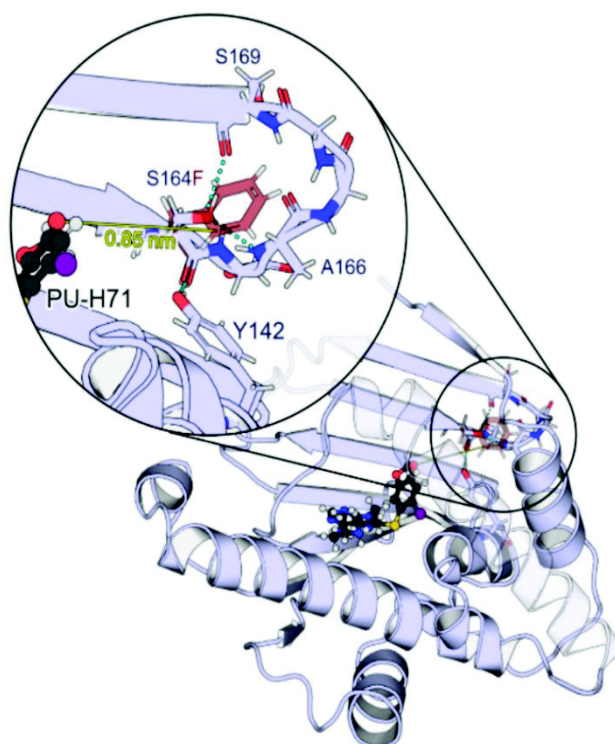
Figure 25: Structural model of the N-terminal domain of HSP90α bound to PU-H71. Based on PDB ID 2fwz. The substitution site S164F is highlighted in red. Depiction was kindly provided by *Dr. David Bickel.* Figure adapted from *Vogt & Dienstbier* et al.[181]

However, wildtype HSP90α demonstrated more flexibility during the simulation (**Figure 26, left panel**), caused by two distinct regions, with one directly adjacent to the mutation site (**Figure 26, right panel**).[181]
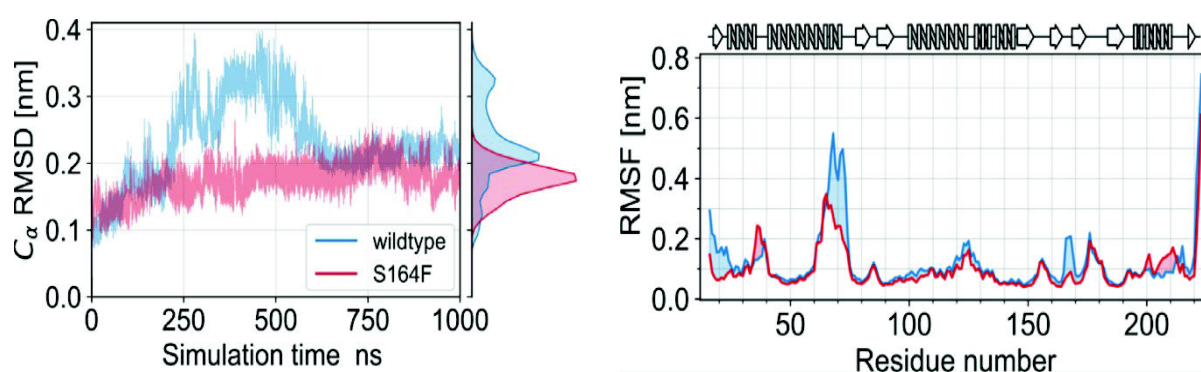
Figure 26: MD simulations of the HSP90α variant S164F versus wildtype. Left panel: Alpha carbon-root mean square deviation (Cα-RMSD) of wild type and variant (S164F) HSP90α over the course of the simulation. Right panel: Alpha carbon-root-mean-square fluctuation (Cα-RMSF) in HSP90α. Above the plot a schematic representation of the secondary structure is given. Simulations performed by *Dr. David Bickel* and *Dr. Munishikha Kalia*. Figure adapted from *Vogt & Dienstbier* et al.[181]

Furthermore, SNP array analysis performed by *Dr. Rabea Wagener* revealed that PUHr cells (compared to the parental DMSOr cells) amplified a region in the 14q32.12q32.3 cytoband of 15 Mb length, including the *HSP90AA1* gene (**Figure 27, A; Table 12**). In contrast, CA1r cells acquired a 1.9 Mb copy number gain on chromosome 7q21.12q21.13 that harbors the *ABCB1* gene, which encodes for the multidrug efflux pump 1 (MDR1) (**Figure 27, B**).
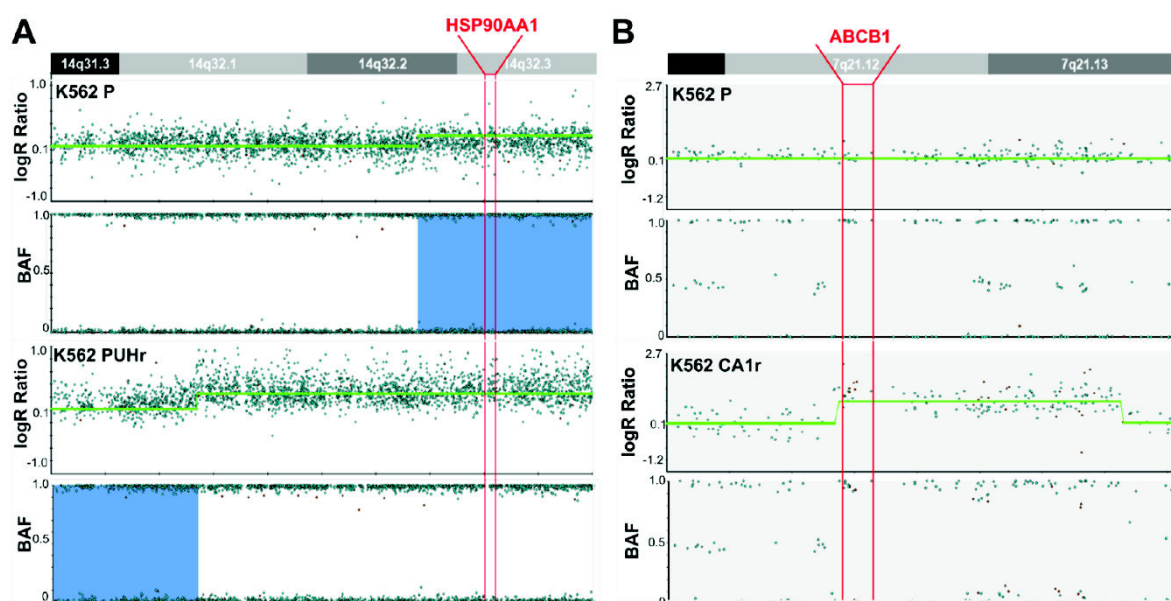
Figure 27: SNP-Array Analysis of PUHr and CA1r cell lines compared to parental K562. PUHr cells acquire a copy-number gain in the 14q32.2 locus where the *HSP90AA1* gene is located **(A)**. CA1r cells acquire a copy-number gain in the 7q21.12 locus where the *ABCB1* gene is located that encodes for the MDR1 protein (**B**). Analysis was performed by *Dr. Rabea Wagener*. Figure adapted from *Vogt & Dienstbier* et al.[181]

In addition, the clonal evolution stages of PUHr cells were assessed utilizing SNP-array technology. Interestingly, copy number gains and amplifications correlate with the evolutionary progression of the resistant clones (**Table 12**, **Figure 28**). While the earliest clone PUHr C1 did not show any copy number variations, progressing aberrations in the *HSP90AA1* locus could be detected in the intermediated C2 clone (copy number gain) and the advanced C3 clone (amplification) (**Table 12**).

Sample	PUHr C1	PUHr C2	PUHr C3
Type	non	Gain	Amplification
Tolerated Dosage	290 nM	660 nM	2 µM
region (hg38)		Chr14:64618208-91874780	Chr14:91874780-104854362
Cytoband		14q23.3-q32.12	14q32.12-q32.33
Length		27256.6 kb	12979.6 kb
Genes		511 genes	429 genes
Overlap with GOI		HSP90AA1	HSP90AA1

Table 12: SNP-Array Analysis of PUHr Evolution. Copy number gains and amplifications of PUHr clones correlate with the evolutionary progression of the resistant clones.
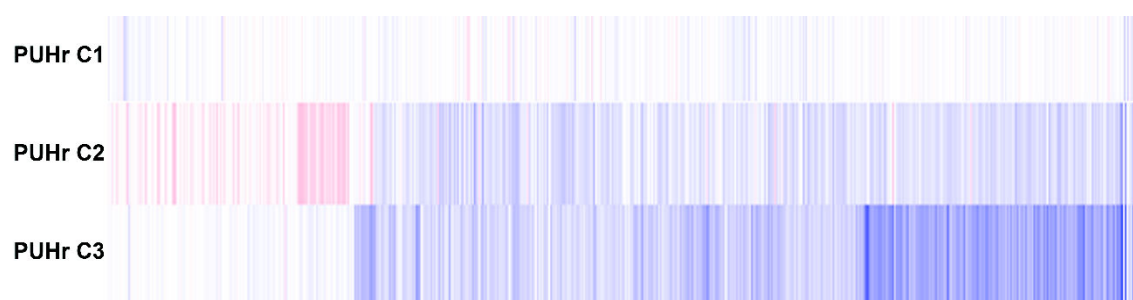
Figure 28: Investigation of PU-H71 resistance evolution by SNP-Array analysis. Copy number gains and amplifications in PUHr clones correlate with the evolutionary progression of the resistant clones.

On top of that, protein levels of MDR1, ALDH1A1, TLR4, and MAPK4 were assessed in resistant cell lines via Western Blot to complement and validate findings on DNA and mRNA levels (**Figure 29**).
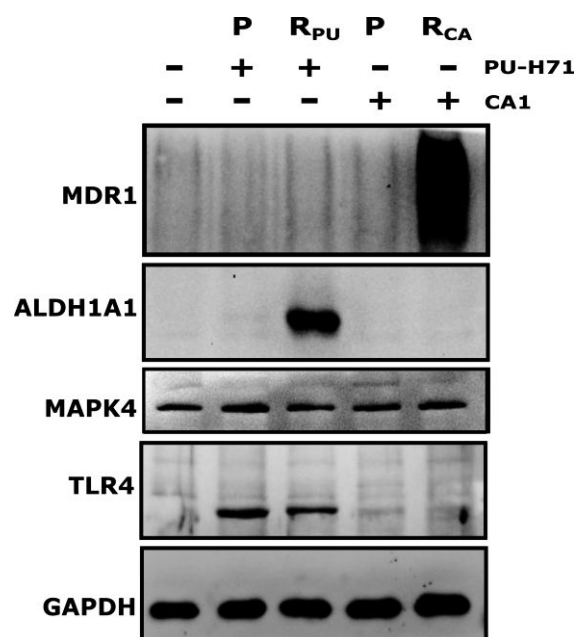
Figure 29: Western Blot validation of mRNA and DNA analysis-based targets. Cells were treated with either PU-H71 (350 nM), Coumermycin A1 (1 μM) or DMSO (-/-) for 24h before being harvested and prepared for protein analysis. P = Parental, R_{PU} = PU-H71 resistant cells, R_{CA} = Coumermycin A1 resistant cells. GAPDH is used as a loading control. Figure adapted from *Vogt & Dienstbier* et al.[181]

In line with the *ABCB1* copy number gain (**Figure 27**), Coumermycin A1-resistant cells demonstrated considerably elevated levels of multi-drug efflux pump (MDR1) protein (**Figure 29, lane 5**). Furthermore, the increase in ALDH1A1 mRNA in PUHr cells detected by mRNA sequencing (**Figure 24**) could be validated by a strong upregulation of total ALDH1A1 protein levels compared to the parental control (**Figure 29**, **lane 3**). On the other hand, differences in TLR4 and MAPK4 mRNA levels did not propagate to the protein level (**Figure 29**).

Next, several relevant reported kinases for HSP90 inhibitor resistance[177,187,188] were evaluated on the protein level to unravel the underlying mechanism of the acquired resistance and concurrent survival benefit (**Figure 30**).
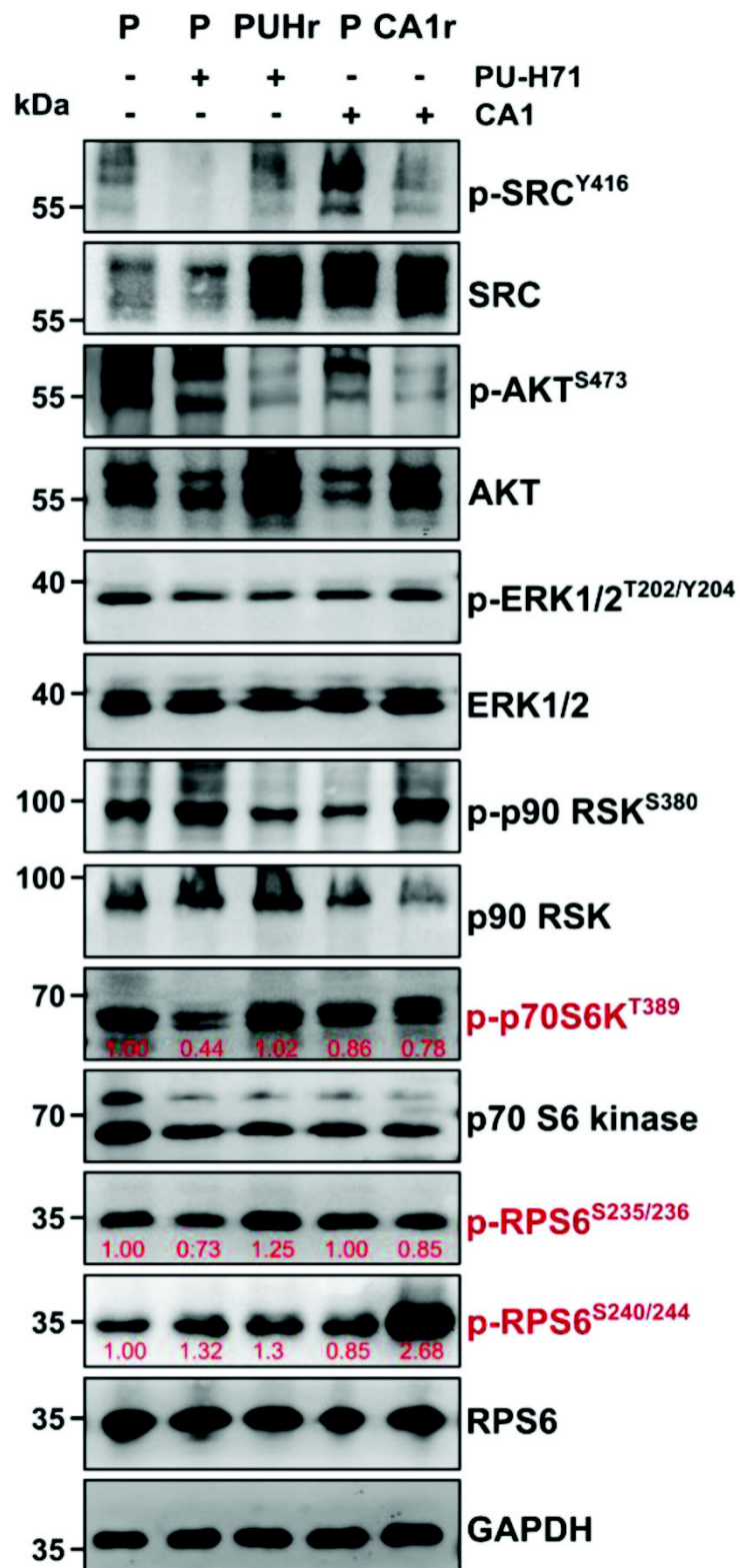
Figure 30: Western Blot analysis of downstream kinases. Cells were treated with either PU-H71 (350 nM), Coumermycin A1 (1 µM) or DMSO (-/-) for 24h before being harvested and prepared for protein analysis. P = Parental, R$_{PU}$ = PU-H71 resistant cells, R$_{CA}$ = Coumermycin A1 resistant cells. Figure adapted from *Vogt & Dienstbier* et al.[181]

First, PUHr cells are characterized by elevated SRC kinase and total AKT levels (**Figure 30, lane 3**). Increased amounts of total AKT result in an activated mTOR pathway confirmed by the hallmark phosphorylation (Thr389) of the p70S6 kinase that subsequently phosphorylates the S6 ribosomal protein at Ser235/236 and thus induces pro-survival signaling and expression of proliferative genes. In addition, PU-H71 treatment in parental cells increased phosphorylation of p90 RSK (S380), which is diminished in PUHr cells (**Figure 30, lane 3**).

In contrast, Coumermycin A1 resistance is accompanied by phosphorylation of p90RSK at S380 with subsequent activation of the ribosomal protein S6 at the phosphorylation site Ser240/244 (**Figure 30, lane 5**). However, classical upstream activators such as ERK1/2[189] appear unaffected. Eventually, both HSP90 resistance mechanisms altered the activity of the ribosomal protein S6 but affected different phosphorylation sides (Ser235/236 in PUHr and Ser240/244 in CAr) (**Figure 30**).

3.3 Development of small molecule inhibitors targeting the HSP90 C-terminal domain

The next aim of the study was to investigate, validate and characterize novel inhibitors of the C-terminal dimerization of HSP90.

Based on previous work on the α-aminooxy-peptide AX (*Bhatia et al*. 2018),[97] and computational predictions performed by the group of *Prof. Holger Gohlke (Computational Pharmaceutical Chemistry, HHU)*, the group of *Prof. Thomas Kurz (Pharmaceutical and Medicinal Chemistry, HHU)* generated tripyrimidonamide scaffold-based compounds with different moieties based on rational design (**Figure 31**).
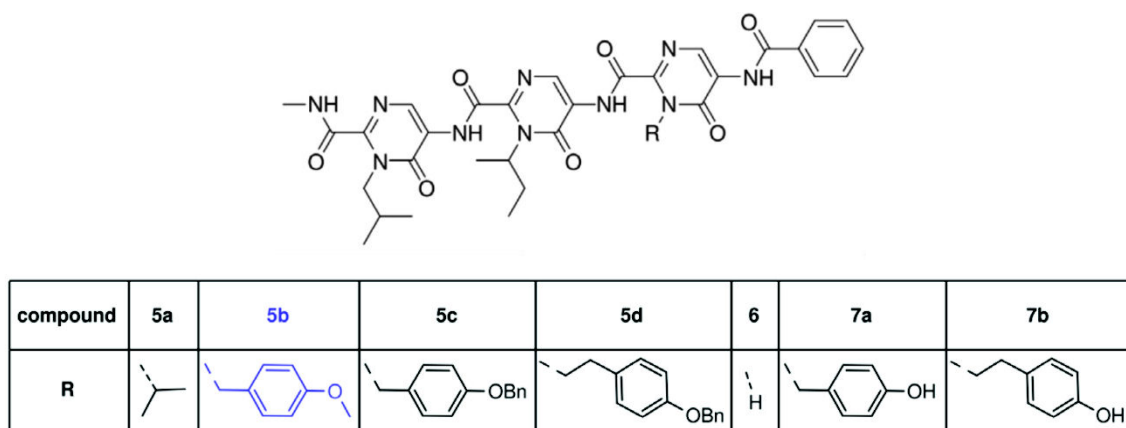
Figure 31: Tripyrimidinonamide scaffold-based drugs. Computational predictions and rational design based on the α-aminooxy-peptide AX[97] yielded tripyrimidonamide scaffold-based compounds. Published in *Bhatia et al.*[182]

After biochemically quantifying the different compounds by microscale thermophoresis and auto-display dimerization assay, the viability of K562 cells was assessed by a drug titration assay utilizing CellTiter-Glo® upon treatment with **5a-7b** (**Figure 32**). At 3 µM, **5b** showed superior potency in reducing cell viability compared to other analogs, with up to 80% reduced viability compared to the control (**Figure 32**). Notably, **7b** displayed similar effects on cell viability but demonstrated lower K_D values assessed by microscale thermophoresis.[182] Considering these findings, **5b** was chosen as the lead compound for further analysis. Additionally, *Dr. Vitalij Woloschin* further modified the **5b** scaffold yielding a tripyrimidoneamide-based compound **VWK147** that was included in the investigation due to hypothesized increased efficacy and solubility.
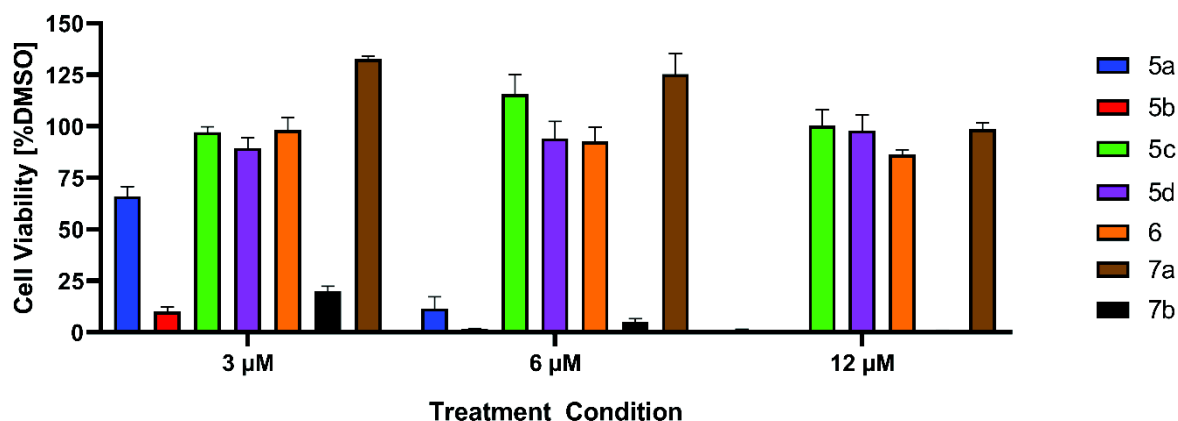
Figure 32: Cell viability screening of Tripyrimidinonamide-based compounds. K562 cells were treated for 72h with indicated inhibitor concentrations and then subjected to CellTiter-Glo® measurement. Viability was normalized to the DMSO control set to 100%. Error bars depict standard deviation of technical replicates (n = 3). Published in *Bhatia et al.*[182]

Following confirmation of **5b** and **VWK147** efficacy in BCR-ABL1 positive K562 cells, the potency of these lead compounds was investigated in a vast panel of cells, including B-ALL, CML, AML, T-ALL, imatinib-resistant cell lines[97], and patient-derived xenograft (PDX) samples (**Figure 33**). **5b** demonstrated profound cell cytotoxicity in most tested leukemia compared to the inactive analog **7a**. Interestingly, **5b** showed efficacy in a PDX sample originating from a relapsed patient (Pat. 3 Relapse) and imatinib-resistant HL60 (HL60r). However, **VWK147** reduced cell viability at a lower dosage in almost all tested leukemia cells, indicating successful optimization. **5b**'s mechanism of action was further evaluated and confirmed by investigating cell cycle, apoptosis, proliferation, survival signaling, and colony-forming capability on several TKI-resistant mutant cell lines.[182]
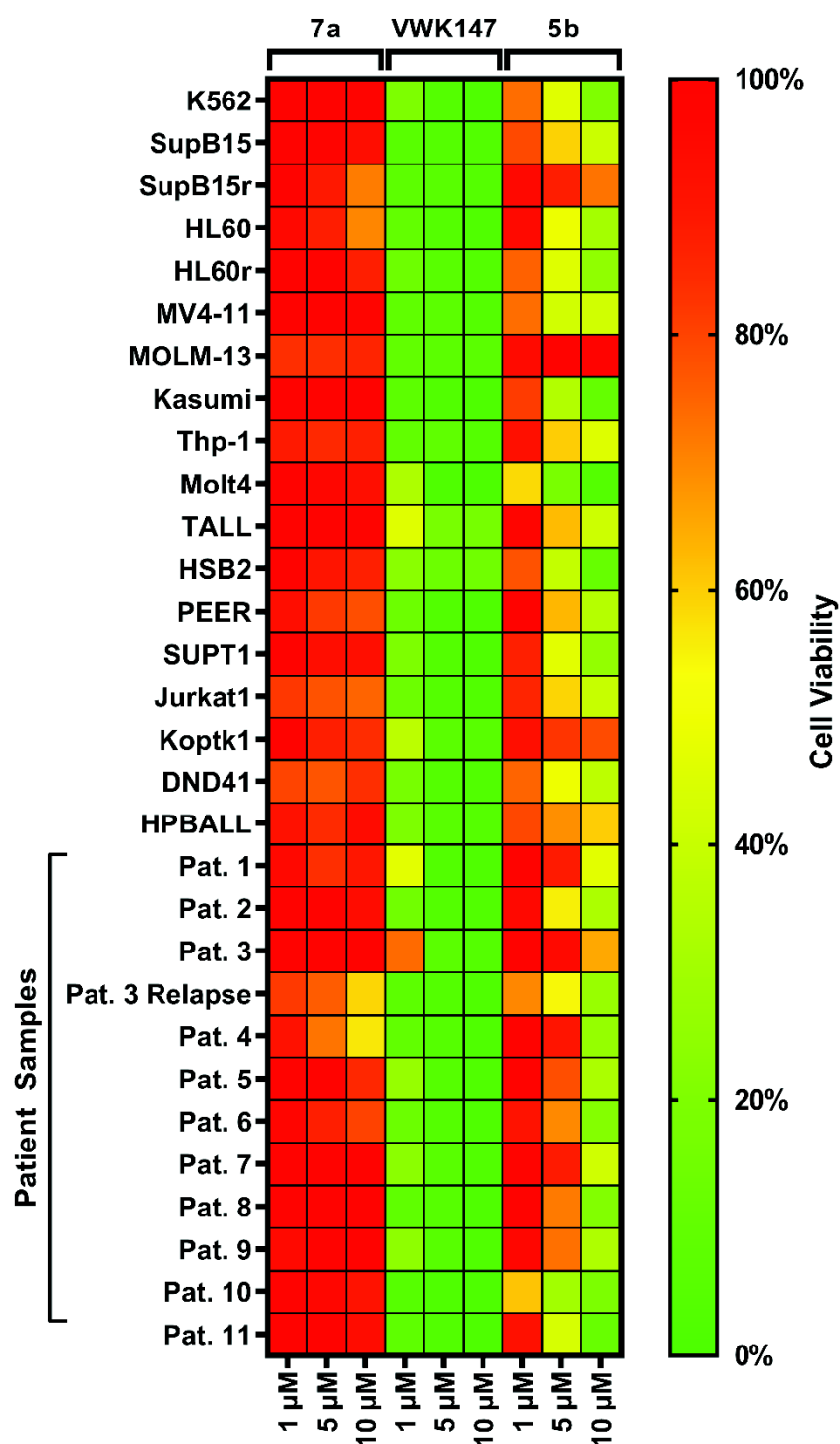
Figure 33: Cell library screening of 7a, VWK147, 5b: A broad spectrum of cell lines different origin including B-ALL, CML, AML, T-ALL, imatinib-resistant cell lines[97] and patient derived xenograft samples were investigated by CellTiter-Glo® measurement after 72h treatment with indicated drugs. Depicted is the cell viability normalized to the vehicle control (0% = no cell viability, 100% = viability comparable to DMSO treatment) as the mean of three technical replicates. To be published in Sun et al.[185]

Next, **5b** and **VWK147** were analyzed in their target specificity, binding mode, and functionality. Binding to HSP90 and its capability to disrupt the chaperone activity of HSP90 was assessed *ex vivo* using a cell-free luciferase refolding assay.[182] Furthermore, a combination of a time-resolved fluorescence energy transfer (FRET)-based and a competitive fluorescence polarization-based biochemical assay was conducted to decipher the binding mode of the compounds.

First, the FRET assay examined the interaction of a truncated C-terminal HSP90 (HSP90-CTD) with Peptidylprolyl isomerase D (PPID), also known as cyclophilin D, a critical C-terminal specific chaperone of HSP90.[179] PPID was labeled with a dye-labeled acceptor whereas HSP90-CTD was modified with terbium to function as FRET donor enabling quantification of the PPID-HSP90-CTD disruption (**Figure 34**).
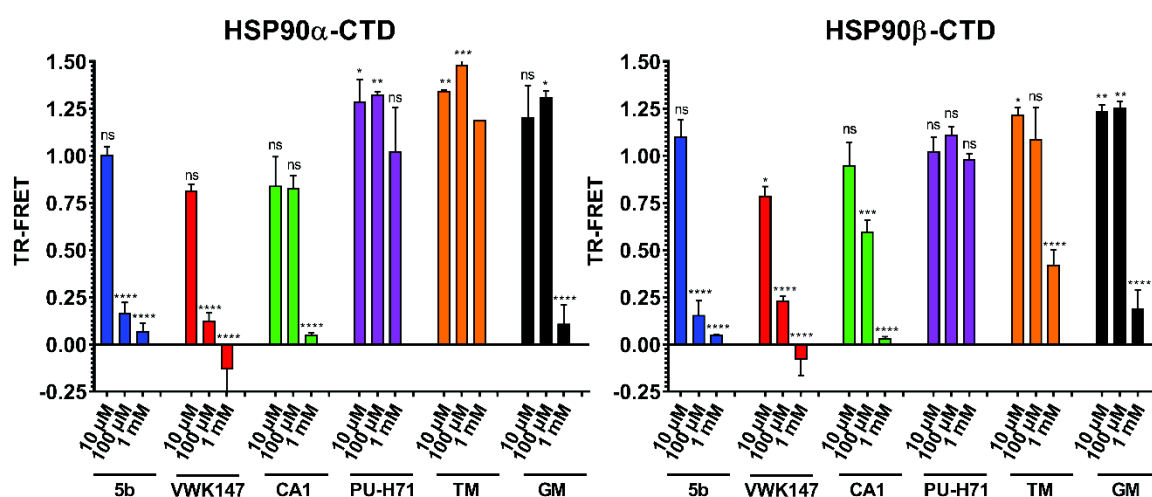
Figure 34: TR-FRET measures the disruption of PPID-HSP90-CTD interaction. TR-FRET ratios were calculated [(FRETsample – FRETneg)/(FRETpos – FRETneg) * 100%]. CA1 = Coumermycin A1, TM = Tanespimycin, GM = Geldanamycin. Depicted are mean values and standard deviation of technical duplicates. Two-way ANOVA was performed to calculate significance against DMSO control. * p = 0.05 **** p = 0.0005. Published in *Bhatia et al.*[182]

5b and **VWK147** disrupted the PPID-HSP90-CTD interaction dose-dependently without apparent isoform specificity to HSP90α or HSP90β. In addition, both compounds were more potent than the C-terminal reference inhibitor Coumermycin A1 at 100 μM. In contrast, the N-terminal inhibitor PU-H71 did not disturb the PPID-HSP90-CTD binding, whereas Tanespimycin (TM) and Geldanamycin (GM) diminished the interaction only at a very high dosage (1 mM) (**Figure 34**).

Secondly, a competitive fluorescence polarization assay was utilized to address potential unspecific binding to the N-terminal domain of HSP90. Therefore, compounds

were incubated together with HSP90 and FITC-labeled GM. If compounds displace the FITC-labeled GM bound to the ATP-binding domain of HSP90, the fluorescence polarization will increase (**Figure 35**).
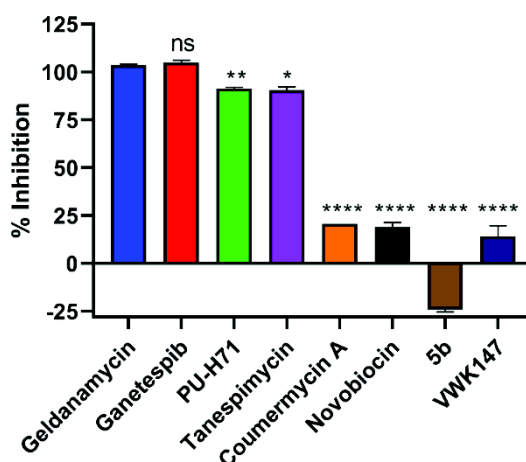
Figure 35: Competitive N-terminal fluorescence polarization assay. Indicated compounds were incubated with HSP90α and FITC-labeled Geldanamycin for 3h. Unlabeled Geldanamycin was used as positive displacement control. The ability to replace FITC-Geldanamycin from the N-terminal binding pocket is expressed as % inhibition. Depicted are mean values of two replicates with error bars (SD). Statistical analysis was performed utilizing two-way ANOVA (* p = 0.05 **** p = 0.0005). Published in *Bhatia et al.*[182]

N-terminal inhibitors such as Ganetespib, PU-H71, and Tanespimycin displaced FITC-labeled GM from the N-terminal HSP90 binding pocket, similarly to unlabeled Geldanamycin. On the other hand, C-terminal reference inhibitors such as Coumermycin A1 and Novobiocin, as well as **5b** and **VWK147,** had only a slight effect on the FITC-GM binding. Interestingly, **5b** increased the FITC-GM binding (**Figure 35**). Taken together, C-terminal TR-FRET and N-terminal FP assay provided evidence that **5b** and **VWK147** indeed bind the HSP90 C-terminal domain *ex vivo*.

Following the *ex vivo* validation, the binding of the lead compounds to HSP90 was assessed *in vitro* by adapting the cellular thermal shifts assay (CETSA),[190] which measures protein stabilization upon ligand binding (**Figure 36**). First, the thermal stabilization of reference inhibitors was quantified. The N-terminal inhibitors Tanespimycin (ΔT_m = +3.25°C) and PU-H71 (ΔT_m = +1.65°C) increased the thermal stability of HSP90 upon treatment, whereas the C-terminal inhibitor Coumermycin A1 negatively affected temperature-induced degradation (ΔT_m = -2.83°C). Notably, **5b** (ΔT_m = +1.86°C) and **VWK147** (ΔT_m = +1.66°C) displayed stabilization capabilities comparable to PU-H71, indicating *in vitro* binding to cellular HSP90 (**Figure 36**).
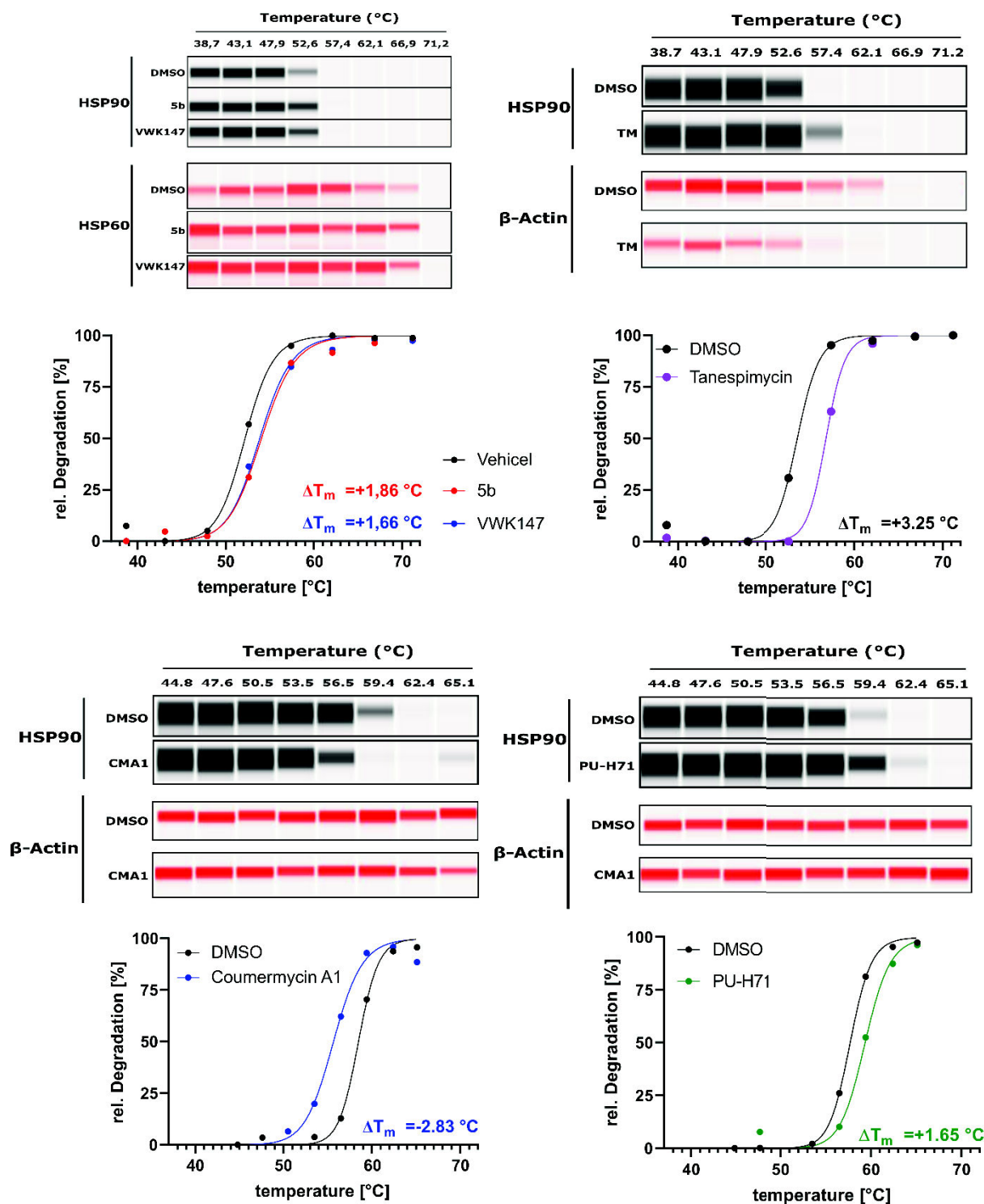
Figure 36: Cellular thermal shift assay (CETSA) of 5b and VWK147. Cells were treated for 24h with indicated concentration of indicated compound or DMSO, harvested and treated with the displayed temperature gradient. Afterwards cells were lysed and analyzed via digital western blotting (JESS). Protein amount depicted as area under the curve of the conditions was normalized to HSP90 level of cells treated with DMSO. Resulting relative protein values were analyzed using non-linear regression (log(antagonist) vs normalized response – variable slope. Published in *Bhatia et al.*[182]

Furthermore, **5b** was evaluated in an isothermal dose-dependent fingerprint (ITDRF) CETSA (CETSA$_{ITDRF}$) to validate that the stabilization is compound-specific and responds to changes in concentration (**Figure 37**). As a result, temperature-induced protein aggregation was prevented dose-dependently by **5b** with a maximum stabilization of 2.68 fold at 5 µM, indicating an on-target effect on cellular HSP90 attributed to the compound (**Figure 37**).
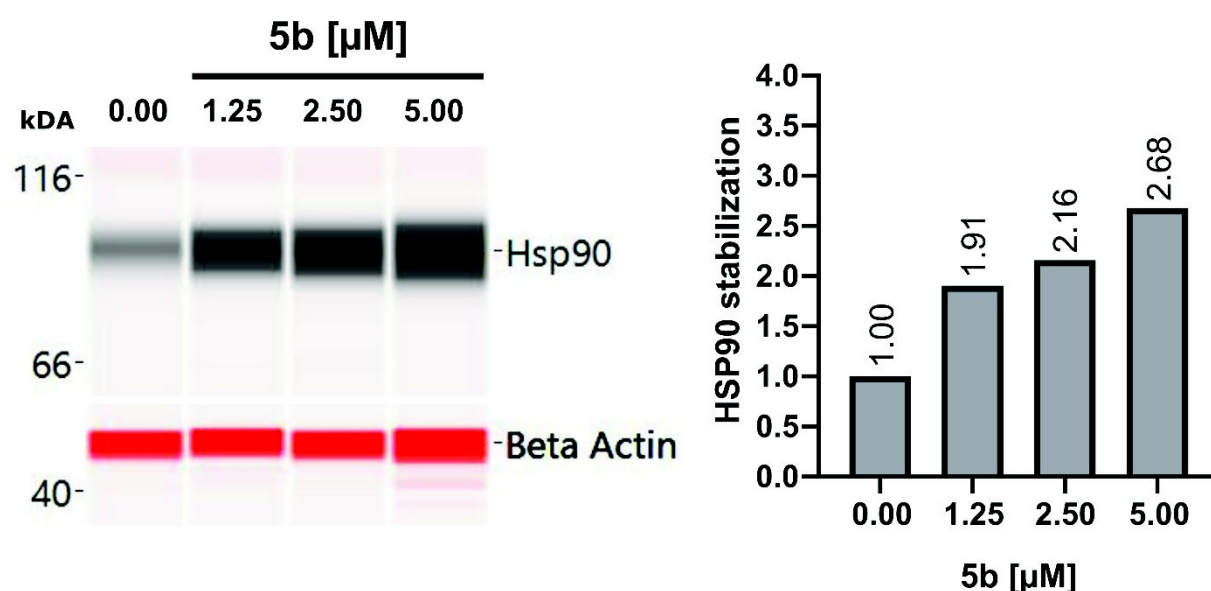
Figure 37: Isothermal dose-dependent fingerprint (ITDRF) CETSA of 5b. Cells were treated for 24h with indicated concentration of **5b** or DMSO, harvested and treated with 54.1°C. Afterwards cells were lysed and analyzed via digital western blotting (JESS). Protein amount depicted as area under the curve of the conditions was normalized to HSP90 level of cells treated with DMSO. Resulting relative protein values were analyzed using non-linear regression (log(antagonist) vs normalized response – variable slope. Published in *Bhatia et al.*[182]

In summary, *ex vivo* and *in vitro* experiments provided complementary evidence for a specific interaction of **5b** and **VWK147** with the HSP90 C-terminal domain (**Table 13**). Subsequently, the group of *Prof. Holger Gohlke (Computational Pharmaceutical Chemistry, HHU)* performed MD simulations indicating a putative binding mechanism in the CTD and MD groove. Additionally, disruption of dimerization was validated by BS[3] crosslinker assay, size exclusion chromatography small-angle X-ray scattering (SEC-SAXS), and BN native gel western blotting.[182]

Compound	Targeting	Cell viability IC$_{50}$ (K562)	Cellular Thermal Shift	TR-FRET HSP90 CTD inhibition		FP HSP90 NTD inhibition
	Domain/Isoform [conc.]	[µM]	ΔTm [°C]	α [1 mM]	β [1 mM]	[10 µM]
LSK82 (5b)	Experimental HSP90 CTD	4.50	+1.86	92.95 ± 2.96 %	94.76 ± 0.03 %	no inhibition
VWK147 (6)	Experimental HSP90 CTD	2.42	+1.66	81.41 ± 2.38 %	78.99 ± 3.28 %	no inhibition
Coumermycin A1	Reference HSP90 CTD	2.67	-2,83	40%	-	no inhibition
Geldanamycin	Reference HSP90 NTD	0.00427	+1,47	94.99 ± 0.86 %	96.54 ± 0.40 %	20.61 ± 0.44 %
Tanespimycin (17-AAG)	Reference HSP90 NTD	0.226	+3.25	89.05 ± 6.94 %	81.16 ± 6.94 %	103.51 ± 0.44 %
Auy922 (Luminespib)	Reference HSP90 NTD	0.00544	-	no Inhibition	57.62 ± 5.53 %	90.36 ± 1.39 %
PU-H71	Reference HSP90 NTD	0.310	+1,65	no Inhibition	no inhibition	105.26 ± 0.44 %

Table 13: Summary of *ex vivo* and *in vitro* target validation. Characteristics of several biochemical target-validation assays. Depicted are mean values of three technical replicates with 95% CI.

Following the completed *ex vivo* and *in vitro* analysis of **5b**, the compound was evaluated *in vivo*. Considering **5b**'s solubility issues, preparing a vehicle suitable for **5b** in *in-vivo* applications was a big challenge. After testing, cyclodextrin-, DMSO-, PEG-, and B2M-based vehicle formulations that failed to solubilize **5b**, 10/18 DRD (10% DMSO, 18% Kolliphor, 3.6% dextrose, 68.4 % H2O) was successfully adapted from *Shimamura* et al.[180] to dissolve **5b. 5b** was mainly limited by DMSO solubility (C$_{max}$ = 10 mM), resulting in an applicable concentration of 1 mM **5b** [10/18 DRD].

Figure 38: Vehicle Formulation and Solubility. (a) **5b** dissolved in DMSO to a concentration up to 10 mM. (b) **5b** precipitated in DMSO over a concentration of 10 mM. (c) **5b** dissolved in 10/18 DRD with a concentration of 1 mM.

The successful vehicle formulation was first used to analyze **5b** efficacy in a zebrafish model by *AG Bajgoli*, Tübingen. GFP-labeled T-ALL cells were transplanted into zebrafish embryos, treated with **5b,** and quantified by flow cytometry. Notably, **5b** reduced T-ALL burden in zebrafish comparable to AUY922, an N-terminal HSP90 inhibitor investigated in several advanced clinical trials (**Figure 39**). In addition, **5b** showed similar or less toxicity than AUY922 (data not shown).
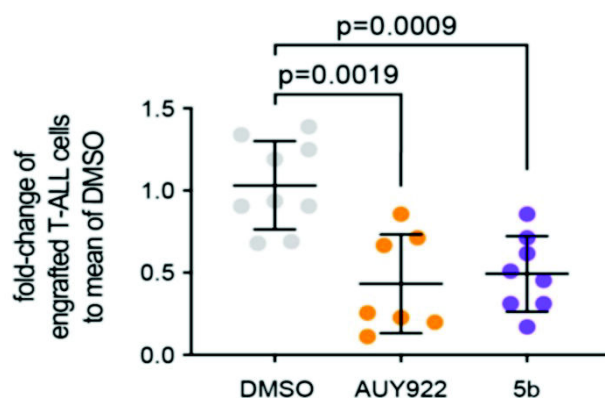
Figure 39: Evaluation of 5b efficacy in a zebrafish model. GFP labeled T-ALL cells were injected into zebrafish embryos, treated with **5b** for indicated timepoints, and counted afterwards by flow cytometry. Image extracted from *Bhatia et al.*[176] All zebrafish work was done by *Narges Aghaallaei* (AG Bagjoli, Tübingen) and is shown for complementary reasons.

After the positive evaluation in the zebrafish model, **5b** was assessed in a mouse xenograft model. But, first, to define treatment parameters (e.g. schedule and dosage) for the 10/18 DRD formulation, dose-escalation and toxicity studies were conducted with Ganetespib [data not shown] and an experimental bispyrimidoneamid-based compound.

The health and weight of NGS mice were monitored twice daily during bi-daily treatment with 30 mg/kg of the compound dissolved in 10/18 DRD. In addition, blood was isolated via retro-orbital bleeding for plasma analysis (**Figure 40**).
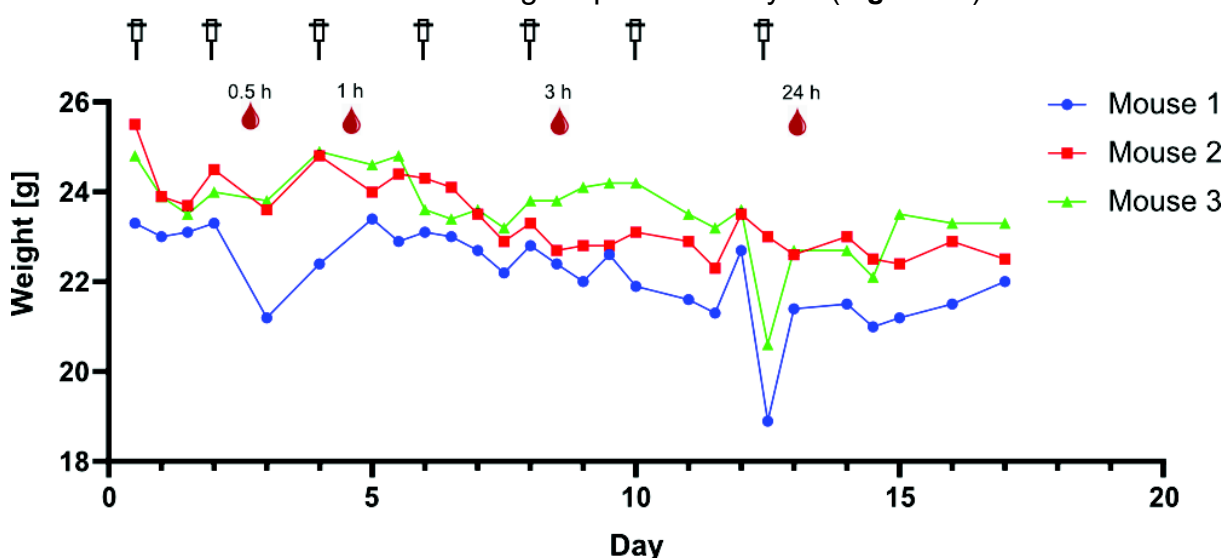
Figure 40: Toxicity Study for the bispyrimidoneamid-based compound. NGS mice were treated bi-daily with 30 mg/kg of an experimental bispyrimidoneamid compound and general health and weight of the mice was monitored. Syringes mark injection days, whereas blood drops express retro-orbital bleeding, after treatment for future plasma level studies.

Injection of the compound led to weight loss not generally exceeding 10% weight per day and was quickly recovered (**Figure 40**). However, after several treatment rounds, mice showed aggressive behavior towards other mice and the handler. Nevertheless, the vehicle is generally well tolerated, and bi-daily treatment appeared to be the minimum recovery period for the mice.

Next, 0.5×10^6 Luciferase-GFP labeled MV-4-11 were transplanted into 11 female NGS mice for the xenograft experiment. Successful engraftment was validated 3 days after D-luciferin injection by live-cell luminescence measurement with the Caliper IVIS Lumina II Multispectral Imaging System. All 11 mice were positively engrafted and randomly assigned to both treatment arms (vehicle, **5b**) (**Figure 41**). However, one mouse showed aggressive behavior and had to be removed from the experiment.
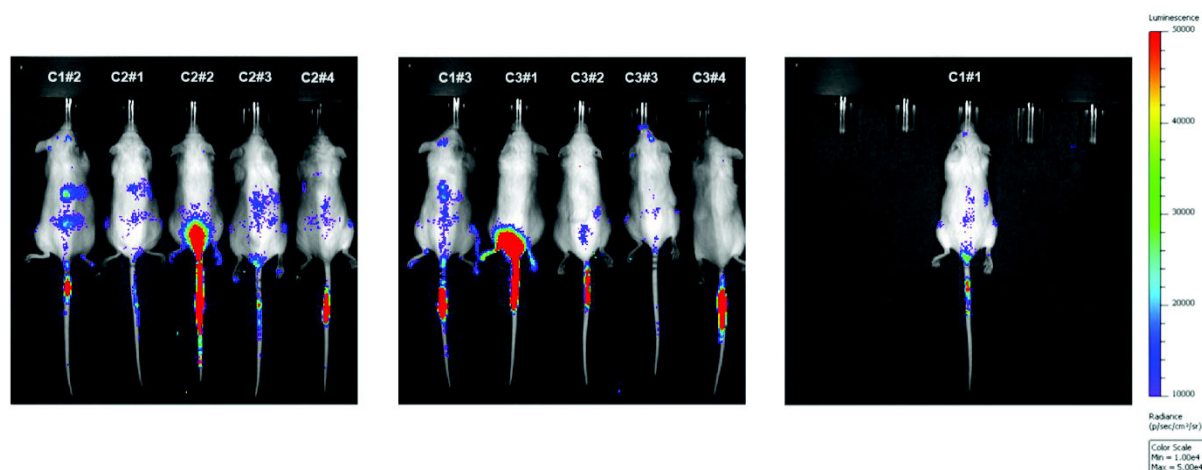
Figure 41: Engraftment validation at day 3. NGS mice were transplanted with 0.5×10^6 Luc-GFP MV-4-11 cells. After 3 days, the tumor burden was monitored with the Caliper IVIS Lumina II Multispectral Imaging System after i.p. injection of D-Luciferin firefly sodium salt monohydrate. Calculations were performed with Living Image Software.

Subsequently, engrafted mice were treated daily with 7 mg/kg **5b** or vehicle control for five consecutive days (days 4-8) (**Figure 42**). One mouse in the **5b** group died unexpectedly on day 4. On day 10, all mice showed an increased tumor burden compared to day 3, whereas no significant difference between both treatment arms was apparent (**Figure 42**). Treatment was continued with a second cycle of 7 mg/kg **5b** or vehicle for another five consecutive days (days 11-15). However, no significant difference between both treatment arms was observed. Mice were monitored and sacrificed upon reaching the humane endpoint. The resulting Kaplan-Maier survival curves did not show a significant survival benefit (p = 0.3022, Mantel-Cox test) for mice treated with **5b** (**Figure 43**).
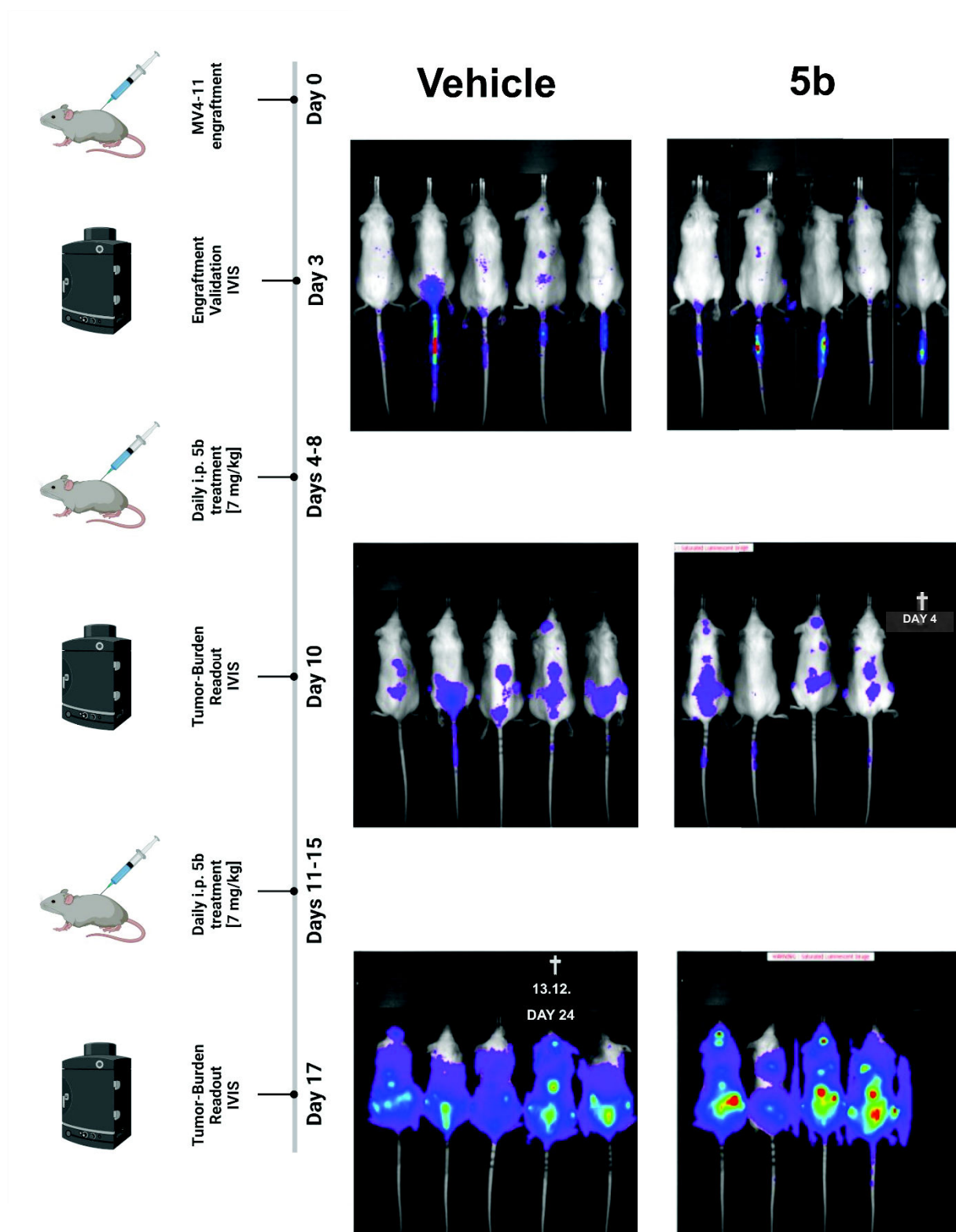
Figure 42. 5b treatment regime and tumor burden evaluation. NGS mice were transplanted with 0.5×10^6 Luc-GFP MV-4-11 cells. The engraftment was monitored after 3, 10 and 17 days with the Caliper IVIS Lumina II Multispectral Imaging System after i.p. injection of D-Luciferin firefly sodium salt monohydrate. Calculations were performed with Living Image Software. Cuts between mice pictures are due to technical reasons (fitting into one imaging chamber, or adjusting wrong mouse order after taking pictures)
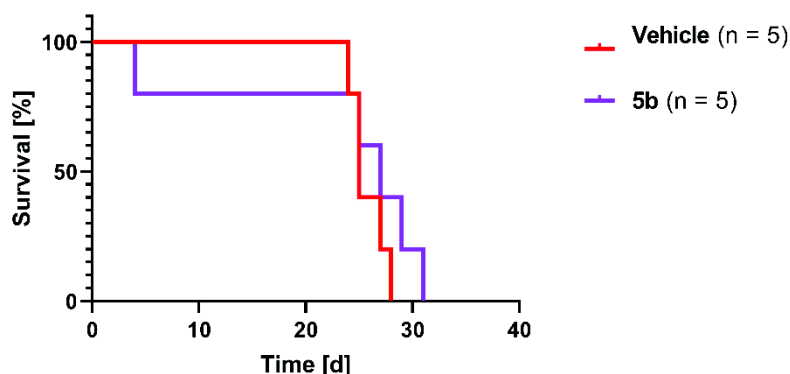
Figure 43: Kaplan-Meier survival analysis of 5b treatment regime. NGS mice were transplanted with 0.5×10^6 Luc-GFP MV-4-11 cells. Humane endpoints were determined by standardized score sheets. Kaplan-Maier Curves were performed in GraphPadPrism. No statistically significant difference p = 0.3022 (Mantel-Cox)

During the experiment, no **5b** treatment-induced weight loss or other signs of toxicity were observable besides the unexpected death (**Figure 44**).
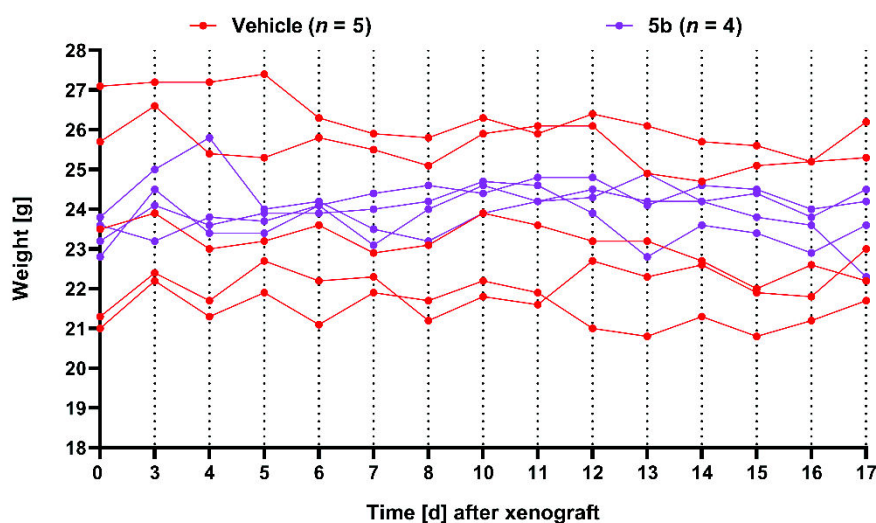
Figure 44: Evaluation of mice weight during xenograft experiment. NGS mice were transplanted with 0.5×10^6 Luc-GFP MV-4-11 cells and subjected to daily treatment of 7 mg/kg **5b** dissolved in 10/18 DRD. Mice were weighted daily to monitor toxicity effects.

In summary, **5b** and **VWK147** are potent, C-terminal specific inhibitors of the HSP90 dimerization that demonstrate efficacy in a broad spectrum of leukemic entities. In addition, **5b** showed promising effects in a zebrafish model, whereas further work and optimization are necessary to evaluate **VWK147** and **5b** in mice accurately.

4 Discussion

4.1 Elucidating the role of HSP90α and β in leukemic cells

Due to their accelerated cell cycle progression, sabotaging of DNA damage surveillance, and other safeguard mechanisms, leukemic cells depend on a high protein turnover resulting in protein instability.[102] To counteract this phenomenon and keep the protein sanity alive, many cancers increase the activity of chaperones, especially HSP90, one of the most ill-regulated chaperones. This phenomenon is called HSP90 addiction.[102] The first aim of the study was to elucidate the distinct roles of HSP90α and β in leukemic cells. Deciphering isoform-specific mechanisms is crucial as it has been shown that high HSP90α levels correlate with poor prognosis in leukemia, whereas HSP90β appears generally less exploited by cancer cells and can, depending on its localization, even facilitate tumor-suppressive functions in a leukemic context.[100,108,122] HSP90α and β expression levels are orchestrated by a complex signaling network not fully understood.[81,108,112–114] Therefore, it is pivotal to investigate the underlying mechanisms that supervise HSP90α and HSP90β expression, function, and activity.

To gain insight into this role allocation, a doxycycline-inducible shRNA-based knockdown of the HSP90 α and β isoforms was performed and validated on mRNA (**Figure 13**) and protein level (**Figure 14**). This model was complemented by constitutive HSP90 knockouts provided by *Melina Vogt*. Although increased levels of HSPA1A (HSP70) mRNA were detected upon HSP90AB1 (HSP90β) knockdown, which partly recapitulates the traditional heat shock response upon HSP90 stress,[172] HSP70 protein expression was not elevated (**Figure 17**). Discrepancies between mRNA and protein levels are common, and elevated HSP70 mRNA levels do not always result in consecutive increases in HSP70 protein.[191,192] However, HSP90 knockout partially induced an HSR on the protein level.[181] Therefore, additional investigation is needed to focus on the underlying kinetic of an HSR caused by genetic HSP90 loss.

Interestingly, the knockdown and knockout model cells maintained their total HSP90 levels upon HSP90α or HSP90β loss by overexpressing the complementary isoform, indicating a balancing mechanism stabilizing the essential HSP90 signaling (**Figure 15, Figure 16**). HSP90α overexpression upon stress and adaptation to the loss of a heat shock family member by upregulation of other family members is well described.[83,85,90,172] Traditionally, HSP90α is referred to as the inducible cytosolic

isoform of HSP90, whereas HSP90 expression is generally believed to be constitutive.[76,193] Recently, several studies have reported HSP90β induction in response to genetic-, heat-, or nutrient stress.[194–196] The demonstrated balancing mechanism indicates an additional role of inducible HSP90β to compensate for HSP90α loss. This phenomenon has to be further validated, especially in light of isoform-specific HSP90 drugs.

The investigation of HSP90 isoforms utilizing the doxycycline-inducible shRNA approach was terminated due to high doxycycline-induced side effects. Exposure of cells to doxycycline disrupts cell proliferation, apoptosis signaling, alters cell line metabolism, and impairs mitochondrial function.[197–199] Considering these effects distort cell signaling significantly, the subsequent *in vitro* and *in vivo* analysis was continued with the HSP90 KO cells.[181]

4.2 Investigation of mechanisms involved in HSP90 resistance

After the successful generation of K562 cells that are resistant to the N-terminal HSP90 inhibitor PU-H71 (PUHr) or the C-terminal inhibitor Coumermycin A1 (CAr) (**Figure 21**), the supplementary downstream analysis revealed two central mechanisms that confer resistance to HSP90 inhibitors (**Figure 45**). First, PUHr cells acquired resistance by overexpressing HSP90α through increased copy numbers of the gene locus of *HSP90AA1* (**Figure 23, Figure 27**), resulting in significantly increased levels of HSP90α protein (**Figure 23**). This overexpression of HSP90α protects cells from re-treatment with PU-H71 by stabilizing SRC and AKT, hijacking the classical RPS6 pathway in response to growth factors (**Figure 24**). It is characterized by AKT-mediated activation of mTORC1, which phosphorylates p70S6 kinase at the hallmark phosphorylation site T389 and thus activates RPS6 (**Figure 45**).[189]

Notably, SRC and AKT maturation depend on HSP90 levels, and both proteins have been implicated in reacting to HSP90 inhibition.[200–202] For example, *Koga et al.* have demonstrated that inhibition of HSP90 by geldanamycin influences the PI3K-AKT signaling axis by directly disrupting the HSP90-SRC binding, resulting in CBL-mediated recruitment of the PI3-kinase p85 subunit.[201] Also, pharmacological inhibition of HSP90 results in decreased AKT protein levels by disrupting an intracellular complex between AKT, HSP90, and Cdc37 that harbors 30% of the total AKT in untreated cells. In this complex, HSP90 protects AKT from proteasomal degradation, providing a

potential mechanism of HSP90α overexpression-driven AKT stabilization in PUHr cells.[203–205]
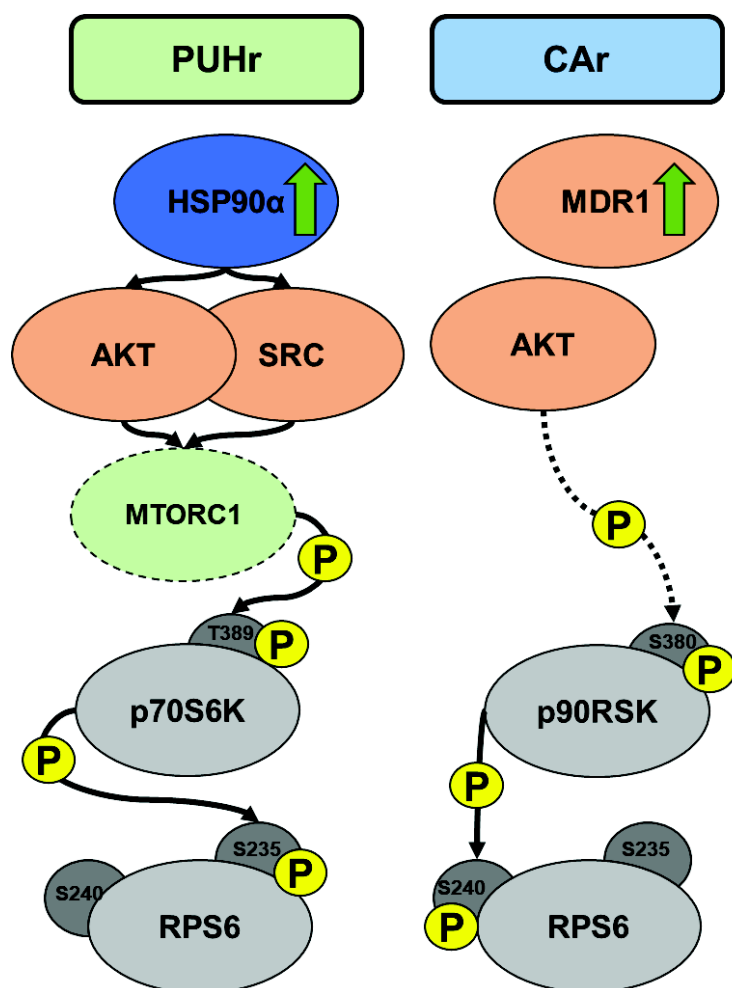
Figure 45: Modes of Kinase-mediated Resistance. Schematic overview of different modes of resistance that cells acquired upon chronic HSP90 inhibitor treatment mediated by the regulation of the kinase signaling system. Published in *Vogt & Dienstbier* et al.[181]

In addition, PUHr cells acquire mutations in the *HSP90AA1* gene resulting in an HSP90α S164F variant as evidenced by whole exome sequencing and PCR validation (**Table 11**). Purine-based inhibitors are especially susceptible to aberrations in the ATP-binding pockets since they mimic the bend conformation of ATP in the N-terminal ATP-binding site.[129,177,206] A similar mutation has been reported as a resistance mechanism to PU-H71 treatment in KRAS-mutated lung cancer affecting Y142N, the hydrogen-bond interaction partner of S164.[177] Y142N substitution led to the abrogation of this hydrogen-bond, destabilizing and disrupting HSP90 function. Nevertheless, S164F substitution will most likely not disturb the hydrogen bond interaction between Y142 and S164 since the hydrogen bonds are formed by the backbone of S164 (**Figure 25**).

Despite a different mode of action, it implies that the interaction between Y142 and S164 is vital in PU-H71 resistance acquisition and relevant across several entities. *In silico* investigation of the HSP90α S164F variant suggests no interference with the PU-H71 binding mode but affected HSP90α flexibility adjacent to the mutation site (**Figure 25**, **Figure 26**). Site-specific mutation and endogenous expression experiments will be necessary to investigate whether HSP90α S164F is sufficient to induce PU-71 resistance or if it is a supporting mechanism accompanying HSP90α overexpression. Additionally, the recombinant expression of HSP90α S164F could elucidate a potential direct disruption of PU-H71 binding measured by biochemical and biophysical validation experiments (e.g. FRET, nFP, Thermal Shift, or CETSA).

Interestingly, PU-H71-resistant cells acquire a strong overexpression of ALDH1A1, which is traditionally involved in the oxidation of ocular retinaldehyde[207] (**Figure 29**). Involvement of the retinoid pathways in leukemia and increased levels of aldehyde dehydrogenase in hematopoietic progenitor cells have been reported.[208,209] More recent studies have shown that ALDH1A1 is indeed involved in stemness characteristics of cancer cells by increasing self-renewal capabilities and cellular detoxification and can be utilized in some cancers as a marker for poor prognosis.[210–212] Notably, high levels of ALDH1A1 confer resistance against EGFR inhibition (erlotinib), chemotherapy (cisplatin), and cyclophosphamides in lung cancer, ovarian cancer, and leukemia, respectively.[213–216] Therefore, simultaneous treating cells with PU-H71 and ALDH1A1 inhibitors may be beneficial. Initial synergism experiments with ALDH1A1- and HSP90 inhibitors did not yield synergistic effects (data not shown).

However, ALDH isoenzymes are characterized by high structural similarities, making the development of isoform-specific inhibitors problematic. That results in unsatisfactory treatment outcomes accompanied by substantial toxicity and low specificity.[217] The discrepancies in the role of ALDH1A1 in different tumor entities and tissues are still controversially discussed, further complicating the topic.[210] Based on current literature, for conferring resistance in PUHr cells, two mechanisms would be imaginable: First, ALD1HA1 might mediate the oxidation of PU-H71, thus inactivating and detoxifying the cells, similar to cyclophosphamide.[210,215,216] Secondly, resistance might be facilitated by the overactivation of the retinoid pathway and consecutive downstream signaling to counteract the missing role of HSP90α.[208,210] Consequently, the mechanism of how ALDHA1A overexpression contributes to PU-H71 resistance

has to be investigated further. Like the proposed further examination of the HSP90α S164F variant, endogenous ALDHA1A overexpression models could be utilized to determine whether elevated ALDHA1A levels are sufficient to induce resistance to PU-H71 treatment or if it is a secondary effect of HSP90α overexpression.

The second mechanism of resistance utilized by Coumermycin A1 resistant cells is based on an acquired copy number gain of the ABCB1 locus (**Figure 27**), resulting in increased protein levels of the multidrug efflux pump MDR1 (**Figure 29**). However, this mechanism is not C-terminal specific since tanespimycin (17-AAG, N-terminal HSP90 inhibitor) resistant cells hijack the exact resistance mechanism (data not shown). Overexpressing the MDR1 is a well-described drug escape mechanism in leukemia.[218,219] In the context of HSP90 inhibition, MDR1-mediated resistance is predominantly reported for benzoquinone ansamycin-type inhibitors like tanespimycin, geldanamycin, and alvespimycin.[165,220,221] However, *Rouhi et al.* also reported MDR1 overexpression as a PU-H71 resistance mechanism.[177] The MDR1 promotor contains heat shock elements connecting MDR1 and HSP90 signaling. Consequently, MDR1 is frequently correlated with constitutive active HSF1, and disruption of HSF1-HSE interaction by quercetin decreases MDR1 levels re-sensitizing cells for therapy.[222–224]

In addition to this common escape mechanism, whole exome sequencing revealed a Coumermycin A1 exclusive mutation (L29F) in the N-terminal region of HSP90α. Considering that the putative binding mode of Coumermycin A1 evolves around interaction with the C-terminal and middle domain, the mutation most likely disrupts the binding of ATP to the N-terminal domain resulting in conformational inaccessibility of the C-terminal grove.[79] However, resistance mechanisms evolving around point mutations targeting the N-terminal binding domain of HSP90 are non-optimal because they decrease ATP binding affinity and thus attenuate HSP90 functionality and cell survival.[165]

Interestingly, both resistance mechanisms were accompanied by increased phosphorylation of ribosomal protein S6 (RPS6). The ribosomal protein S6 is highly conserved throughout organisms and functions as an central regulator of cell cycle progression,.[189] The role of RPS6 in cancer development, cell survival, and resistance is well described.[225–227] Overexpression of RSK isoforms has been found to induce *de novo* resistance to ganetespib *in vitro* and *in vivo*. Additionally, lung cancer cells have been re-sensitized to ganetespib treatment by p90 RSK knockdown.[188] RPS6 has five

conserved serine residues (S235, S236, S240, S244, S247). It has been proposed that these residues are phosphorylated in a strictly sequential pattern.[228–230] Both resistance models activated discrete upstream kinases with PUHr cells phosphorylating $p70S6K_{T389}$, whereas CA1r cells activate $p90RSK_{S380}$ (**Figure 30**). Subsequently, PUHr and CA1r cells phosphorylate $RPS6_{S235/236}$ and $RPS6_{S240}$, respectively (**Figure 31, Figure 45**). Differential phosphorylation of the serine sites S235 and S236 of RPS6 during heat shock in yeast,[231,232] might indicate why the HSR-inducing inhibitor PU-H71 affects those sites, while CA1 does not. p90RSK involvement in HSP90i resistance has been described in KRAS-mutant lung cancer embedded in the ERK-p90RSK-mTOR axis, which differs from the findings of this study, showing differentially regulated ERK (**Figure 24**).[188] HSP90 is involved in regulating rpS3 and RPS6 by preventing the ubiquitin-mediated degradation due to the formation of HSP90-rpS3 and HSP90-RPS6 complexes that can be disrupted by geldanamycin treatment resulting in dissociation of the complex and degradation of free RPS6.[233] Additionally, there are some efforts to exploit the reduced phosphorylation of RPS6 following HSP90 inhibition as a pharmacodynamic marker for successful HSP90inhibition (patent: WO/2007/090032). Furthermore, RSK-mediated protection of the efflux pump P-glycoprotein against proteasomal degradation is also complementing the findings on MDR1 overexpression.[234]

In summary, PUHr cells genetically overexpress mutated HSP90α S164F, resulting in enhanced SRC and AKT maturation and stabilization, which confers accelerated survival by utilizing the classical RPS6 pathway in response to growth factors. The HSP90α S164F variant and the ALD1HA1 overexpression support this mechanism. In contrast, CA1r cells elevate MDR1 levels by copy number gains of the *ABCB1* gene and acquire a supporting L29F mutation in the HSP90α N-terminus. Aberrations of the RPS6 signaling pathway accompany both mechanisms. However, drug resistance in leukemia has been demonstrated to be a multifactorial process suggesting an interplay between those mechanisms.[118,219,235]

4.3 Development of a first-in-class C-terminal inhibitor of HSP90 dimerization

Although significant progress in developing new treatment options for leukemia was achieved in the last decades, relapsed and therapy refractory leukemias are still associated with poor survival outcomes due to unsatisfactory second-line therapy

options.[44] In addition, chemotherapy and tyrosine kinase inhibitors induce extensive adverse side effects, including liver toxicity, organ failure, and vascular events, and cause poor quality of life for patients and treatment-induced mortality.[49,50] Thus, developing new therapeutic options for therapy refractory and relapsed patients is crucial.

This integrative study between the labs of *Dr. Sanil Bhatia (Department of Pediatric Oncology, Hematology and Clinical Immunology, HHU)*, *Prof. Holger Gohlke (Computational Pharmaceutical Chemistry, HHU)*, and *Prof. Thomas Kurz (Pharmaceutical and Medicinal Chemistry, HHU)* builds on recent advances in developing novel C-terminal specific HSP90 inhibitors. Those inhibitors are particularly attractive as drugs compared to classical HSP90 inhibitors because most do not induce the HSR and thus reduce the occurrence of severe side effects.[129,156,236] Therefore, this study aimed to develop a small molecule inhibitor with enhanced pharmacological drug properties compared to bulky lipophilic peptide-based peptidomimetics like AX.[97,182] Due to the integration of computational modeling, structure-activity relationship studies (SAR), extensive *in vitro* and initial *in vivo* validation, **5b** was developed as a first-in-class C-terminal inhibitor of the HSP90 dimerization interface.

Concentration-dependent cell viability and KD assessment of different tripyrimidonamide analogs revealed that **5b** is the most potent candidate of all synthesized compounds (**Figure 32**). Next, the engagement of **5b** and **VWK147** with HSP90 was validated by DARTS, thermal shift assay, CETSA, and ITDFR$_{CETSA}$ (**Figure 36, Figure 37**). Additionally, it was confirmed that **5b** and **VWK147** engage the HSP90 C-terminus without unspecific N-terminal interaction by combining an N-terminal specific competitive fluorescence polarization assay (**Figure 35**) and a C-terminal specific time-resolved FRET (**Figure 34**). However, identifying the binding pocket of **5b** or **VWK147** in the C-terminus of HSP90 **5b** remains elusive. A literature review of HSP90 inhibitors suggests four potential target sites in the HSP90 C-terminus: A C-terminal ATP binding site, the MEEVD motif, the dimerization interface, and a region between the MD and CTD in proximity to the NTD that mediates potential allosteric effects.[129,237–239]. Consequently, high-resolution binding studies, mutational/truncation studies, and, ideally, co-crystal structures will be necessary to elucidate **5b**'s C-terminal binding pocket. However, initial co-crystalization attempts of **5b** with the HSP90 CTD were unsuccessful (data not shown). Considering the two ATP binding

sites (N- and C-terminal) in HSP90 are structurally highly similar, it is challenging to design drugs that preferentially target the N- or C-terminal ATP pocket. However, the N-terminal ATP binding site (NTD) prefers adenine derivates, whereas the C-terminal site is more specific for purine and pyrimidine nucleotides opening the possibility for site-specific drug interactions.[240] Targeting the MEEVD motif as a potential binding site to disrupt the HSP90 dimerization may also be promising.[79] The novelty of this study was driven by developing a first-in-class inhibitor of C-terminal mediated HSP90 dimerization. Therefore, **5b** and **VWK17** are rationally designed to target the dimerization interface based on hot-spot predictions made by the working group of *Prof. Holger Gohlke* also utilized in the prototype compound AX.[97,157,159,241]

Understanding HSP90 dimerization remains incomplete because of the complex co-chaperone dynamics and the conformational cycle of HSP90.[97,242] Therefore, experimentally validating the disruption of dimerization was emphasized. The complementary results of the auto display dimerization assay established by AG Jose, BS[3] crosslinker assay (*Melina Vogt*), size exclusion chromatography small-angle X-ray scattering (SEC-SAXS) by AG Smits and MD simulations by AG Gohlke based on previous investigations [97,243–245] validated dimerization disruption from different angels and taken together provided significant evidence of successful disruption of HSP90 dimerization.[182]

N-terminal HSP90 inhibitors often acquire dose-limiting toxicity based on induction of the heat shock response resulting in overexpression of cognate chaperones like HSP70 and HSP27. However, it is not yet completely understood why C-terminal inhibitors tend not to induce HSR.[186,246] Interestingly, there is a discrepancy between the efficacy of N-terminal HSP90 inhibitors in cell viability and biochemical binding assays (sub-nanomolar vs. sub-micromolar concentrations) indicating potential off-targets effects that confer this cytotoxicity.[168,247,248] Further work will be necessary to elucidate what characteristics of a novel drug confer HSR induction.

Considering the low overall solubility of peptidomimetics and **5b**, preparation for *in vivo* studies required extensive research for *in vivo* applicable formulations. Thus, significant effort was put into developing and testing different vehicle formulations to overcome the solubility limitations of **5b**. Finally, the emulsifier Kolliphor RH40 in a 10/18 DRD (10% DMSO, 18% RH40, 3.6% dextrose, water) formulation was adapted[180], and **5b** solubility was further improved by a combination of dilution series,

heat-application, and ultra-sonification. After ensuring sufficient stability of **5b** in aqueous solutions, the compound was evaluated in a zebrafish T-ALL engraftment model by AG Bagjohli. Overall, **5b** showed promising anti-leukemic effects with low unspecific toxicity (**Figure 39**). Next, **5b** was tested in a mouse xenograft model with BCR-ABL1 positive CML cells (**Figure 42**). Unfortunately, although **5b** treatment did not induce any toxic side effects and was well tolerated (**Figure 44**), it was also ineffective in reducing tumor burden (**Figure 42**) or improving overall survival (**Figure 43**). These underwhelming results are most likely caused by low dosage (7 mg/kg) application due to solubility limitations compared to other HSP90 inhibitors customarily used at 25 mg/kg or higher.[180] In summary, **5b** is a promising first-in-class compound, achieved by interdisciplinary teamwork, that can be used together with the optimized **VWK147** as a milestone to design more advanced compounds disrupting C-terminal mediated dimerization of HSP90.

HSP90 inhibitors are an attractive therapeutic target with promising initial results in clinical trials laying the foundation for further progression and development in this field. However, HSP90 inhibitors show underwhelming results in monotherapy usage, characterized by significant limitations, including solubility and stability issues, hepato- and ocular toxicity, and the development of resistance.[164] Nevertheless, many cancers are highly addicted to HSP90. In addition, many cancer cells depend on an HSP90 super-chaperone complex preferentially targeted by HSP90 drugs and not present in healthy cells. Both differences open up potential therapeutic windows to specifically target malignant cells. In addition, new interest in HSP90 drugs in cancers is sparked by "undruggable" proteins like KRAS and c-Myc.[164,249]

Given the obstacles HSP90 drug monotherapy faces in clinical trials, recent advances utilize HSP90 inhibitors as a complementary therapy in highly treatment-resistant cancer entities to overcome drug resistance or sensitize to chemo- or targeted therapy. For example, it has been shown that treating BCR-ABL1 positive leukemic cells with geldanamycin synergistically induces apoptosis upon doxorubicin and paclitaxel treatment, enabling reduced chemotherapy dosage.[250] Furthermore, c-kit mutated AML cells can be sensitized to imatinib treatment utilizing HSP90 inhibitors.[251] Simultaneous treatment of KRAS-mutant lung cancer with HSP90 inhibitors in combination with mTOR, PI3K, ERK, or p90RSK drugs demonstrated promising effects in xenograft and cellular models.[188,252,253] In clinical trials, ganetespib or Auy922

sensitize Her2/Erb2 overexpressing breast cancer against trastuzumab treatment, resulting in an overall reduced tumor burden.[254,255] Similar studies have been performed in epidermal growth factor receptor (EGFR) mutant lung cancers to investigate erlotinib-AUY922 combination treatment. Despite achieving a partial response in some patients, the trial was terminated due to limiting toxicities, including night blindness.[256] Furthermore, targeting HSP90 and histone deacetylases (HDACs) has documented synergistic effects considering they mutually orchestrate protein homeostasis and the proteasome machinery.[257] This is based on the bilateral regulation of both proteins. HDAC6 acetylates HSP90 at critical lysine sites, including K294, whereas HSP90 mediates the stabilization and maturation of HDAC6 and HDAC1.[257–259] Changes in HSP90 acetylation can disrupt co-chaperone interactions and enhance the depletion of downstream survival factors enabling utilization of both drugs at lower concentrations.[260,261]

Another unique and novel mechanism of HSP90 inhibition is the deliberate induction of HSP90 cleavage. Various conditions, including HDAC inhibitors like vorinostat, proteasome inhibitors like MG132, or other chemicals, have been reported to induce HSP90 cleavage.[163] Most of these mechanisms evolve around an increase in reactive oxygen species (ROS) that cause caspase-mediated hydrolysis of HSP90 and thus disrupt downstream survival signaling in highly resistant tumor entities.[262–264] Indeed, over two decades ago, *Gorman et al.* demonstrated the importance of ROS in HSP and HSF1 signaling by treating cells with antioxidants resulting in attenuated HSP levels in leukemic cells.[265] Interestingly, the ROS-dependent HSP90 hydrolysis mechanism seems selective for tumor cells and does not affect healthy cells due to differences in the microenvironment and oxidative stress mechanism of tumor entities compared to healthy tissue.[266,267] However, the clinical implication of deliberate HSP90 cleavage is unknown since this mechanism has been studied solely *in vitro* and requires additional research.

In summary, further research will focus on the development of highly specific HSP90 inhibitors and utilizing them as sensitizers in combination with additional agents targeting cancer-specific signaling axis to overcome acquired resistance and decrease treatment-associated side effects,

4.4 Outlook:

The role of HSP90α and β loss must be investigated in an *in vivo* context. Therefore, further experiments included a mouse xenograft model with HSP90α and β knockout and implications on mouse tumor burden and survival. Follow-up experiments should decipher the complex involved kinetic orchestrated by co-chaperone regulation. In addition, the kinetic should yield further insights into HSP90 loss-induced heat shock response in a genetic context.

Furthermore, both proposed resistance mechanisms to HSP90 inhibition described in this study need further investigation. Since point mutations are a favored tool of cancer cells to circumvent treatment pressure[268], thorough characterization of the reported single nucleotide polymorphism will be necessary. Exogenous and endogenous expression of HSP90α (p.S164F) and HSP90α L29F variants utilizing site-specific mutations in HSP90α knock out cancer cells elucidate whether these acquired SNPs are sufficient to reduce the efficacy of PU-H71 and coumermycin A1 treatment. In addition, mutation and truncation studies targeting similar regions could help enlighten drug resistance and decipher the binding modes of HSP90 drugs. On top of that, the correlation of ALDH1A1 overexpression and differential phosphorylation of ribosomal protein S6 as a resistance mechanism to HSP90 stress should be addressed in further projects, focusing on the regulatory machinery involved. All reported findings must be reproduced in additional BCR-ABL1 positive leukemic cell lines.

The effectiveness of **5b** in cells harboring clinically relevant BCR-ABL1 mutations of refractory or relapse patient leukemia cells was demonstrated.[269,270] This potentially enables the utilization of **5b**-based advanced compounds as a secondary or tertiary treatment after TKI inhibitors fail or to overcome TKI-induced mutations in BCR-ABL1.[269] However, significant optimization of pharmacokinetic properties, and further improvements in specificity and potency are necessary to lay the foundation for extensive *in vivo* studies. In addition, structure-activity relationship (SAR) studies must be performed to enhance specificity and potency to achieve this optimization. Therefore, AG Kurz is developing 3rd generation HSP90 inhibitors based on a bispyrimidonamide scaffold with improved solubility in aqueous solvents, maintaining potency and specificity. Interestingly, initial experiments with **5b** and **VWK147** showed promising efficacy in PU-H71-resistant or Coumermycin A1-resistant cell lines.

5 References

1. BioRender.com. Blood Cancers. Available at https://app.biorender.com/biorender-templates (2022).

2. Sawyers, C. L., Denny, C. T. & Witte, O. N. Leukemia and the disruption of normal hematopoiesis. *Cell* **64,** 337–350; 10.1016/0092-8674(91)90643-D (1991).

3. Monroe, J. G. & Dorshkind, K. Fate decisions regulating bone marrow and peripheral B lymphocyte development. *Advances in immunology* **95,** 1–50; 10.1016/S0065-2776(07)95001-4 (2007).

4. Shlush, L. I. *et al.* Identification of pre-leukemic hematopoietic stem cells in acute leukemia. *Nature* **506,** 328–333; 10.1038/nature13038 (2014).

5. Alexander, T. B. & Mullighan, C. G. Molecular Biology of Childhood Leukemia. *Annu. Rev. Cancer Biol.* **5,** 95–117; 10.1146/annurev-cancerbio-043020-110055 (2021).

6. Greaves, M. & Janossy, G. Patterns of gene expression and the cellular origins of human leukaemias. *Biochimica et biophysica acta* **516,** 193–230; 10.1016/0304-419X(78)90008-2 (1978).

7. Hutter, J. J. Childhood leukemia. *Pediatrics in review* **31,** 234–241; 10.1542/pir.31-6-234 (2010).

8. Döhner, H., Weisdorf, D. J. & Bloomfield, C. D. Acute Myeloid Leukemia. *The New England journal of medicine* **373,** 1136–1152; 10.1056/NEJMra1406184 (2015).

9. Cui, P. *et al.* Leukemia cells impair normal hematopoiesis and induce functionally loss of hematopoietic stem cells through immune cells and inflammation. *Leukemia Research* **65,** 49–54; 10.1016/j.leukres.2018.01.002 (2018).

10. Minciacchi, V. R., Kumar, R. & Krause, D. S. Chronic Myeloid Leukemia: A Model Disease of the Past, Present and Future. *Cells* **10**; 10.3390/cells10010117 (2021).

11. Khoury, J. D. *et al.* The 5th edition of the World Health Organization Classification of Haematolymphoid Tumours: Myeloid and Histiocytic/Dendritic Neoplasms. *Leukemia* **36,** 1703–1719; 10.1038/s41375-022-01613-1 (2022).

12. Ward, E., DeSantis, C., Robbins, A., Kohler, B. & Jemal, A. Childhood and adolescent cancer statistics, 2014. *CA: a cancer journal for clinicians* **64,** 83–103; 10.3322/caac.21219 (2014).

13. Bolouri, H. *et al.* The molecular landscape of pediatric acute myeloid leukemia reveals recurrent structural alterations and age-specific mutational interactions. *Nature medicine* **24,** 103–112; 10.1038/nm.4439 (2018).

14. Wiemels, J. L. *et al.* In utero origin of t(8;21) AML1-ETO translocations in childhood acute myeloid leukemia. *Blood* **99,** 3801–3805; 10.1182/blood.v99.10.3801 (2002).

15. Mori, H. *et al.* Chromosome translocations and covert leukemic clones are generated during normal fetal development. *Proc. Natl. Acad. Sci. U.S.A.* **99,** 8242–8247; 10.1073/pnas.112218799 (2002).

16. Andersson, A. K. *et al.* The landscape of somatic mutations in infant MLL-rearranged acute lymphoblastic leukemias. *Nature genetics* **47,** 330–337; 10.1038/ng.3230 (2015).

17. Schäfer, D. *et al.* Five percent of healthy newborns have an ETV6-RUNX1 fusion as revealed by DNA-based GIPFEL screening. *Blood* **131,** 821–826; 10.1182/blood-2017-09-808402 (2018).

18. Hauer, J., Martín-Lorenzo, A. & Sánchez-García, I. Infection causes childhood leukemia. *Aging (Albany NY)* **7,** 607–608 (2015).

19. Kinlen, L. J. Epidemiological evidence for an infective basis in childhood leukaemia. *Br J Cancer* **71,** 1–5; 10.1038/bjc.1995.1 (1995).

20. Greaves, M. F. & Alexander, F. E. An infectious etiology for common acute lymphoblastic leukemia in childhood? *Leukemia* **7,** 349–360 (1993).

21. Bartenhagen, C. *et al.* Infection as a cause of childhood leukemia: virus detection employing whole genome sequencing. *Haematologica* **102,** e179-83; 10.3324/haematol.2016.155382 (2017).

22. Martín-Lorenzo, A. *et al.* Infection Exposure is a Causal Factor in B-cell Precursor Acute Lymphoblastic Leukemia as a Result of Pax5-Inherited Susceptibility. *Cancer Discovery* **5,** 1328–1343; 10.1158/2159-8290.CD-15-0892 (2015).

23. Rodríguez-Hernández, G. *et al.* Infection Exposure Promotes ETV6-RUNX1 Precursor B-cell Leukemia via Impaired H3K4 Demethylases. *Cancer Res* **77,** 4365–4377; 10.1158/0008-5472.CAN-17-0701 (2017).

24. Rowley, J. D. Letter: A new consistent chromosomal abnormality in chronic myelogenous leukaemia identified by quinacrine fluorescence and Giemsa staining. *Nature* **243,** 290–293; 10.1038/243290a0 (1973).

25. Groffen, J. *et al.* Philadelphia chromosomal breakpoints are clustered within a limited region, bcr, on chromosome 22. *Cell* **36,** 93–99; 10.1016/0092-8674(84)90077-1 (1984).

26. Heisterkamp, N. *et al.* Localization of the c-ab1 oncogene adjacent to a translocation break point in chronic myelocytic leukaemia. *Nature* **306,** 239–242; 10.1038/306239a0 (1983).

27. Jain, P. *et al.* Impact of BCR-ABL transcript type on outcome in patients with chronic-phase CML treated with tyrosine kinase inhibitors. *Blood* **127,** 1269–1275; 10.1182/blood-2015-10-674242 (2016).

28. Stam, K. *et al.* Evidence of a new chimeric bcr/c-abl mRNA in patients with chronic myelocytic leukemia and the Philadelphia chromosome. *The New England journal of medicine* **313,** 1429–1433; 10.1056/NEJM198512053132301 (1985).

29. Pluk, H., Dorey, K. & Superti-Furga, G. Autoinhibition of c-Abl. *Cell* **108,** 247–259; 10.1016/S0092-8674(02)00623-2 (2002).

30. Muller, A. J. *et al.* BCR first exon sequences specifically activate the BCR/ABL tyrosine kinase oncogene of Philadelphia chromosome-positive human leukemias. *Mol. Cell. Biol.* **11,** 1785–1792; 10.1128/MCB.11.4.1785 (1991).

31. Daley, G. Q., van Etten, R. A. & Baltimore, D. Induction of chronic myelogenous leukemia in mice by the P210bcr/abl gene of the Philadelphia chromosome. *Science* **247,** 824–830; 10.1126/science.2406902 (1990).

32. Steelman, L. S. *et al.* Contributions of the Raf/MEK/ERK, PI3K/PTEN/Akt/mTOR and Jak/STAT pathways to leukemia. *Leukemia* **22,** 686–707; 10.1038/leu.2008.26 (2008).

33. Ilaria, R. L. & van Etten, R. A. P210 and P190(BCR/ABL) induce the tyrosine phosphorylation and DNA binding activity of multiple specific STAT family members. *Journal of Biological Chemistry* **271,** 31704–31710; 10.1074/jbc.271.49.31704 (1996).

34. Moriggl, R. *et al.* Stat5 tetramer formation is associated with leukemogenesis. *Cancer cell* **7,** 87–99; 10.1016/j.ccr.2004.12.010 (2005).

35. Franke, T. F., Kaplan, D. R. & Cantley, L. C. PI3K: Downstream AKTion Blocks Apoptosis. *Cell* **88,** 435–437; 10.1016/S0092-8674(00)81883-8 (1997).

36. Skorski, T. *et al.* Phosphatidylinositol-3 kinase activity is regulated by BCR/ABL and is required for the growth of Philadelphia chromosome-positive cells. *Blood* **86,** 726–736; 10.1182/blood.V86.2.726.bloodjournal862726 (1995).

37. Sawyers, C. L., McLaughlin, J. & Witte, O. N. Genetic requirement for Ras in the transformation of fibroblasts and hematopoietic cells by the Bcr-Abl oncogene. *The Journal of experimental medicine* **181,** 307–313; 10.1084/jem.181.1.307 (1995).

38. Ye, D., Wolff, N., Li, L., Zhang, S. & Ilaria, R. L. STAT5 signaling is required for the efficient induction and maintenance of CML in mice. *Blood* **107,** 4917–4925; 10.1182/blood-2005-10-4110 (2006).

39. Agarwal, A. *et al.* BCR-ABL1 promotes leukemia by converting p27 into a cytoplasmic oncoprotein. *Blood* **124,** 3260–3273; 10.1182/blood-2013-04-497040 (2014).

40. Jonuleit, T. *et al.* Bcr-Abl kinase down-regulates cyclin-dependent kinase inhibitor p27 in human and murine cell lines. *Blood* **96,** 1933–1939 (2000).

41. Konopka, J. B., Watanabe, S. M. & Witte, O. N. An alteration of the human c-abl protein in K562 leukemia cells unmasks associated tyrosine kinase activity. *Cell* **37,** 1035–1042; 10.1016/0092-8674(84)90438-0 (1984).

42. Ben-Neriah, Y., Daley, G. Q., Mes-Masson, A. M., Witte, O. N. & Baltimore, D. The chronic myelogenous leukemia-specific P210 protein is the product of the bcr/abl hybrid gene. *Science* **233,** 212–214; 10.1126/science.3460176 (1986).

43. Lugo, T. G., Pendergast, A. M., Muller, A. J. & Witte, O. N. Tyrosine kinase activity and transformation potency of bcr-abl oncogene products. *Science* **247,** 1079–1082; 10.1126/science.2408149 (1990).

44. Drozdov, D., Bonaventure, A., Nakata, K., Suttorp, M. & Belot, A. Temporal trends in the proportion of "cure" in children, adolescents, and young adults diagnosed with chronic myeloid leukemia in England: A population-based study. *Pediatric blood & cancer* **65,** e27422; 10.1002/pbc.27422 (2018).

45. Druker, B. J. *et al.* Activity of a specific inhibitor of the BCR-ABL tyrosine kinase in the blast crisis of chronic myeloid leukemia and acute lymphoblastic leukemia with the Philadelphia chromosome. *The New England journal of medicine* **344,** 1038–1042; 10.1056/NEJM200104053441402 (2001).

46. Reddy, E. P. & Aggarwal, A. K. The ins and outs of bcr-abl inhibition. *Genes & cancer* **3,** 447–454; 10.1177/1947601912462126 (2012).

47. Hochhaus, A. *et al.* European LeukemiaNet 2020 recommendations for treating chronic myeloid leukemia. *Leukemia* **34,** 966–984; 10.1038/s41375-020-0776-2 (2020).

48. Smith, S. M., Hijiya, N. & Sakamoto, K. M. Chronic Myelogenous Leukemia in Childhood. *Current oncology reports* **23,** 40; 10.1007/s11912-021-01025-x (2021).

49. Williams, L. A. *et al.* Measuring the symptom burden associated with the treatment of chronic myeloid leukemia. *Blood* **122,** 641–647; 10.1182/blood-2013-01-477687 (2013).

50. Efficace, F. *et al.* Health-related quality of life in chronic myeloid leukemia patients receiving long-term therapy with imatinib compared with the general population. *Blood* **118,** 4554–4560; 10.1182/blood-2011-04-347575 (2011).

51. Chai-Adisaksopha, C., Lam, W. & Hillis, C. Major arterial events in patients with chronic myeloid leukemia treated with tyrosine kinase inhibitors: a meta-analysis. *Leukemia & lymphoma* **57,** 1300–1310; 10.3109/10428194.2015.1091929 (2016).

52. Wieczorek, A. & Uharek, L. Management of Chronic Myeloid Leukemia Patients Resistant to Tyrosine Kinase Inhibitors Treatment. *Biomarker insights* **10,** 49–54; 10.4137/BMI.S22431 (2015).

53. Ursan, I. D. *et al.* Emergence of BCR-ABL kinase domain mutations associated with newly diagnosed chronic myeloid leukemia: a meta-analysis of clinical trials of tyrosine kinase inhibitors. *Journal of managed care & specialty pharmacy* **21,** 114–122; 10.18553/jmcp.2015.21.2.114 (2015).

54. Vetrie, D., Helgason, G. V. & Copland, M. The leukaemia stem cell: similarities, differences and clinical prospects in CML and AML. *Nature reviews. Cancer* **20,** 158–173; 10.1038/s41568-019-0230-9 (2020).

55. Herrmann, H. *et al.* Dipeptidylpeptidase IV (CD26) defines leukemic stem cells (LSC) in chronic myeloid leukemia. *Blood* **123,** 3951–3962; 10.1182/blood-2013-10-536078 (2014).

56. Landberg, N. *et al.* CD36 defines primitive chronic myeloid leukemia cells less responsive to imatinib but vulnerable to antibody-based therapeutic targeting. *Haematologica* **103,** 447–455; 10.3324/haematol.2017.169946 (2018).

57. Kinstrie, R. *et al.* CD93 is expressed on chronic myeloid leukemia stem cells and identifies a quiescent population which persists after tyrosine kinase inhibitor therapy. *Leukemia* **34,** 1613–1625; 10.1038/s41375-019-0684-5 (2020).

58. Jamieson, C. H. M. *et al.* Granulocyte-macrophage progenitors as candidate leukemic stem cells in blast-crisis CML. *The New England journal of medicine* **351,** 657–667; 10.1056/NEJMoa040258 (2004).

59. Neviani, P. *et al.* PP2A-activating drugs selectively eradicate TKI-resistant chronic myeloid leukemic stem cells. *The Journal of clinical investigation* **123,** 4144–4157; 10.1172/JCI68951 (2013).

60. Branford, S. *et al.* Detection of BCR-ABL mutations in patients with CML treated with imatinib is virtually always accompanied by clinical resistance, and mutations in the ATP phosphate-binding loop (P-loop) are associated with a poor prognosis. *Blood* **102,** 276–283; 10.1182/blood-2002-09-2896 (2003).

61. Cowan-Jacob, S. W. *et al.* Structural biology contributions to the discovery of drugs to treat chronic myelogenous leukaemia. *Acta crystallographica. Section D, Biological crystallography* **63,** 80–93; 10.1107/S0907444906047287 (2007).

62. Skora, L., Mestan, J., Fabbro, D., Jahnke, W. & Grzesiek, S. NMR reveals the allosteric opening and closing of Abelson tyrosine kinase by ATP-site and myristoyl pocket inhibitors. *Proc. Natl. Acad. Sci. U.S.A.* **110,** E4437-45; 10.1073/pnas.1314712110 (2013).

63. Jabbour, E. *et al.* Characteristics and outcomes of patients with chronic myeloid leukemia and T315I mutation following failure of imatinib mesylate therapy. *Blood* **112,** 53–55; 10.1182/blood-2007-11-123950 (2008).

64. Cortes, J. E. *et al.* Ponatinib in refractory Philadelphia chromosome-positive leukemias. *The New England journal of medicine* **367,** 2075–2088; 10.1056/NEJMoa1205127 (2012).

65. Taipale, M. *et al.* Quantitative analysis of HSP90-client interactions reveals principles of substrate recognition. *Cell* **150,** 987–1001; 10.1016/j.cell.2012.06.047 (2012).

66. Lindquist, S. & Craig, E. A. The heat-shock proteins. *Annual review of genetics* **22,** 631–677; 10.1146/annurev.ge.22.120188.003215 (1988).

67. Dollins, D. E., Warren, J. J., Immormino, R. M. & Gewirth, D. T. Structures of GRP94-nucleotide complexes reveal mechanistic differences between the hsp90 chaperones. *Molecular cell* **28,** 41–56; 10.1016/j.molcel.2007.08.024 (2007).

68. Shiau, A. K., Harris, S. F., Southworth, D. R. & Agard, D. A. Structural Analysis of E. coli hsp90 reveals dramatic nucleotide-dependent conformational rearrangements. *Cell* **127,** 329–340; 10.1016/j.cell.2006.09.027 (2006).

69. Harris, S. F., Shiau, A. K. & Agard, D. A. The crystal structure of the carboxy-terminal dimerization domain of htpG, the Escherichia coli Hsp90, reveals a potential substrate binding site. *Structure (London, England : 1993)* **12,** 1087–1097; 10.1016/j.str.2004.03.020 (2004).

70. Prodromou, C. *et al.* Identification and Structural Characterization of the ATP/ADP-Binding Site in the Hsp90 Molecular Chaperone. *Cell* **90,** 65–75; 10.1016/s0092-8674(00)80314-1 (1997).

71. Grenert, J. P. *et al.* The amino-terminal domain of heat shock protein 90 (hsp90) that binds geldanamycin is an ATP/ADP switch domain that regulates hsp90 conformation. *Journal of Biological Chemistry* **272,** 23843–23850; 10.1074/jbc.272.38.23843 (1997).

72. Stebbins, C. E. *et al.* Crystal Structure of an Hsp90–Geldanamycin Complex: Targeting of a Protein Chaperone by an Antitumor Agent. *Cell* **89,** 239–250; 10.1016/S0092-8674(00)80203-2 (1997).

73. Cadepond, F. *et al.* Interaction of glucocorticosteroid receptor and wild-type or mutated 90-kDa heat shock protein coexpressed in baculovirus-infected Sf9 cells. *Proc. Natl. Acad. Sci. U.S.A.* **90,** 10434–10438; 10.1073/pnas.90.22.10434 (1993).

74. Realini, C., Rogers, S. W. & Rechsteiner, M. KEKE motifs. *FEBS letters* **348,** 109–113; 10.1016/0014-5793(94)00569-9 (1994).

75. Szyszka, R., Kramer, G. & Hardesty, B. The phosphorylation state of the reticulocyte 90-kDa heat shock protein affects its ability to increase phosphorylation of peptide initiation factor 2 alpha subunit by the heme-sensitive kinase. *Biochemistry* **28,** 1435–1438; 10.1021/bi00430a001 (1989).

76. Csermely, P., Schnaider, T., So″ti, C., Prohászka, Z. & Nardai, G. The 90-kDa Molecular Chaperone Family. *Pharmacology & Therapeutics* **79,** 129–168; 10.1016/S0163-7258(98)00013-8 (1998).

77. Louvion, J. F., Warth, R. & Picard, D. Two eukaryote-specific regions of Hsp82 are dispensable for its viability and signal transduction functions in yeast. *Proc. Natl. Acad. Sci. U.S.A.* **93,** 13937–13942; 10.1073/pnas.93.24.13937 (1996).

78. Hessling, M., Richter, K. & Buchner, J. Dissection of the ATP-induced conformational cycle of the molecular chaperone Hsp90. *Nature structural & molecular biology* **16,** 287–293; 10.1038/nsmb.1565 (2009).

79. Schopf, F. H., Biebl, M. M. & Buchner, J. The HSP90 chaperone machinery. *Nat Rev Mol Cell Biol* **18,** 345–360; 10.1038/nrm.2017.20 (2017).

80. Buchner, J. Hsp90 & Co. - a holding for folding. *Trends in Biochemical Sciences* **24,** 136–141; 10.1016/s0968-0004(99)01373-0 (1999).

81. Sreedhar, A. S., Kalmár, E., Csermely, P. & Shen, Y.-F. Hsp90 isoforms: functions, expression and clinical importance. *FEBS letters* **562,** 11–15; 10.1016/s0014-5793(04)00229-7 (2004).

82. Gupta, R. S. Phylogenetic analysis of the 90 kD heat shock family of protein sequences and an examination of the relationship among animals, plants, and fungi species. *Molecular biology and evolution* **12,** 1063–1073; 10.1093/oxfordjournals.molbev.a040281 (1995).

83. Zuehlke, A. D., Beebe, K., Neckers, L. & Prince, T. Regulation and function of the human HSP90AA1 gene. *Gene* **570,** 8–16; 10.1016/j.gene.2015.06.018 (2015).

84. Rebbe, N. F., Hickman, W. S., Ley, T. J., Stafford, D. W. & Hickman, S. Nucleotide sequence and regulation of a human 90-kDa heat shock protein gene. *Journal of Biological Chemistry* **264,** 15006–15011 (1989).

85. Zhang, S. L. *et al.* Regulation of human hsp90alpha gene expression. *FEBS letters* **444,** 130–135; 10.1016/s0014-5793(99)00044-7 (1999).

86. Ciocca, D. R., Arrigo, A. P. & Calderwood, S. K. Heat shock proteins and heat shock factor 1 in carcinogenesis and tumor development: an update. *Archives of toxicology* **87,** 19–48; 10.1007/s00204-012-0918-z (2013).

87. Muller, P. *et al.* C-terminal phosphorylation of Hsp70 and Hsp90 regulates alternate binding to co-chaperones CHIP and HOP to determine cellular protein folding/degradation balances. *Oncogene* **32,** 3101–3110; 10.1038/onc.2012.314 (2013).

88. Quanz, M. *et al.* Heat shock protein 90α (Hsp90α) is phosphorylated in response to DNA damage and accumulates in repair foci. *The Journal of biological chemistry* **287,** 8803–8815; 10.1074/jbc.M111.320887 (2012).

89. Toma-Jonik, A., Vydra, N., Janus, P. & Widłak, W. Interplay between HSF1 and p53 signaling pathways in cancer initiation and progression: non-oncogene and oncogene addiction. *Cellular oncology (Dordrecht)* **42,** 579–589; 10.1007/s13402-019-00452-0 (2019).

90. Craig, E. A. The heat shock response. *CRC critical reviews in biochemistry* **18,** 239–280; 10.3109/10409238509085135 (1985).

91. Zou, J., Guo, Y., Guettouche, T., Smith, D. F. & Voellmy, R. Repression of heat shock transcription factor HSF1 activation by HSP90 (HSP90 complex) that forms a stress-sensitive complex with HSF1. *Cell* **94,** 471–480; 10.1016/s0092-8674(00)81588-3 (1998).

92. Guettouche, T., Boellmann, F., Lane, W. S. & Voellmy, R. Analysis of phosphorylation of human heat shock factor 1 in cells experiencing a stress. *BMC biochemistry* **6,** 4; 10.1186/1471-2091-6-4 (2005).

93. Kampinga, H. H. *et al.* Guidelines for the nomenclature of the human heat shock proteins. *Cell stress & chaperones* **14,** 105–111; 10.1007/s12192-008-0068-7 (2009).

94. Woessner, D. W. *et al.* A coiled-coil mimetic intercepts BCR-ABL1 dimerization in native and kinase-mutant chronic myeloid leukemia. *Leukemia* **29,** 1668–1675; 10.1038/leu.2015.53 (2015).

95. Huang, Z.-L. *et al.* Induction of apoptosis by directing oncogenic Bcr-Abl into the nucleus. *Oncotarget* **4,** 2249–2260; 10.18632/oncotarget.1339 (2013).

96. Li, Q. *et al.* Blockade of Y177 and Nuclear Translocation of Bcr-Abl Inhibits Proliferation and Promotes Apoptosis in Chronic Myeloid Leukemia Cells. *International journal of molecular sciences* **18**; 10.3390/ijms18030537 (2017).

97. Bhatia, S. *et al.* Targeting HSP90 dimerization via the C terminus is effective in imatinib-resistant CML and lacks the heat shock response. *Blood* **132,** 307–320; 10.1182/blood-2017-10-810986 (2018).

98. Nimmanapalli, R., O'Bryan, E. & Bhalla, K. Geldanamycin and its analogue 17-allylamino-17-demethoxygeldanamycin lowers Bcr-Abl levels and induces apoptosis and differentiation of Bcr-Abl-positive human leukemic blasts. *Cancer Res* **61,** 1799–1804 (2001).

99. Wu, L. X. *et al.* Disruption of the Bcr-Abl/Hsp90 protein complex: a possible mechanism to inhibit Bcr-Abl-positive human leukemic blasts by novobiocin. *Leukemia* **22,** 1402–1409; 10.1038/leu.2008.89 (2008).

100. Peng, Y. *et al.* Effect of HSP90AB1 and CC domain interaction on Bcr-Abl protein cytoplasm localization and function in chronic myeloid leukemia cells. *Cell communication and signaling : CCS* **19,** 71; 10.1186/s12964-021-00752-9 (2021).

101. Echeverría, P. C., Bernthaler, A., Dupuis, P., Mayer, B. & Picard, D. An interaction network predicted from public data as a discovery tool: application to the Hsp90 molecular chaperone machine. *PLoS ONE* **6,** e26044; 10.1371/journal.pone.0026044 (2011).

102. Miyata, Y., Nakamoto, H. & Neckers, L. The therapeutic target Hsp90 and cancer hallmarks. *Current pharmaceutical design* **19,** 347–365; 10.2174/138161213804143725 (2013).

103. Misso, G. *et al.* Pharmacological inhibition of HSP90 and ras activity as a new strategy in the treatment of HNSCC. *Journal of cellular physiology* **228,** 130–141; 10.1002/jcp.24112 (2013).

104. Sato, S., Fujita, N. & Tsuruo, T. Modulation of Akt kinase activity by binding to Hsp90. *Proc. Natl. Acad. Sci. U.S.A.* **97,** 10832–10837; 10.1073/pnas.170276797 (2000).

105. Jego, G., Hazoumé, A., Seigneuric, R. & Garrido, C. Targeting heat shock proteins in cancer. *Cancer letters* **332,** 275–285; 10.1016/j.canlet.2010.10.014 (2013).

106. Hanahan, D. & Weinberg, R. A. The hallmarks of cancer. *Cell* **100,** 57–70; 10.1016/s0092-8674(00)81683-9 (2000).

107. Hanahan, D. & Weinberg, R. A. Hallmarks of cancer: the next generation. *Cell* **144,** 646–674; 10.1016/j.cell.2011.02.013 (2011).

108. Yufu, Y., Nishimura, J. & Nawata, H. High constitutive expression of heat shock protein 90 alpha in human acute leukemia cells. *Leukemia Research* **16,** 597–605; 10.1016/0145-2126(92)90008-u (1992).

109. Jameel, A. *et al.* Clinical and biological significance of HSP89 alpha in human breast cancer. *International journal of cancer* **50,** 409–415; 10.1002/ijc.2910500315 (1992).

110. Gress, T. M. *et al.* Differential expression of heat shock proteins in pancreatic carcinoma. *Cancer Res* **54,** 547–551 (1994).

111. Ogata, M., Naito, Z., Tanaka, S., Moriyama, Y. & Asano, G. Overexpression and localization of heat shock proteins mRNA in pancreatic carcinoma. *Journal of Nippon Medical School = Nippon Ika Daigaku zasshi* **67,** 177–185; 10.1272/jnms.67.177 (2000).

112. Jérôme, V., Vourc'h, C., Baulieu, E. E. & Catelli, M. G. Cell cycle regulation of the chicken hsp90 alpha expression. *Experimental cell research* **205,** 44–51; 10.1006/excr.1993.1056 (1993).

113. Jérôme, V., Léger, J., Devin, J., Baulieu, E. E. & Catelli, M. G. Growth factors acting via tyrosine kinase receptors induce HSP90 alpha gene expression. *Growth factors (Chur, Switzerland)* **4,** 317–327; 10.3109/08977199109043917 (1991).

114. Teng, S.-C. *et al.* Direct activation of HSP90A transcription by c-Myc contributes to c-Myc-induced transformation. *Journal of Biological Chemistry* **279,** 14649–14655; 10.1074/jbc.M308842200 (2004).

115. Fumo, G., Akin, C., Metcalfe, D. D. & Neckers, L. 17-Allylamino-17-demethoxygeldanamycin (17-AAG) is effective in down-regulating mutated, constitutively activated KIT protein in human mast cells. *Blood* **103,** 1078–1084; 10.1182/blood-2003-07-2477 (2004).

116. Lin, T.-Y. *et al.* The novel HSP90 inhibitor STA-9090 exhibits activity against Kit-dependent and -independent malignant mast cell tumors. *Experimental hematology* **36,** 1266–1277; 10.1016/j.exphem.2008.05.001 (2008).

117. Yao, Q. *et al.* FLT3 expressing leukemias are selectively sensitive to inhibitors of the molecular chaperone heat shock protein 90 through destabilization of signal transduction-associated kinases. *Clinical cancer research : an official journal of the American Association for Cancer Research* **9,** 4483–4493 (2003).

118. Thomas, X. *et al.* Expression of heat-shock proteins is associated with major adverse prognostic factors in acute myeloid leukemia. *Leukemia Research* **29,** 1049–1058; 10.1016/j.leukres.2005.02.010 (2005).

119. Xiao, K., Liu, W., Qu, S., Sun, H. & Tang, J. Study of heat shock protein HSP90 alpha, HSP70, HSP27 mRNA expression in human acute leukemia cells. *Journal of Tongji Medical University = Tong ji yi ke da xue xue bao* **16,** 212–216; 10.1007/BF02888109 (1996).

120. Yufu, Y., Nishimura, J., Ideguchi, H. & Nawata, H. Heterogeneity of the synthesis of heat shock proteins in human leukaemic cells. *Br J Cancer* **62,** 65–68; 10.1038/bjc.1990.230 (1990).

121. Sedlackova, L., Spacek, M., Holler, E., Imryskova, Z. & Hromadnikova, I. Heat-shock protein expression in leukemia. *Tumour biology : the journal of the International Society for Oncodevelopmental Biology and Medicine* **32,** 33–44; 10.1007/s13277-010-0088-7 (2011).

122. Tian, W.-L. *et al.* High expression of heat shock protein 90 alpha and its significance in human acute leukemia cells. *Gene* **542,** 122–128; 10.1016/j.gene.2014.03.046 (2014).

123. Duval, A. *et al.* Expression and prognostic significance of heat-shock proteins in myelodysplastic syndromes. *Haematologica* **91,** 713–714 (2006).

124. Elia, G., Marco, A. de, Rossi, A. & Santoro, M. G. Inhibition of HSP70 expression by calcium ionophore A23187 in human cells. An effect independent of the acquisition of DNA-binding activity by the heat shock transcription factor. *Journal of Biological Chemistry* **271,** 16111–16118; 10.1074/jbc.271.27.16111 (1996).

125. Pirkkala, L., Alastalo, T. P., Nykanen, P., Seppa, L. & Sistonen, L. Differentiation lineage-specific expression of human heat shock transcription factor 2. *FASEB journal : official publication of the Federation of American Societies for Experimental Biology* **13,** 1089–1098; 10.1096/fasebj.13.9.1089 (1999).

126. Roe, S. M. *et al.* Structural basis for inhibition of the Hsp90 molecular chaperone by the antitumor antibiotics radicicol and geldanamycin. *J. Med. Chem.* **42,** 260–266; 10.1021/jm980403y (1999).

127. Le Brazidec, J.-Y. *et al.* Synthesis and biological evaluation of a new class of geldanamycin derivatives as potent inhibitors of Hsp90. *J. Med. Chem.* **47,** 3865–3873; 10.1021/jm0306125 (2004).

128. Tian, Z.-Q. *et al.* Synthesis and biological activities of novel 17-aminogeldanamycin derivatives. *Bioorganic & Medicinal Chemistry* **12,** 5317–5329; 10.1016/j.bmc.2004.07.053 (2004).

129. Bickel, D. & Gohlke, H. C-terminal modulators of heat shock protein of 90 kDa (HSP90): State of development and modes of action. *Bioorganic & Medicinal Chemistry* **27,** 115080; 10.1016/j.bmc.2019.115080 (2019).

130. Zhou, H., Qiao, K., Gao, Z., Vederas, J. C. & Tang, Y. Insights into radicicol biosynthesis via heterologous synthesis of intermediates and analogs. *The Journal of biological chemistry* **285,** 41412–41421; 10.1074/jbc.M110.183574 (2010).

131. Cheung, K.-M. J. *et al.* The identification, synthesis, protein crystal structure and in vitro biochemical evaluation of a new 3,4-diarylpyrazole class of Hsp90 inhibitors. *Bioorganic & Medicinal Chemistry Letters* **15,** 3338–3343; 10.1016/j.bmcl.2005.05.046 (2005).

132. Eccles, S. A. *et al.* NVP-AUY922: a novel heat shock protein 90 inhibitor active against xenograft tumor growth, angiogenesis, and metastasis. *Cancer Research* **68,** 2850–2860; 10.1158/0008-5472.CAN-07-5256 (2008).

133. Nakashima, T. *et al.* New molecular and biological mechanism of antitumor activities of KW-2478, a novel nonansamycin heat shock protein 90 inhibitor, in multiple myeloma cells. *Clinical cancer research : an official journal of the American Association for Cancer Research* **16,** 2792–2802; 10.1158/1078-0432.CCR-09-3112 (2010).

134. Woodhead, A. J. *et al.* Discovery of (2,4-dihydroxy-5-isopropylphenyl)-5-(4-methylpiperazin-1-ylmethyl)-1,3-dihydroisoindol-2-ylmethanone (AT13387), a novel inhibitor of the molecular chaperone Hsp90 by fragment based drug design. *Journal of medicinal chemistry* **53,** 5956–5969; 10.1021/jm100060b (2010).

135. Chiosis, G. *et al.* A small molecule designed to bind to the adenine nucleotide pocket of Hsp90 causes Her2 degradation and the growth arrest and differentiation of breast cancer cells. *Chemistry & biology* **8,** 289–299; 10.1016/s1074-5521(01)00015-1 (2001).

136. Wright, L. *et al.* Structure-activity relationships in purine-based inhibitor binding to HSP90 isoforms. *Chemistry & biology* **11,** 775–785; 10.1016/j.chembiol.2004.03.033 (2004).

137. He, H. *et al.* Identification of potent water soluble purine-scaffold inhibitors of the heat shock protein 90. *J. Med. Chem.* **49,** 381–390; 10.1021/jm0508078 (2006).

138. Cerchietti, L. C. *et al.* A purine scaffold Hsp90 inhibitor destabilizes BCL-6 and has specific antitumor activity in BCL-6-dependent B cell lymphomas. *Nature medicine* **15,** 1369–1376; 10.1038/nm.2059 (2009).

139. Caldas-Lopes, E. *et al.* Hsp90 inhibitor PU-H71, a multimodal inhibitor of malignancy, induces complete responses in triple-negative breast cancer models. *Proc. Natl. Acad. Sci. U.S.A.* **106,** 8368–8373; 10.1073/pnas.0903392106 (2009).

140. Marcu, M. G., Schulte, T. W. & Neckers, L. Novobiocin and related coumarins and depletion of heat shock protein 90-dependent signaling proteins. *Journal of the National Cancer Institute* **92,** 242–248; 10.1093/jnci/92.3.242 (2000).

141. Marcu, M. G., Chadli, A., Bouhouche, I., Catelli, M. & Neckers, L. M. The heat shock protein 90 antagonist novobiocin interacts with a previously unrecognized ATP-binding domain in the carboxyl terminus of the chaperone. *The Journal of biological chemistry* **275,** 37181–37186; 10.1074/jbc.M003701200 (2000).

142. Chai, R. C. *et al.* Molecular stress-inducing compounds increase osteoclast formation in a heat shock factor 1 protein-dependent manner. *The Journal of biological chemistry* **289,** 13602–13614; 10.1074/jbc.M113.530626 (2014).

143. Shelton, S. N. *et al.* KU135, a novel novobiocin-derived C-terminal inhibitor of the 90-kDa heat shock protein, exerts potent antiproliferative effects in human leukemic cells. *Molecular pharmacology* **76,** 1314–1322; 10.1124/mol.109.058545 (2009).

144. Conde, R., Belak, Z. R., Nair, M., O'Carroll, R. F. & Ovsenek, N. Modulation of Hsf1 activity by novobiocin and geldanamycin. *Biochemistry and cell biology = Biochimie et biologie cellulaire* **87,** 845–851; 10.1139/o09-049 (2009).

145. Zhao, H. *et al.* Engineering an antibiotic to fight cancer: optimization of the novobiocin scaffold to produce anti-proliferative agents. *Journal of medicinal chemistry* **54,** 3839–3853; 10.1021/jm200148p (2011).

146. Donnelly, A. C. *et al.* The design, synthesis, and evaluation of coumarin ring derivatives of the novobiocin scaffold that exhibit antiproliferative activity. *The Journal of organic chemistry* **73,** 8901–8920; 10.1021/jo801312r (2008).

147. Burlison, J. A., Neckers, L., Smith, A. B., Maxwell, A. & Blagg, B. S. J. Novobiocin: redesigning a DNA gyrase inhibitor for selective inhibition of hsp90. *Journal of the American Chemical Society* **128,** 15529–15536; 10.1021/ja065793p (2006).

148. Yu, X. M. *et al.* Hsp90 inhibitors identified from a library of novobiocin analogues. *Journal of the American Chemical Society* **127,** 12778–12779; 10.1021/ja0535864 (2005).

149. Byrd, K. M., Kent, C. N. & Blagg, B. S. J. Synthesis and Biological Evaluation of Stilbene Analogues as Hsp90 C-Terminal Inhibitors. *ChemMedChem* **12,** 2022–2029; 10.1002/cmdc.201700630 (2017).

150. Ghosh, S. *et al.* Diverging Novobiocin Anti-Cancer Activity from Neuroprotective Activity through Modification of the Amide Tail. *ACS medicinal chemistry letters* **7,** 813–818; 10.1021/acsmedchemlett.6b00224 (2016).

151. Anyika, M., McMullen, M., Forsberg, L. K., Dobrowsky, R. T. & Blagg, B. S. J. Development of Noviomimetics as C-Terminal Hsp90 Inhibitors. *ACS medicinal chemistry letters* **7,** 67–71; 10.1021/acsmedchemlett.5b00331 (2016).

152. Zhao, H. *et al.* Design, synthesis and biological evaluation of biphenylamide derivatives as Hsp90 C-terminal inhibitors. *European Journal of Medicinal Chemistry* **89,** 442–466; 10.1016/j.ejmech.2014.10.034 (2015).

153. Byrd, K. M. *et al.* Synthesis and Biological Evaluation of Novobiocin Core Analogues as Hsp90 Inhibitors. *Chem. Eur. J.* **22,** 6921–6931; 10.1002/chem.201504955 (2016).

154. Zhao, J. *et al.* Triazole Containing Novobiocin and Biphenyl Amides as Hsp90 C-Terminal Inhibitors. *MedChemComm* **5,** 1317–1323; 10.1039/C4MD00102H (2014).

155. Matts, R. L. *et al.* Elucidation of the Hsp90 C-terminal inhibitor binding site. *ACS chemical biology* **6,** 800–807; 10.1021/cb200052x (2011).

156. Allan, R. K., Mok, D., Ward, B. K. & Ratajczak, T. Modulation of Chaperone Function and Cochaperone Interaction by Novobiocin in the C-terminal Domain of Hsp90. *Journal of Biological Chemistry* **281,** 7161–7171; 10.1074/jbc.M512406200 (2006).

157. Krieger, V. *et al.* α-Aminoxy Peptoids: A Unique Peptoid Backbone with a Preference for cis -Amide Bonds. *Chem. Eur. J.* **23,** 3699–3707; 10.1002/chem.201605100 (2017).

158. Bopp, B. *et al.* Design and biological testing of peptidic dimerization inhibitors of human Hsp90 that target the C-terminal domain. *Biochimica et biophysica acta* **1860,** 1043–1055; 10.1016/j.bbagen.2016.01.005 (2016).

159. Ciglia, E. *et al.* Resolving hot spots in the C-terminal dimerization domain that determine the stability of the molecular chaperone Hsp90. *PLoS ONE* **9,** e96031; 10.1371/journal.pone.0096031 (2014).

160. Di, L. Strategic approaches to optimizing peptide ADME properties. *The AAPS journal* **17,** 134–143; 10.1208/s12248-014-9687-3. (2015).

161. Banerji, U. *et al.* Phase I pharmacokinetic and pharmacodynamic study of 17-allylamino, 17-demethoxygeldanamycin in patients with advanced malignancies. *JCO* **23,** 4152–4161; 10.1200/JCO.2005.00.612 (2005).

162. Pacey, S. *et al.* A Phase II trial of 17-allylamino, 17-demethoxygeldanamycin (17-AAG, tanespimycin) in patients with metastatic melanoma. *Invest New Drugs* **30,** 341–349; 10.1007/s10637-010-9493-4 (2012).

163. Park, S., Park, J.-A., Jeon, J.-H. & Lee, Y. Traditional and Novel Mechanisms of Heat Shock Protein 90 (HSP90) Inhibition in Cancer Chemotherapy Including HSP90 Cleavage. *Biomolecules & therapeutics* **27,** 423–434; 10.4062/biomolther.2019.051 (2019).

164. Sharp, S. & Workman, P. Inhibitors of the HSP90 molecular chaperone: current status. *Advances in cancer research* **95,** 323–348; 10.1016/S0065-230X(06)95009-X (2006).

165. Piper, P. W. & Millson, S. H. Mechanisms of Resistance to Hsp90 Inhibitor Drugs: A Complex Mosaic Emerges. *Pharmaceuticals (Basel, Switzerland)* **4,** 1400–1422; 10.3390/ph4111400 (2011).

166. Jhaveri, K., Taldone, T., Modi, S. & Chiosis, G. Advances in the clinical development of heat shock protein 90 (Hsp90) inhibitors in cancers. *Biochimica et biophysica acta* **1823,** 742–755; 10.1016/j.bbamcr.2011.10.008. (2012).

167. Supko, J. G., Hickman, R. L., Grever, M. R. & Malspeis, L. Preclinical pharmacologic evaluation of geldanamycin as an antitumor agent. *Cancer chemotherapy and pharmacology* **36,** 305–315; 10.1007/BF00689048. (1995).

168. Wang, Y. & McAlpine, S. R. N-terminal and C-terminal modulation of Hsp90 produce dissimilar phenotypes. *Chemical communications (Cambridge, England)* **51,** 1410–1413; 10.1039/c4cc07284g (2015).

169. Eskew, J. D. *et al.* Development and characterization of a novel C-terminal inhibitor of Hsp90 in androgen dependent and independent prostate cancer cells. *BMC Cancer* **11,** 468; 10.1186/1471-2407-11-468 (2011).

170. Kurokawa, Y. *et al.* Pimitespib in patients with advanced gastrointestinal stromal tumor (CHAPTER-GIST-301): a randomized, double-blind, placebo-controlled phase III trial.

Annals of oncology : official journal of the European Society for Medical Oncology **33,** 959–967; 10.1016/j.annonc.2022.05.518 (2022).

171. Whitesell, L., Santagata, S. & Lin, N. U. Inhibiting HSP90 to treat cancer: a strategy in evolution. *Current molecular medicine* **12,** 1108–1124; 10.2174/156652412803306657 (2012).

172. Hatfield, M. P. D. & Lovas, S. Role of Hsp70 in cancer growth and survival. *Protein and peptide letters* **19,** 616–624; 10.2174/092986612800493968 (2012).

173. Jäättelä, M., Wissing, D., Kokholm, K., Kallunki, T. & Egeblad, M. Hsp70 exerts its anti-apoptotic function downstream of caspase-3-like proteases. *The EMBO journal* **17,** 6124–6134; 10.1093/emboj/17.21.6124 (1998).

174. Bruey, J. M. *et al.* Hsp27 negatively regulates cell death by interacting with cytochrome c. *Nature cell biology* **2,** 645–652; 10.1038/35023595 (2000).

175. Zhang, H. *et al.* BIIB021, a synthetic Hsp90 inhibitor, has broad application against tumors with acquired multidrug resistance. *International journal of cancer* **126,** 1226–1234; 10.1002/ijc.24825 (2010).

176. Benchekroun, M. N., Schneider, E., Safa, A. R., Townsend, A. J. & Sinha, B. K. Mechanisms of resistance to ansamycin antibiotics in human breast cancer cell lines. *Molecular pharmacology* **46,** 677–684 (1994).

177. Rouhi, A. *et al.* Prospective identification of resistance mechanisms to HSP90 inhibition in KRAS mutant cancer cells. *Oncotarget* **8,** 7678–7690; 10.18632/oncotarget.13841 (2017).

178. Gaspar, N. *et al.* Acquired resistance to 17-allylamino-17-demethoxygeldanamycin (17-AAG, tanespimycin) in glioblastoma cells. *Cancer Res* **69,** 1966–1975; 10.1158/0008-5472.CAN-08-3131 (2009).

179. Ward, B. K. *et al.* A structure-based mutational analysis of cyclophilin 40 identifies key residues in the core tetratricopeptide repeat domain that mediate binding to Hsp90. *Journal of Biological Chemistry* **277,** 40799–40809; 10.1074/jbc.M207097200 (2002).

180. Shimamura, T. *et al.* Ganetespib (STA-9090), a nongeldanamycin HSP90 inhibitor, has potent antitumor activity in in vitro and in vivo models of non-small cell lung cancer. *Clinical cancer research : an official journal of the American Association for Cancer Research* **18,** 4973–4985; 10.1158/1078-0432.CCR-11-2967 (2012).

181. Vogt, M. *et al.* Co-targeting HSP90 alpha and CDK7 overcomes resistance against HSP90 inhibitors in BCR-ABL1+ leukemia cells. *Cell death & disease* **14,** 799; 10.1038/s41419-023-06337-3 (2023).

182. Bhatia, S. *et al.* Development of a First-in-Class Small-Molecule Inhibitor of the C-Terminal Hsp90 Dimerization. *ACS central science* **8,** 636–655; 10.1021/acscentsci.2c00013 (2022).

183. Sinatra, L. *et al.* Solid-Phase Synthesis of Cereblon-Recruiting Selective Histone Deacetylase 6 Degraders (HDAC6 PROTACs) with Antileukemic Activity. *J. Med. Chem.* **65,** 16860–16878; 10.1021/acs.jmedchem.2c01659 (2022).

184. Wurnig, S. L. *et al.* Development of the first Geldanamycin-Based HSP90 Degraders.

185. Sun, Y. *et al.* Small-molecule inhibitor of C-terminal HSP90 dimerization modulates autophagy and functions synergistically with mTOR inhibition to kill bladder cancer cells.

186. Li, L., Wang, L., You, Q.-D. & Xu, X.-L. Heat Shock Protein 90 Inhibitors: An Update on Achievements, Challenges, and Future Directions. *J. Med. Chem.* **63,** 1798–1822; 10.1021/acs.jmedchem.9b00940 (2020).

187. Mumin, N. H. *et al.* Overcoming acquired resistance to HSP90 inhibition by targeting JAK-STAT signalling in triple-negative breast cancer. *BMC Cancer* **19,** 102; 10.1186/s12885-019-5295-z (2019).

188. Chatterjee, S., Huang, E. H.-B., Christie, I., Kurland, B. F. & Burns, T. F. Acquired Resistance to the Hsp90 Inhibitor, Ganetespib, in KRAS-Mutant NSCLC Is Mediated via Reactivation of the ERK-p90RSK-mTOR Signaling Network. *Mol Cancer Ther* **16,** 793–804; 10.1158/1535-7163.MCT-16-0677 (2017).

189. Meyuhas, O. Ribosomal Protein S6 Phosphorylation: Four Decades of Research. *International review of cell and molecular biology* **320,** 41–73; 10.1016/bs.ircmb.2015.07.006 (2015).

190. Jafari, R. *et al.* The cellular thermal shift assay for evaluating drug target interactions in cells. *Nat Protoc* **9,** 2100–2122; 10.1038/nprot.2014.138 (2014).

191. Wang, D. Discrepancy between mRNA and protein abundance: insight from information retrieval process in computers. *Computational biology and chemistry* **32,** 462–468; 10.1016/j.compbiolchem.2008.07.014 (2008).

192. Lewis, M. *et al.* Different Relationship between hsp70 mRNA and hsp70 Levels in the Heat Shock Response of Two Salmonids with Dissimilar Temperature Preference. *Frontiers in physiology* **7,** 511; 10.3389/fphys.2016.00511 (2016).

193. Ullrich, S. J., Moore, S. K. & Appella, E. Transcriptional and Translational Analysis of the Murine 84- and 86-kDa Heat Shock Proteins. *Journal of Biological Chemistry* **264,** 6810–6816; 10.1016/S0021-9258(18)83502-5 (1989).

194. Bhattacharya, K. *et al.* Translational reprogramming in response to accumulating stressors ensures critical threshold levels of Hsp90 for mammalian life. *Nat Commun* **13,** 6271; 10.1038/s41467-022-33916-3 (2022).

195. Jing, E. *et al.* Hsp90β knockdown in DIO mice reverses insulin resistance and improves glucose tolerance. *Nutrition & metabolism* **15,** 11; 10.1186/s12986-018-0242-6 (2018).

196. Maiti, S. & Picard, D. Cytosolic Hsp90 Isoform-Specific Functions and Clinical Significance. *Biomolecules* **12**; 10.3390/biom12091166 (2022).

197. Ahler, E. *et al.* Doxycycline alters metabolism and proliferation of human cell lines. *PLoS ONE* **8,** e64561; 10.1371/journal.pone.0064561 (2013).

198. Luger, A.-L. *et al.* Doxycycline Impairs Mitochondrial Function and Protects Human Glioma Cells from Hypoxia-Induced Cell Death: Implications of Using Tet-Inducible Systems. *International journal of molecular sciences* **19**; 10.3390/ijms19051504 (2018).

199. Dijk, S. N., Protasoni, M., Elpidorou, M., Kroon, A. M. & Taanman, J.-W. Mitochondria as target to inhibit proliferation and induce apoptosis of cancer cells: the effects of doxycycline and gemcitabine. *Sci Rep* **10,** 4363; 10.1038/s41598-020-61381-9 (2020).

200. Mshaik, R. *et al.* HSP90 inhibitor NVP-BEP800 affects stability of SRC kinases and growth of T-cell and B-cell acute lymphoblastic leukemias. *Blood cancer journal* **11,** 61; 10.1038/s41408-021-00450-2 (2021).

201. Koga, F. *et al.* Hsp90 inhibition transiently activates Src kinase and promotes Src-dependent Akt and Erk activation. *Proc. Natl. Acad. Sci. U.S.A.* **103,** 11318–11322; 10.1073/pnas.0604705103 (2006).

202. Xu, Y., Singer, M. A. & Lindquist, S. Maturation of the tyrosine kinase c-src as a kinase and as a substrate depends on the molecular chaperone Hsp90. *Proc. Natl. Acad. Sci. U.S.A.* **96,** 109–114; 10.1073/pnas.96.1.109 (1999).

203. Basso, A. D., Solit, D. B., Munster, P. N. & Rosen, N. Ansamycin antibiotics inhibit Akt activation and cyclin D expression in breast cancer cells that overexpress HER2. *Oncogene* **21,** 1159–1166; 10.1038/sj.onc.1205184 (2002).

204. Hostein, I., Robertson, D., DiStefano, F., Workman, P. & Andrew Clarke, P. Inhibition of Signal Transduction by the Hsp90 Inhibitor 17-Allylamino-17-demethoxygeldanamycin Results in Cytostasis and Apoptosis. *Cancer Res* **61,** 4003–4009 (2001).

205. Basso, A. D. *et al.* Akt Forms an Intracellular Complex with Heat Shock Protein 90 (Hsp90) and Cdc37 and Is Destabilized by Inhibitors of Hsp90 Function. *Journal of Biological Chemistry* **277,** 39858–39866; 10.1074/jbc.M206322200 (2002).

206. Huck, J. D. *et al.* Structures of Hsp90α and Hsp90β bound to a purine-scaffold inhibitor reveal an exploitable residue for drug selectivity. *Proteins* **87,** 869–877; 10.1002/prot.25750 (2019).

207. Chen, Y., Thompson, D. C., Koppaka, V., Jester, J. V. & Vasiliou, V. Ocular aldehyde dehydrogenases: protection against ultraviolet damage and maintenance of transparency for vision. *Progress in retinal and eye research* **33,** 28–39; 10.1016/j.preteyeres.2012.10.001 (2013).

208. Qiu, J. J. *et al.* Critical role of retinoid/rexinoid signaling in mediating transformation and therapeutic response of NUP98-RARG leukemia. *Leukemia* **29,** 1153–1162; 10.1038/leu.2014.334 (2015).

209. Kastan, M. B. *et al.* Direct demonstration of elevated aldehyde dehydrogenase in human hematopoietic progenitor cells. *Blood* **75,** 1947–1950 (1990).

210. Tomita, H., Tanaka, K., Tanaka, T. & Hara, A. Aldehyde dehydrogenase 1A1 in stem cells and cancer. *Oncotarget* **7,** 11018–11032; 10.18632/oncotarget.6920 (2016).

211. Ginestier, C. *et al.* ALDH1 is a marker of normal and malignant human mammary stem cells and a predictor of poor clinical outcome. *Cell stem cell* **1,** 555–567; 10.1016/j.stem.2007.08.014 (2007).

212. Alamgeer, M. *et al.* The prognostic significance of aldehyde dehydrogenase 1A1 (ALDH1A1) and CD133 expression in early stage non-small cell lung cancer. *Thorax* **68,** 1095–1104; 10.1136/thoraxjnl-2012-203021 (2013).

213. Uddin, M. H., Kim, B., Cho, U., Azmi, A. S. & Song, Y. S. Association of ALDH1A1-NEK-2 axis in cisplatin resistance in ovarian cancer cells. *Heliyon* **6,** e05442; 10.1016/j.heliyon.2020.e05442 (2020).

214. Lei, H.-M. *et al.* Aldehyde dehydrogenase 1A1 confers erlotinib resistance via facilitating the reactive oxygen species-reactive carbonyl species metabolic pathway in lung adenocarcinomas. *Theranostics* **9,** 7122–7139; 10.7150/thno.35729 (2019).

215. Hilton, J. Role of aldehyde dehydrogenase in cyclophosphamide-resistant L1210 leukemia. *Cancer Res* **44,** 5156–5160 (1984).

216. Sladek, N. E. & Landkamer, G. J. Restoration of sensitivity to oxazaphosphorines by inhibitors of aldehyde dehydrogenase activity in cultured oxazaphosphorine-resistant L1210 and cross-linking agent-resistant P388 cell lines. *Cancer Res* **45,** 1549–1555 (1985).

217. Koppaka, V. *et al.* Aldehyde dehydrogenase inhibitors: a comprehensive review of the pharmacology, mechanism of action, substrate specificity, and clinical application. *Pharmacological reviews* **64,** 520–539; 10.1124/pr.111.005538 (2012).

218. Agrawal, M. *et al.* MDR1 expression predicts outcome of Ph+ chronic phase CML patients on second-line nilotinib therapy after imatinib failure. *Leukemia* **28,** 1478–1485; 10.1038/leu.2014.6 (2014).

219. Kasimir-Bauer, S. *et al.* In acute myeloid leukemia, coexpression of at least two proteins, including P-glycoprotein, the multidrug resistance-related protein, bcl-2, mutant p53, and heat-shock protein 27, is predictive of the response to induction chemotherapy. *Experimental hematology* **26,** 1111–1117 (1998).

220. Kim, H. J. *et al.* P-glycoprotein confers acquired resistance to 17-DMAG in lung cancers with an ALK rearrangement. *BMC Cancer* **15,** 553; 10.1186/s12885-015-1543-z (2015).

221. Kelland, L. R., Sharp, S. Y., Rogers, P. M., Myers, T. G. & Workman, P. DT-Diaphorase expression and tumor cell sensitivity to 17-allylamino, 17-demethoxygeldanamycin, an inhibitor of heat shock protein 90. *Journal of the National Cancer Institute* **91,** 1940–1949; 10.1093/jnci/91.22.1940 (1999).

222. Vilaboa, N. E., Galán, A., Troyano, A., Blas, E. de & Aller, P. Regulation of multidrug resistance 1 (MDR1)/P-glycoprotein gene expression and activity by heat-shock transcription factor 1 (HSF1). *Journal of Biological Chemistry* **275,** 24970–24976; 10.1074/jbc.M909136199 (2000).

223. Kim, S. H. *et al.* Involvement of heat shock factor in regulating transcriptional activation of MDR1 gene in multidrug-resistant cells. *Cancer letters* **115,** 9–14; 10.1016/s0304-3835(97)04725-3 (1997).

224. Kim, S. H. *et al.* Suppression of multidrug resistance via inhibition of heat shock factor by quercetin in MDR cells. *Experimental & molecular medicine* **30,** 87–92; 10.1038/emm.1998.13 (1998).

225. Grundy, M. *et al.* Early changes in rpS6 phosphorylation and BH3 profiling predict response to chemotherapy in AML cells. *PLoS ONE* **13,** e0196805; 10.1371/journal.pone.0196805 (2018).

226. Yang, X. *et al.* Knockdown of ribosomal protein S6 suppresses proliferation, migration, and invasion in epithelial ovarian cancer. *Journal of ovarian research* **13,** 100; 10.1186/s13048-020-00707-7 (2020).

227. Yi, Y. W., You, K. S., Park, J.-S., Lee, S.-G. & Seong, Y.-S. Ribosomal Protein S6: A Potential Therapeutic Target against Cancer? *International journal of molecular sciences* **23**; 10.3390/ijms23010048 (2021).

228. Meyuhas, O. Physiological roles of ribosomal protein S6: one of its kind. *International review of cell and molecular biology* **268,** 1–37; 10.1016/S1937-6448(08)00801-0 (2008).

229. Flotow, H. & Thomas, G. Substrate recognition determinants of the mitogen-activated 70K S6 kinase from rat liver. *Journal of Biological Chemistry* **267,** 3074–3078 (1992).

230. Wettenhall, R. E., Erikson, E. & Maller, J. L. Ordered multisite phosphorylation of Xenopus ribosomal protein S6 by S6 kinase II. *Journal of Biological Chemistry* **267,** 9021–9027 (1992).

231. Jakubowicz, T. Phosphorylation-dephosphorylation changes in yeast ribosomal proteins S2 and S6 during growth under normal and hyperthermal conditions. *Acta biochimica Polonica* **32,** 7–12 (1985).

232. Szyszka, R. & Gasior, E. Phosphorylation of ribosomal proteins during differentiation of Saccharomyces cerevisiae. *Acta biochimica Polonica* **31,** 375–382 (1984).

233. Kim, T.-S. *et al.* Interaction of Hsp90 with Ribosomal Proteins Protects from Ubiquitination and Proteasome-dependent Degradation□. *Molecular Biology of the Cell* **17,** 824–833; 10.1091/mbc.E05-08-0713 (2006).

234. Katayama, K., Fujiwara, C., Noguchi, K. & Sugimoto, Y. RSK1 protects P-glycoprotein/ABCB1 against ubiquitin-proteasomal degradation by downregulating the ubiquitin-conjugating enzyme E2 R1. *Sci Rep* **6,** 36134; 10.1038/srep36134 (2016).

235. Kasimir-Bauer, S. *et al.* Impact of the expression of P glycoprotein, the multidrug resistance-related protein, bcl-2, mutant p53, and heat shock protein 27 on response to induction therapy and long-term survival in patients with de novo acute myeloid leukemia. *Experimental hematology* **30,** 1302–1308; 10.1016/s0301-472x(02)00926-8 (2002).

236. Goode, K. M. *et al.* Targeting the Hsp90 C-terminal domain to induce allosteric inhibition and selective client downregulation. *Biochimica et Biophysica Acta (BBA) - General Subjects* **1861,** 1992–2006; 10.1016/j.bbagen.2017.05.006 (2017).

237. D'Annessa, I., Raniolo, S., Limongelli, V., Di Marino, D. & Colombo, G. Ligand Binding, Unbinding, and Allosteric Effects: Deciphering Small-Molecule Modulation of HSP90. *J. Chem. Theory Comput.* **15,** 6368–6381; 10.1021/acs.jctc.9b00319 (2019).

238. Sanchez-Martin, C., Serapian, S. A., Colombo, G. & Rasola, A. Dynamically Shaping Chaperones. Allosteric Modulators of HSP90 Family as Regulatory Tools of Cell Metabolism in Neoplastic Progression. *Frontiers in oncology* **10,** 1177; 10.3389/fonc.2020.01177 (2020).

239. Sanchez, J., Carter, T. R., Cohen, M. S. & Blagg, B. S. Old and New Approaches to Target the Hsp90 Chaperone. *CCDT* **20,** 253–270; 10.2174/1568009619666191202101330 (2020).

240. Söti, C., Rácz, A. & Csermely, P. A Nucleotide-dependent Molecular Switch Controls ATP Binding at the C-terminal Domain of Hsp90. *Journal of Biological Chemistry* **277,** 7066–7075; 10.1074/jbc.M105568200 (2002).

241. Diedrich, D. *et al.* α-Aminoxy Oligopeptides: Synthesis, Secondary Structure, and Cytotoxicity of a New Class of Anticancer Foldamers. *Chemistry (Weinheim an der Bergstrasse, Germany)* **22,** 17600–17611; 10.1002/chem.201602521 (2016).

242. Ratzke, C., Mickler, M., Hellenkamp, B., Buchner, J. & Hugel, T. Dynamics of heat shock protein 90 C-terminal dimerization is an important part of its conformational cycle. *Proc. Natl. Acad. Sci. U.S.A.* **107,** 16101–16106; 10.1073/pnas.1000916107 (2010).

243. Frieg, B., Gremer, L., Heise, H., Willbold, D. & Gohlke, H. Binding modes of thioflavin T and Congo red to the fibril structure of amyloid-β(1-42). *Chem. Commun.* **56,** 7589–7592; 10.1039/D0CC01161D (2020).

244. Milić, D. *et al.* Recognition motif and mechanism of ripening inhibitory peptides in plant hormone receptor ETR1. *Sci Rep* **8**; 10.1038/s41598-018-21952-3 (2018).

245. Gohlke, H. *et al.* Binding region of alanopine dehydrogenase predicted by unbiased molecular dynamics simulations of ligand diffusion. *Journal of chemical information and modeling* **53,** 2493–2498; 10.1021/ci400370y (2013).

246. Trepel, J., Mollapour, M., Giaccone, G. & Neckers, L. Targeting the dynamic HSP90 complex in cancer. *Nature reviews. Cancer* **10,** 537–549; 10.1038/nrc2887 (2010).

247. Wang, Y., Koay, Y. C. & McAlpine, S. R. How Selective are Hsp90 Inhibitors for Cancer Cells over Normal Cells? *ChemMedChem* **12,** 353–357; 10.1002/cmdc.201600595 (2017).

248. Wang, Y. & McAlpine, S. R. Heat-shock protein 90 inhibitors: will they ever succeed as chemotherapeutics? *Future Medicinal Chemistry* **7,** 87–90; 10.4155/fmc.14.154 (2015).

249. Kamal, A. *et al.* A high-affinity conformation of Hsp90 confers tumour selectivity on Hsp90 inhibitors. *Nature* **425,** 407–410; 10.1038/nature01913 (2003).

250. Blagosklonny, M. V. *et al.* The Hsp90 inhibitor geldanamycin selectively sensitizes Bcr-Abl-expressing leukemia cells to cytotoxic chemotherapy. *Leukemia* **15,** 1537–1543; 10.1038/sj.leu.2402257 (2001).

251. Tsujimura, A. *et al.* Selective KIT inhibitor KI-328 and HSP90 inhibitor show different potency against the type of KIT mutations recurrently identified in acute myeloid leukemia. *International journal of hematology* **92,** 624–633; 10.1007/s12185-010-0692-8 (2010).

252. Acquaviva, J. *et al.* Targeting KRAS-mutant non-small cell lung cancer with the Hsp90 inhibitor ganetespib. *Mol Cancer Ther* **11,** 2633–2643; 10.1158/1535-7163.MCT-12-0615 (2012).

253. Raedt, T. de *et al.* Exploiting cancer cell vulnerabilities to develop a combination therapy for ras-driven tumors. *Cancer cell* **20,** 400–413; 10.1016/j.ccr.2011.08.014 (2011).

254. Kong, A. *et al.* Phase 1B/2 study of the HSP90 inhibitor AUY922 plus trastuzumab in metastatic HER2-positive breast cancer patients who have progressed on trastuzumab-based regimen. *Oncotarget* **7,** 37680–37692; 10.18632/oncotarget.8974 (2016).

255. Jhaveri, K. *et al.* A phase I trial of ganetespib in combination with paclitaxel and trastuzumab in patients with human epidermal growth factor receptor-2 (HER2)-positive metastatic breast cancer. *Breast cancer research : BCR* **19,** 89; 10.1186/s13058-017-0879-5 (2017).

256. Johnson, M. L. *et al.* Phase I/II Study of HSP90 Inhibitor AUY922 and Erlotinib for EGFR-Mutant Lung Cancer With Acquired Resistance to Epidermal Growth Factor Receptor Tyrosine Kinase Inhibitors. *JCO* **33,** 1666–1673; 10.1200/JCO.2014.59.7328 (2015).

257. Bonanni, D. *et al.* Dual Targeting Strategies on Histone Deacetylase 6 (HDAC6) and Heat Shock Protein 90 (Hsp90). *Current medicinal chemistry* **29,** 1474–1502; 10.2174/0929867328666210902145102 (2022).

258. Bali, P. *et al.* Inhibition of histone deacetylase 6 acetylates and disrupts the chaperone function of heat shock protein 90: a novel basis for antileukemia activity of histone deacetylase inhibitors. *Journal of Biological Chemistry* **280,** 26729–26734; 10.1074/jbc.C500186200 (2005).

259. Scroggins, B. T. *et al.* An acetylation site in the middle domain of Hsp90 regulates chaperone function. *Molecular cell* **25,** 151–159; 10.1016/j.molcel.2006.12.008 (2007).

260. Edwards, A., Li, J., Atadja, P., Bhalla, K. & Haura, E. B. Effect of the histone deacetylase inhibitor LBH589 against epidermal growth factor receptor-dependent human lung cancer cells. *Mol Cancer Ther* **6,** 2515–2524; 10.1158/1535-7163.MCT-06-0761 (2007).

261. Nishioka, C. *et al.* MS-275, a novel histone deacetylase inhibitor with selectivity against HDAC1, induces degradation of FLT3 via inhibition of chaperone function of heat shock protein 90 in AML cells. *Leukemia Research* **32,** 1382–1392; 10.1016/j.leukres.2008.02.018 (2008).

262. Park, S. *et al.* Suberoylanilide hydroxamic acid induces ROS-mediated cleavage of HSP90 in leukemia cells. *Cell stress & chaperones* **20,** 149–157; 10.1007/s12192-014-0533-4 (2015).

263. Park, S., Park, J.-A., Yoo, H., Park, H.-B. & Lee, Y. Proteasome inhibitor-induced cleavage of HSP90 is mediated by ROS generation and caspase 10-activation in human leukemic cells. *Redox biology* **13,** 470–476; 10.1016/j.redox.2017.07.010 (2017).

264. Park, S. E. *et al.* Vorinostat enhances gefitinib-induced cell death through reactive oxygen species-dependent cleavage of HSP90 and its clients in non-small cell lung cancer with the EGFR mutation. *Oncology reports* **41,** 525–533; 10.3892/or.2018.6814 (2019).

265. Gorman, A. M., Heavey, B., Creagh, E., Cotter, T. G. & Samali, A. Antioxidant-mediated inhibition of the heat shock response leads to apoptosis. *FEBS letters* **445,** 98–102; 10.1016/s0014-5793(99)00094-0 (1999).

266. Beck, R. *et al.* Hsp90 cleavage by an oxidative stress leads to its client proteins degradation and cancer cell death. *Biochemical Pharmacology* **77,** 375–383; 10.1016/j.bcp.2008.10.019 (2009).

267. Beck, R. *et al.* Hsp90 is cleaved by reactive oxygen species at a highly conserved N-terminal amino acid motif. *PLoS ONE* **7,** e40795; 10.1371/journal.pone.0040795 (2012).

268. Duesberg, P., Stindl, R. & Hehlmann, R. Explaining the high mutation rates of cancer cells to drug and multidrug resistance by chromosome reassortments that are catalyzed by aneuploidy. *Proc. Natl. Acad. Sci. U.S.A.* **97,** 14295–14300; 10.1073/pnas.97.26.14295 (2000).

269. O'Hare, T., Eide, C. A. & Deininger, M. W. N. Bcr-Abl kinase domain mutations, drug resistance, and the road to a cure for chronic myeloid leukemia. *Blood* **110,** 2242–2249; 10.1182/blood-2007-03-066936 (2007).

270. Soverini, S. *et al.* BCR-ABL kinase domain mutation analysis in chronic myeloid leukemia patients treated with tyrosine kinase inhibitors: recommendations from an expert panel on behalf of European LeukemiaNet. *Blood* **118,** 1208–1215; 10.1182/blood-2010-12-326405 (2011).

Publications & Presentations:

Co-targeting HSP90 alpha and CDK7 overcomes resistance against HSP90 inhibitors in BCR-ABL1+ leukemia cells. [181]

Vogt, Melina*; **Dienstbier, Niklas***; Schliehe-Diecks, Julian; Scharov, Katerina; Tu, Jia-Wey; Gebing, Philip; Hogenkamp, Julian; Bilen, Berna-Selin; Furlan, Silke; Picard, Daniel; Remke, Marc; Yasin, Layal; Bickel, David; Kalia, Munishikha; Iacoangeli, Alfredo; Lenz, Thomas; Stühler, Kai; Pandyra, Aleksandra; Hauer, Julia; Fischer, Ute; Wagener, Rabea; Borkhardt, Arndt; Bhatia, Sanil (2023):
In *Cell death & disease* 14 (12), p. 799. DOI: 10.1038/s41419-023-06337-3.

Development of a First-in-Class Small-Molecule Inhibitor of the C-Terminal HSP90 Dimerization.[182]

Bhatia, Sanil; Spanier, Lukas; Bickel, David; **Dienstbier, Niklas**; Woloschin, Vitalij; Vogt, Melina; Pols, Henrik; Lungerich, Beate; Reiners, Jens; Aghaallaei, Narges; Diedrich, Daniela; Frieg, Benedikt; Schliehe-Diecks, Julian; Bopp, Bertan; Lang, Franziska; Gopalswamy, Mohanraj; Loschwitz, Jennifer; Bajohgli, Baubak; Skokowa, Julia; Borkhardt, Arndt; Hauer, Julia; Hansen, Finn K.; Smits, Sander H. J.; Jose, Joachim; Gohlke, Holger; Kurz, Thomas (2022):
In *ACS central science* 8 (5), pp. 636–655. DOI: 10.1021/acscentsci.2c00013.

Solid-Phase Synthesis of Cereblon-Recruiting Selective Histone Deacetylase 6 Degraders (HDAC6 PROTACs) with Antileukemic Activity.[183]

Sinatra, Laura; Yang, Jing; Schliehe-Diecks, Julian; **Dienstbier, Niklas**; Vogt, Melina; Gebing, Philip; Bachmann, Luisa M.; Sönnichsen, Melf; Lenz, Thomas; Stühler, Kai; Schöler, Andrea; Borkhardt, Arndt; Bhatia, Sanil; Hansen, Finn K. (2022):
In *J. Med. Chem.* 65 (24), pp. 16860–16878. DOI: 10.1021/acs.jmedchem.2c01659.

Development of the first Geldanamycin-Based HSP90 Degraders[184]

Wurnig, Silas L.*; Vogt, Melina*; Hogenkamp, Julian; **Dienstbier, Niklas**; Borkhardt, Arndt; Bhatia, Sanil*; Hansen, Finn K.* (2023):
In *Frontiers in Chemistry*. DOI: 10.3389/fchem.2023.1219883

Small-molecule inhibitor of C-terminal HSP90 dimerization modulates autophagy and functions synergistically with mTOR inhibition to kill bladder cancer cells[185]

Sun, Yadong; Woloschin, Vitalij; Vogt, Melina; **Dienstbier, Niklas**; David, Céline; Schlütermann, David; Berning, Lena; Opitz, Heinz; Friedrich, Annabelle; Akgün, Seda; Mendiburo, María José; Borkhardt, Arndt; Wesselborg, Sebastian; Bhatia, Sanil*; Kurz, Thomas*; Stork, Björn* (2023):
Manuscript in preparation

* contributed equally to this work

Detailed contributions to the manuscripts mentioned above:

Co-targeting HSP90 alpha and CDK7 overcomes resistance against HSP90 inhibitors in BCR-ABL1+ leukemia cells.

In *Cell death & disease* 14 (12), p. 799. DOI: 10.1038/s41419-023-06337-3.

Contribution:

I have designed, performed, and analyzed most experiments related to the unraveling of the resistance phenotype including generation and validation of resistance cell lines and Western Blots. I have written the majority of the results section for the investigation of the resistance mechanism and have written several paragraphs of the introduction, method section and discussion. I have reviewed the manuscript.

Development of a First-in-Class Small-Molecule Inhibitor of the C-Terminal HSP90 Dimerization.

In *ACS central science* 8 (5), pp. 636–655. DOI: 10.1021/acscentsci.2c00013.

Contribution:

I have performed and analyzed the cell viability assays to identify 5b as a suitable lead candidate (Fig. 2 d-e). I have elucidated the putative binding mode by cFRET, CETSA and n-terminal FP assays (Fig. 3 c, e, f, Fig S23, Table S1). I have adapted a successful vehicle formulation to test 5b in the zebrafish experiment. I have written several paragraphs of the results and methods section especially belonging to Fig 3. I have reviewed the manuscript.

Solid-Phase Synthesis of Cereblon-Recruiting Selective Histone Deacetylase 6 Degraders (HDAC6 PROTACs) with Antileukemic Activity.

In *J. Med. Chem.* 65 (24), pp. 16860–16878. DOI: 10.1021/acs.jmedchem.2c01659.

Contribution:

I have developed, optimized, performed, and analyzed the digital western blot quantification method (Fig 3a.). I have written the results section for the quantification experiment and method section. I have reviewed the manuscript.

Development of the first Geldanamycin-Based HSP90 Degraders

In *Frontiers in Chemistry*. DOI: 10.3389/fchem.2023.1219883

Contribution:

I have performed and analyzed the initial selection screen to identify the most potent Hsp90 Degrader via digital western blotting (Fig. S1 a). I have validated the binding mode by performing and analyzing the nFP assay (Fig. 2 a). I have established and optimized the degradation efficacy digital western blotting assay and have performed one replicate (Fig. 2 b-c) I have written the method sections belonging to digital western blotting and nFP. I have reviewed the manuscript.

Small-molecule inhibitor of C-terminal HSP90 dimerization modulates autophagy and functions synergistically with mTOR inhibition to kill bladder cancer cells

Manuscript in preparation

Contribution:

I have performed and optimized the binding mode investigation by performing nFP, cFRET and thermal shift assay. I have performed and analyzed the cell viability screening in the cell line panel to validate VWK147 efficacy. I have written several paragraphs of the results and method section regarding the binding mode investigation.

Conference Paper:

Vogt, M.; **Dienstbier, N**.; Schliehe-Diecks, J.; Scharov, K.; Tu, J.-W.; Gebing, P. et al. (2022):
S153: DECRYPTING THE ROLE OF HSP90A AND B ISOFORMS TO OVERCOME RESISTANCE IN BCR-ABL1 LEUKEMIA.
In HemaSphere 6, pp. 54–55. DOI: 10.1097/01.hs9.0000843504.70313.ba.

S. Bhatia; H. Ahlert; **N. Dienstbier**; J. Schliehe-Diecks; M. Sönnichsen; M. Remke;U. Fischer;J. Hauer; A. Borkhardt:
Therapeutic stratification of acute leukemia using high throughput drug screening
33. Jahrestagung der Kind-Philipp-Stiftung für pädiatr. onkolog. Forschung (2020).
33. Jahrestagung der Kind-Philipp-Stiftung für pädiatr. onkolog. Forschung. Wilsede, 27/03/2020 - 27/03/2020: © Georg Thieme Verlag KG (Klinische Pädiatrie).

Ahlert, H.; Bhatia, S.; Sönnichsen, M.; **Dienstbier, N**.; Remke, M.; Fischer, U.; Hauer, J.; Borkhardt, A. (2019):
PB1648 THE CLINICAL RELEVANCE OF INDIRECT MYC INHIBITORS FOR PERSONALIZED T-ALL TREATMENT.
In HemaSphere 3 (S1), pp. 762–763. DOI: 10.1097/01.HS9.0000564840.77885.3e.

Ahlert, Heinz; Bhatia, Sanil; Remke, Marc; Sönnichsen, Melf; **Dienstbier, Niklas**; Fischer, Ute; Hauer, Julia; Borkhardt, Arndt (2019):
Therapeutic Stratification of PTEN-MYC Axis Appears to be Promising for Molecular Targeted Therapies in Refractory and Relapsed T-Cell Acute Lymphoblastic Leukemia. In Blood 134 (Supplement_1), p. 3883. DOI: 10.1182/blood-2019-128136.

Acknowledgment

Affirmation

I hereby declare on oath that I have written this dissertation independently. I have used only the sources and aids indicated in this thesis. With the exception of such citations, the work presented in this thesis is my own. I have identified all sources that have helped me as such. This dissertation has never been submitted or presented in a similar form to any other institution or examination board. I have not yet passed any doctoral examination without success.

Ich versichere an Eides Statt, dass die Dissertation von mir selbständig und ohne unzulässige fremde Hilfe unter Beachtung der „Grundsätze zur Sicherung guter wissenschaftlicher Praxis an der Heinrich-Heine-Universität Düsseldorf" erstellt worden ist. Die Dissertation ist nicht einer anderen Fakultät vorgelegt worden. Es sind keine weiteren erfolglosen oder erfolgreichen Promotionsvorhaben unternommen worden.

Die Disputation soll in englischer Sprache abgelegt werden. Es wird kein Ausschluss der Öffentlichkeit beantragt. Es soll der Grad „Doktor der Naturwissenschaften" (doctor rerum naturalium - Dr. rer.nat.) verliehen werden.

_____

Dienstbier, Niklas

20.06.2023